

# Development of a novel colon anastomosis procedure and an endoscopic, single-use platform by using additive manufacturing

Jana Simone Steger

Vollständiger Abdruck der von der TUM School of Engineering and Design der Technischen Universität München zur Erlangung des akademischen Grades einer

Doktorin der Ingenieurwissenschaften (Dr.-Ing.)

genehmigten Dissertation.

Vorsitz: Prof. Dr. Tim C. Lüth

Prüfer\*innen der Dissertation:

1. Prof. Dr. Petra Mela
2. apl. Prof. Dr. Dirk Wilhelm
3. Jun.-Prof. Dr. Franziska Mathis-Ullrich

Die Dissertation wurde am 18.07.2022 bei der Technischen Universität München eingereicht und durch die TUM School of Engineering and Design am 12.02.2023 angenommen.



## **Acknowledgements**

This dissertation is the completion of my doctoral research at the Chair of Medical Materials and Implants at the Technical University of Munich by Prof. Dr. Ing. Petra Mela.

I would like to express my sincere gratitude to my doctoral supervisor Prof. Mela for her courteous guidance, support and the inspiring collaboration throughout the entire time of my doctoral thesis.

Most of the content of this thesis was developed within the scope of the project “CONNECT”, funded by the German Research Foundation (DFG-Project number: 386233407), at the Institute for Minimally Invasive Interdisciplinary Therapeutic Intervention of Prof. Dr. med. Dirk Wilhelm. I want to express my special gratitude to him as my mentor, for his devoted supervision and the intensive encouragement. I am thankful to have had the possibility to work and learn in a really special environment, which allowed me to grow, both on a professional, and personal level.

Furthermore, I would like to thank the examination board for their review and examination of my work and my colleagues at the MMI and the institute MITI for all the discussions, brainstorming sessions, as well as for the familial atmosphere and close team cohesion, so that I have been looking forward to coming to work every day. Furthermore, I would like to express special thanks to Prof. Dr. med Hubertus Feußner, who founded the institute and created a stimulating environment of applied research, and to our secretary and good soul Mrs. Tereza Baude, who always had an open ear and was always there to help and advise me.

Lastly, my heartfelt thanks go to my friends and family, especially to my parents Sabine and Alexander Steger, who always supported me, for the conversations and words of encouragement during the often work-intensive and challenging phases of my doctorate, and for always believing in me.

## **Prologue**

Within the scope of this work, studies and relevant investigations for the development of a novel anastomosis procedure and a patient-adaptable, single-use endoscopic manipulator were summarized. This comprised a meta-analysis of state of the art anastomosis techniques, biomechanical investigations of the colon, the examination of fundamental technologies to enable complex surgical manipulation tasks purely endoluminally, the development of a comprehensive approach for the endoscopic anastomosis application device, using additive manufacturing, and the development of a validation environment. Relevant publications are referenced at the respective passages in the text.

---

## Abstract

**Motivation:** The creation of anastomoses following resective interventions is one of the core challenges in abdominal surgery. Surgeons can choose from a considerable range of different techniques and devices, all of which still show similar complication rates and shortcomings, especially with respect to the intraoperative trauma. To enhance patient care, a novel procedure to create the ideal anastomosis was derived by means of a systematic literature review, and a patient-adaptable, endoscopic single-use anastomosis device was developed. Key challenges of endoluminal manipulation were addressed, including grasping and approximating the bowel endings in an inverted manner, adapting the device size to the patient's anatomy, forming the anastomosis by closing a compression implant and detaching the implant endoscopically.

**Methods:** The development process followed the VDI guideline 2221 for the "Design of technical products and systems". Biomechanical investigations of the colon were performed on porcine samples to determine procedure relevant parameters and requirements for the implant closing process, and derive design guidelines for the device. The knowledge gained was translated into the design of competing prototypes, which were experimentally assessed by evaluating the interaction with porcine colon tissue. Solution principles were integrated into a combined applicator concept, which was examined with regard to its ability to meet the mechanical challenges outlined.

**Results:** In order to enhance manipulation freedom, and to grasp and approximate the bowel endings in an inverted manner, the final applicator comprised two units. An aboral entity, which was free to move along the endoscope shaft, and an oral applicator head, which was fixed just below the steerable tip by a friction locked mechanism with a holding force of  $F_{oral\ fixation}^{mean} = 54.8 \pm 2.0\ N$  to withstand the forces occurring during navigation throughout the colon ( $\sim 11.6\ N$  for axial push and  $\sim 10.7\ N$  for axial pull movements [1]). All components were realized according to an over-the-tube design, using a conventional endoscope as carrier and as visualizing system. Suction air channels were integrated into the applicator, allowing to establish a holding force of 2.0 N orally and of 1.6 N aborally. A two stage telescope hydraulic unit, incorporated into the applicator body, proved to be the most suitable solution to configure the implant in three different device diameter configurations. Implant mounts were assembled to the hydraulics by scissor joints, enabling parallel orientation of compression faces and a fixed distance between the implant halves in all configurations. A maximum realizable expansion force of 41.7 N was determined and with respect to the counteracting bearing forces of 128.3 N, rules for an optimized implant suspension were deduced to reduce leverage effects. Axial congruence between the oral and aboral applicator and implant units was achieved by a snap connection with a closing force of  $F_{snap\ closure}^{mean} = 15.2 \pm 1.0\ N$ . For the implant closing process, biomechanical investigations showed that among the groups compared, neither variations in piercing body trajectory velocities ( $v = 5, 10, 15\ mms^{-1}$ ), nor accelerations ( $a = 5, 10, 15\ mms^{-2}$ ), nor variations in tissue fixation point arrangements had a statistically significant

---

effect on the forces required to pierce colon tissue. However, for the implant design it has to be considered that an increase in spikes (4, 8, 12) resulted in a statistically significant increase in piercing forces ( $6.4\pm 1.5$  N,  $13.6\pm 1.4$  N,  $21.7\pm 5.8$  N). Comparing the measured holding force of the snap connector  $F_{snap\ holding}^{mean} = 43.6\pm 3.9$  N to the required maximum piercing forces of  $\sim 28$  N from the biomechanic investigations, it is concluded that the connection provides sufficient abutment. With respect to the implant closing process, a hydraulic overtube unit was developed, which proved to be a feasible approach to establish appropriate closing forces and pierce through the tissue in the compression zone.

**Conclusion:** It can be summarized that within the scope of this project, solutions were found to overcome key challenges of endoluminal manipulation tasks. These concepts were then translated into an applicator design to form the ideal, endoscopic colon anastomosis. Biomechanical investigations allowed to derive design guidelines for force-efficient, endoscopic implant closure processes, that can be applied to anastomosis procedures, but can also be transferred to alternative interventions. The device establishes a novel approach to cope with the challenge of endoscopic force application in flexible instruments, showing promising results to overcome the problems of conventionally used Bowden wires.

---

## Table of Contents

<b>Motivation</b> .....	<b>1</b>
<b>Background</b> .....	<b>2</b>
2.1 Anatomy: Basics of the gastrointestinal tract.....	2
2.2 Basics of anastomosis formation in the colon.....	3
2.3 Influence of bowel wall layers on anastomotic healing.....	4
2.4 Overview of anastomosing techniques: Identification of a feasible approach towards an endoscopic anastomosis device.....	5
<b>State of the art</b> .....	<b>6</b>
3.1 Comparison of techniques and identification of shortcomings.....	6
3.2 Detailed description of compression anastomosis implants and procedures.....	8
3.2.1 Form-fit based compression anastomosis devices.....	9
3.2.2 Shape-memory based compression anastomosis devices.....	9
3.2.3 Endoscopic compression anastomosis devices.....	10
3.3 Shortcomings of existing endoscopic anastomosis techniques.....	11
3.4 The ideal anastomosis procedure.....	12
<b>Material and Methods</b> .....	<b>15</b>
4.1 Anatomical and mechanical characterization of colon tissue.....	15
4.1.1 Setup design.....	15
4.1.2 Investigated design parameters.....	17
4.1.3 Sample preparation.....	19
4.1.4 Experimental preparation.....	20
4.1.5 Statistical analysis.....	20
4.2 Development and evaluation of solutions to enable basic endoluminal manipulation tasks.....	20
4.2.1 Design and test methods: Grasping/ inversion of colonic margins and patient adaptation ( <i>Theses b, c</i> ).....	21
4.2.2 Design and test methods: Applicator integrated implant closing unit ( <i>Thesis d</i> )..	27
4.2.3 Design and test methods: Endoscopic implant detachment using electromagnets ( <i>Thesis e</i> ).....	31
4.3 Final design approach and mechanical assessment.....	35
4.3.1 Design and test methods: Handling concept of final applicator prototype.....	36
4.3.2 Design and test method: Patient adaptation of final applicator prototype.....	39
4.3.3 Design and test method: Anastomosis formation unit of final applicator prototype.....	41
<b>Results</b> .....	<b>42</b>
5.1 Biological and mechanical characterization of colon tissue: Derivations for an endoscopic applicator closure unit.....	42
5.2 Results of task specific solutions to enable endoluminal manipulation.....	43

---

5.2.1 Results: Grasping/ inversion of colonic margins and patient adaptation ( <i>Theses b, c</i> ) .....	43
5.2.2 Results: Applicator integrated implant closing unit ( <i>Thesis d</i> ) .....	45
5.2.3 Results: Endoscopic implant detachment using electromagnets ( <i>Thesis e</i> ).....	46
5.2.4 Resumé .....	49
5.3 Design of a scalable, single-use endoscopic device for the creation of inverting, end-to-end anastomoses .....	51
5.4 Results of mechanical assessment .....	57
5.4.1 Results: Handling concept of final applicator prototype .....	57
5.4.2 Results: Patient adaptation of final applicator prototype.....	58
5.4.3 Results: Anastomosis formation unit of final applicator prototype.....	62
<b>Discussion.....</b>	<b>62</b>
6.1 Feasibility assessment of final concept with respect to procedure related mechanical requirements .....	62
6.1.1 Tissue manipulation and handling .....	63
6.1.2 Expansion unit .....	64
6.1.3 Closing unit.....	65
6.1.4 Device dimensions.....	67
6.1.5 Using electromagnets for implant detachment .....	68
6.1.6 Using additive manufacturing for the development of novel endoscopic instruments.....	69
6.2 Using hydraulics vs. Bowden wires in endoscopic platforms: Future potentials.....	70
<b>Acknowledgement .....</b>	<b>71</b>
<b>Appendix .....</b>	<b>72</b>
8.1 Formula Directory .....	72
8.2 List of publications .....	73
8.3 List of patents .....	73
8.4 List of supervised student theses .....	74
<b>References .....</b>	<b>75</b>

---

## Motivation

Surgery, as an academic discipline, evolved about 150 years ago [2]. Always in focus, is the preservation of life and the increase in the quality of human life. Since the 1990s, a rapid and continuous trend has started to characterize modern surgery, which aims at minimizing surgical trauma. Ever since, the advantages of trauma reduction have been proven scientifically in various studies. Shortened hospitalization, accelerated convalescence, less pain and medication, improved cosmetic results as well as reduced impairment of immune system and pulmonary function result not only in physical and psychological benefits for patients, but also in economic benefits for the healthcare system [3].

While laparoscopy, allowing resections and interventions on organs purely via a few small incisions, was only the first step, more elaborated approaches have evolved subsequently. As a common principle all of them aim at reducing the number of access sites to only one, while using artificial transabdominal or natural orifices. In this context and as a motor for further trauma reduction, flexible endoscopy has matured tremendously and has become of central interest. In this regard and to completely avoid external incisions, endoscopy shifted from pure diagnostic applications to the performance of smaller therapeutic interventions. Fundamental prerequisite for the translation of surgical procedures to flexible endoscopic interventions, is the development of potent auxiliary instrumentation to overcome the surgical challenges, resulting from limited access possibilities. Despite significant advances and technical innovations that were introduced to routine practice, most procedures still need to be performed transabdominally and with rigid instruments, either via an open or laparoscopic approach. This inability of endoscopy was intensively discussed during the NOTES era, initiated in 2004, which led to a consensus conference to identify the existing barriers for more advanced endoscopic surgery. Here it was derived that technical solutions for even more complex endoluminal tasks, such as relevant for the formation of anastomoses, would be required to take the next step in endoscopic surgery. [4]

The goal of the research herein presented was to develop and examine fundamental technologies to enable complex manipulation tasks purely endoluminally, with a special focus on the establishment of gastrointestinal anastomoses. Therefore, the colonic environment was biomechanically characterized with respect to procedure relevant parameters [5]. The knowledge gained was translated into the concept and design of an endoscopic device to provide an instrument for the creation of a patient adapted, scalable anastomosis in the colon. As single-use products hold advantages in terms of sterility, licensing and economic implementation, all concepts were designed for the producibility with polymers. Using additive manufacturing opened up new possibilities, providing a broad range of task optimized materials, allowing to fabricate miniaturized, filigree and complex geometries, and enabling highly function integrated monolithic structures.

---

## Background

### 2.1 Anatomy: Basics of the gastrointestinal tract

The gastrointestinal tract represents one major part of the digestive system and extends from the end of the pharynx to the anus [6]. It is divided into the esophagus, stomach, small intestine and large intestine. In its entirety these organs are responsible for the transportation and digestion of food and for the removal of waste products [6, 7]. The patency and integrity of the gastrointestinal tract is therefore of specific importance for the absorption of nutrients [7] and for the energy supply of the organism.

Each segment is specialized to correspond to dedicated requirements, as, for example, for transport (esophagus), for resorption (small intestine) or for the thickening of stool (colon). The stomach (gaster) is followed by the small intestine, which has an average length of about 5 – 6 m. In the large intestine, water is removed from the chyme over a period of 25 to 30 hours before it is stored in the rectum, until it is excreted through the anal canal (canalis analis), which ends in the anus. [7] As the research presented herein was strongly focused on the colon, this anatomical region will be explained more in detail in the following.

**Colon:** The colon is divided into seven segments. The caecum extends to about 7 cm below the ileocolic junction (valva ileocaecalis). The appendix (appendix vermiformis) is attached to this part of the colon. The ascending colon (colon ascendens) ( $\approx 15$  cm) begins above the ileocecal valve and extends to the lower boarder of the liver. The ascending colon is fixed to the retroperitoneum and thus keeps its position more or less stable. Here it may cause an impression to the right lobe of the liver (impression colica) by contact with the so-called flexura colica dextra (or hepatic flexure). This flexure also represents the transition to the next part of the colon, the transverse colon ( $\approx 15 - 25$  cm), which lies within the peritoneal cavity and extends across the abdomen to the left colonic flexure. Both, the right and left flexures are held in position by ligaments. The transverse colon is fixed to and supplied by the mesenteric root. It has a varying length, depending on the individual constitution, which determines the patient specific mobility and flexibility of this section. Via the gastrocolic ligament, it is connected to the large curvature of the stomach. Irrespective of that, the left flexure can differ individually in its exact localization. From the left colonic flexure, the colon transits to the descending colon, which may have a length of about 15 cm and which, just as on the opposite side, is fixed to the retroperitoneum. At the site where the colon loses its retroperitoneal fixation to run free into the peritoneal cavity, it is labeled sigmoid colon. Most often, this point is found at the height of the iliac crest. The length of the sigmoid colon varies significantly and is subject to individual and age-dependent variations, as to its location. It can measure between 30 - 45 cm in length. Due to its unfixed localization, also the sigmoid colon possesses a mesentery. [7] Figure 1 illustrates the segments of the Colon.

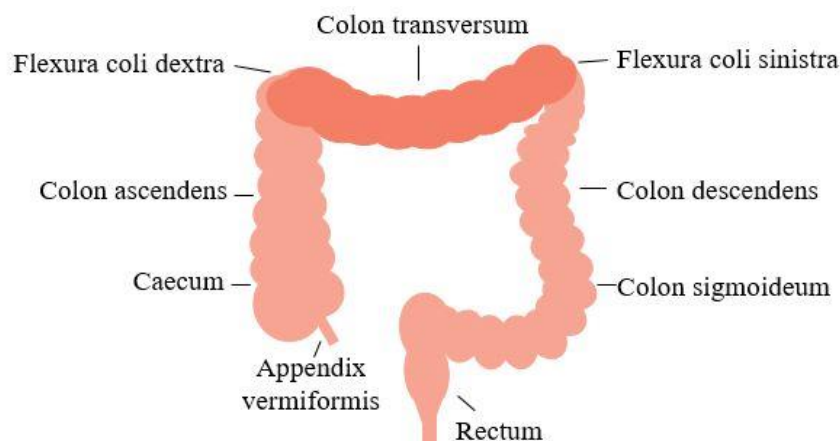


Figure 1 Illustration of the human colon and anatomical segments.

The mesentery, best to be found at the transverse and sigmoid colon, but existing in any part of the colon, is a connective peritoneal duplication, which contains the blood vessels and the lymphatic tissue (nodes and vessels). As mentioned before, it is fused to the posterior abdominal wall along the ascending and descending colon. Thus, these segments are labeled retroperitoneally fixed. Along the transverse and sigmoid colon, the intestine runs intraperitoneally, allowing for nearly free range of motion. This unfixed position eases colonic surgery, but complicates colonoscopy sometimes. [8]

## 2.2 Basics of anastomosis formation in the colon

The term “anastomosis” refers to the reconnection of two hollow organs after the resection of a pathological segment, to restore continuity of the digestive system. Colorectal resections are performed at a high frequency and for different reasons, such as cancer or inflammatory diseases. In 2008, there were approximately 2.1 million new diagnoses of colorectal carcinoma worldwide [9], with a high percentage of them requiring surgery. As for diverticular disease, only in the US, more than 22.000 surgical resections are conducted per year, for instance in 2005 [10]. Considering various other indications, it can be assumed that globally more than 1 million individuals have to undergo colon resection every year.

The procedure of anastomosing two intestinal residual endings after the resection of pathologic tissue is one of the core competences of visceral surgery. In most patients, colonic anastomoses are still performed at least partially open, and techniques vary widely depending on the operating surgeon's preferences and the accessibility of the anastomosis site.

Variations exist in terms of bowel lumen configurations (side-to-side, end-to-side, end-to-end), bowel wall contact (such as inverting, everting, butt-to-butt), and the type of instrumentation used (hand suture, linear or circular stapler, compression implant). A complication-free anastomosis technique and subsequent tissue healing is of essential relevance for the successful convalescence of the patient.

In side-to-side anastomoses, the intestinal stumps are each permanently closed at their ends by means of staple sutures, laterally adjusted and fixed to each other. The new lumen is then

---

artificially cut into the legs, which are subsequently or simultaneously connected to ensure patency.

In the end-to-side configuration, one hollow organ stump is attached to the limb of the second stump. Again, an artificially created incision is cut into the limb side while the other ending's opening is directly attached to it, leaving a portion of the occluded stump protruding from the connection zone. In the end-to-end connection, both intestinal openings are directly connected in axial alignment.

The bowel wall contact describes which layers of the intestinal stumps are connected to each other. While for butt-to-butt anastomoses the entire wall cross-section is brought into contact, everting anastomoses imply the outward reversion of bowel margins, so that only the mucosal layers are attached to each other. Finally, the inverting attachment brings the outermost layers, the serosa, into contact by folding bowel margins towards the lumen center.

### 2.3 Influence of bowel wall layers on anastomotic healing

The bowel wall anatomy and physiology significantly influences the colonic healing behavior in regions of rejoined intestinal margins [11], which has to be taken into consideration when choosing an anastomosis configuration.

In general, the hollow organs of the gastrointestinal tract represent muscle tubes, which all have a similar wall layering in common. Variations result from the segment's individual function within the digestive process. From the inside to the outside, the intestinal wall consists of the mucosal layer, followed by the submucosal layer, the main muscular layer (in general two overlaying layers) and the serosa [7].

The mucosal layer consists of epithelium, lamina propria (loose connective tissue containing collagen, elastic fibers, capillaries, nerves and immune cells, such as macrophages) and the muscularis mucosa (a thin layer of smooth muscle cells) [7]. Healing of the mucosal layer in the anastomosis happens via migration and hyperplasia of the epithelial cells, which seals the defect against the digestive products inside the lumen. Completion of sealing can be achieved within 3 days, if the bowel wall layers are directly brought in contact, while mucosal eversion and inversion delay the process. [11]

The adjacent submucosal layer is a shifting layer, which consists of loose connective tissue, a dense network of blood and lymph vessels, nerve fiber bundles, ganglion cells, glands and lymph follicles [7]. It contains the majority of collagen and determines the tensile strength of the intestinal lumen. In the context of anastomosis formation, it is largely responsible for anchoring the sutures in the intestinal lumen to be rejoined. [11]

The muscularis propria consists of smooth muscle cells, which are intermixed with a network of collagen. It comprises two different muscle layers, the inner circularly oriented muscle layer (stratum circulare) and an outer, longitudinally oriented muscle layer (stratum longitudinale). The connective tissue between the muscle layers contains a nerve network and ganglion cells.

---

Both muscle tubes collaborate for peristalsis, which is the typical movement of the intestinal wall and which causes the transport of the intestinal content. Peristalsis requires a well-balanced contraction of the two muscle layers, which is controlled by the enteric nervous system. [7]

For segments that lie within the abdominal cavity, the muscle tube is covered by the serosal layer, consisting of the visceral peritoneum, which is a single-layered flat epithelium (mesothelium). [7] Good serosal apposition in an anastomosis enables gas and fluid tight closure within the first few hours after formation by fibrin exsudation, to minimize the risk of leakage [11, 12]. Segments that run outside the abdominal cavity are covered by the so-called adventitia, which is a loose layer of connective tissue that connects the organs with surrounding structures of the organism. [7]

## 2.4 Overview of anastomosing techniques: Identification of a feasible approach towards an endoscopic anastomosis device

In general, three different techniques to reconnect the bowel lumen and restore continuity can be differentiated, namely hand suturing, stapling or compression implants.

**Hand-suture** represents the classical anastomosis method and is primarily used in open surgery. Absorbable or non-absorbable suture materials can be used to sew bowel endings together [13–16]. Generally, the design of the hand seam is determined by the number of rows, the layering, the suturing technique and the adaptation technique [16, 17].

However, most surgeons apply running sutures, while interrupted sutures are reserved for complex situations and in narrow regions, such as the lower pelvis or the esophagus. Hand-suture anastomoses require a certain level of experience and represent one of the main skills young surgeons have to acquire during their training. Nevertheless, anastomotic leak is still one of the main complications after resective surgery and accounts for almost 10% of revisions. For this reason, alternative techniques which are less dependent on the surgeons' expertise were attracting the innovative spirit of both physicians and engineers.

With the beginning of laparoscopy in the 1990s, alternative principles for anastomoses were no longer only nice-to-have, but would become decisive, since the reduction of the access trauma and the impaired exposure of the surgical site made hand-sewn anastomosis almost impossible. This alternative to hand-sewn anastomosis had to reduce the complexity of intra-abdominal manipulation and the demands on dexterity.

Accordingly, assistive instruments, so-called **stapling devices**, were developed and manufactured, which also allowed for a higher standardization of surgical outcomes. Since then, stapling systems became increasingly important and quickly developed into the most commonly used anastomosis technique [12, 16, 18].

Releasing the applicator, U-shaped titanium clamps that are pierced into the readjusted intestinal stumps, are cold formed into a B-shape, permanently compressing the tissue in

---

between [12]. Depending on the number and arrangement of the staple seams, 2- and 3-row linear, transverse and circular staplers, available for both open surgery and laparoscopic procedures, can be distinguished. [16] Furthermore, pure stapling devices can be confined from stapler-knife combinations in so-called GIAs (Gastrointestinal Anastomosis) [12]. Using linear, multi-row staplers with a knife, the intestine can be cut while simultaneously closing the lumina linearly at multiple points. In this way, two separated but firmly closed intestinal segments are obtained. [12]

Circular staplers consist of a main body with a staple cartridge and a removable counter-pressure plate. Two tissue parts can be connected in the form of an inverting or everting anastomosis [12], while simultaneously punching a lumen inside the circular staple suture with an integrated annular knife, to ensure patency. Adaptation to different intestinal lumen diameters is enabled by a selection of systems in different diameters (21 - 34 mm) [12] or lengths (e.g. 30 – 90 mm). Staplers in general feature a rigid body and vary according to their diameter and length to be used in open or laparoscopic surgery.

**Compression implants** complete the techniques for anastomosis formation. One implant half is inserted into each of the intestinal lumina. This is done either by multi-port laparoscopy, endoluminally or using hybrid techniques combining both approaches. Upon fusion of the implant halves, the tissue in between is subjected to permanent compression. Depending on the implant design, a compression gradient is induced. The innermost tissue circle becomes necrotic, while in the direct vicinity tissue healing is stimulated and promoted. As a result, the necrotic region is excreted together with the implant via natural digestion after one to two weeks (depending on the system), while in the healing zone the intestinal layers grow together and build a permanent connection. The size and shape of the implants determine the immediate postoperative patency through a central opening. [19–21]

## State of the art

### 3.1 Comparison of techniques and identification of shortcomings

Besides postoperative patient safety, which is assessed primarily by the risk of leakage and secondly by the rate of obstruction, reoperation, mortality and wound healing complications, other aspects, such as technique standardization, associated intraoperative trauma, device complexity and usability are important aspects to be considered when rating anastomosis procedures [22–26]. This comparison supports delimitation of possible development approaches and technologies, which have to be feasible for the integration into an endoscopic system.

A review and meta-analysis was performed in terms of the research project, to compare the techniques with respect to the associated trauma and their potential for further trauma minimization. [27] The review was based on the methodology of the preferred reporting items for systematic reviews and meta-analyses (PRISMA) guidelines. Controlled and uncontrolled

---

clinical trials from their inception up to and including December 2021 were extracted from three electronic databases, MEDLINE, Scopus and Cochrane Library. Only data rendered in German and English language was considered. The following keywords were used in association with the Boolean operators AND and OR to perform the search: ‘colorectal surgery’, ‘comparative studies’, ‘surgical staplers’, ‘sutures’, ‘compression anastomosis’, ‘anastomosis ring’. In addition, reference lists and reviews were processed to identify missed studies.

The systematic meta-analysis revealed only a statistically significant superiority of hand-suture over stapling anastomoses with respect to the occurrence of obstructions. For the other assessment criteria there were no statistically significant differences for colorectal anastomoses between any of the groups [27]. Comparable results were found by other research groups, such as Slessor et al., who were unable to identify any differences in the incidence of leakage or mortality in a meta-analysis of 10 randomized controlled trials comparing compression versus conventional (hand-suture or stapler) colorectal anastomoses [28].

Thus, criteria such as the potential for procedure and outcome standardization, as well as the techniques’ and devices’ applicability in regions with a lack of manipulation space as a measure for the usability via minimal (amount and size) incisions, become even more important. In other words, and due to the missing superiority of any of these techniques in terms of postoperative outcome, the aspect of how the anastomosis can be established is more critical than that of how it performs. Of note, this is just about what already paved the way for mechanical anastomosis [22].

All techniques still show significant shortcomings. This applies first and foremost to the hand-suture anastomosis. Most problematic here, is its time intensity, the susceptibility to errors and the long training phases for surgeons. Wound healing capabilities in anastomoses significantly depend on the tissue compression, which must not restrict adequate blood supply and sufficient oxygenation. As anastomosis compression is related to the suture tension, the quality of hand suturing is highly dependent on the surgeon’s level of expertise.

However, there is still the question, whether stapling anastomoses are really the better option. Staplers indeed allow for an anastomosis formation, which is less dependent on the surgeons’ individual skills and save operating time. Nevertheless, even if the meta-analysis does not reveal a clear superiority of one or the other technique in general, a correlation between staple lines and the susceptibility to stenosis formation was identified also by others [23, 24, 29]. Polese et al. specifically identified the staple-suture as one of the most critical risk factors for anastomosis stenoses in their study [24]. Additionally, various groups have identified an increased risk of anastomosis leakage associated with an increasing number of stapler releases [30–33] and an increasing stapler device diameter (for circular anastomoses) [30].

---

More relevant and even critical in terms of further reducing the interventional trauma, as for example by using natural orifices for access, become technical aspects of stapled anastomoses, or the high forces required to enable plastic deformation of staple seams [34].

Even though other approaches, such as the use of mechatronic devices, or motorized stapler systems, aim to overcome this problem, demonstrating easier intraoperative handling and reduced malformation of staples in most recent evaluations [35, 36], these systems still have rigid bodies. Therefore, this technology is limited to the transabdominal application apart from anastomoses in the lower sigma or rectum. This accounts also for most of currently available compression anastomosis devices.

Endoluminal stapling or compression anastomosis in higher parts of the colon would require flexible device solutions. Due to the lack of miniaturized, potent mechanisms to either transmit forces along flexible shafts, or apply them directly at the endoscope tip, these approaches are not applicable in higher regions of the colon up to today. Furthermore, the available instruments lack visual components and thus control, which is why the advancement through the colon requires a skilled operator and is only possible if a sufficient lumen width is available.

The approximation of anastomosed colon endings demands direct accessibility and complex manipulation from the outside for the available devices. Both, the counter pressure plate for stapler anastomoses and the compression segments for compression anastomoses, must be tied into the intestinal segments, which usually requires an additional cut in the abdomen increasing the trauma.

However, it seems that the principle of a two-part implant holds the potential for a highly standardized and intuitive lumen reconnection, by reducing the complexity of intraabdominal manipulation (compared to hand suture) and using force-efficient implant designs and closure mechanisms (compared to cold metal forming during stapling). This could bring about a significant step towards enabling endoscopic anastomosis formation via natural access routes. With respect to stenosis occurrence, the expulsion of the compression implants deserves particular notion, leading to a foreign body free healing process and less scarring.

Even though the number of patients with compression implant anastomoses included in available studies is low and thus the evidence of compared postoperative outcomes is limited, results published to date are at least promising. [27]

### 3.2 Detailed description of compression anastomosis implants and procedures

Decisive for the design of a manipulator is the way of how force must be induced to close an implant and how compression is applied. Assessing available technology in the field of compression anastomosis implants, systems can be classified into form-fit, shape-memory and magnet based devices. With respect to the overarching goal of developing an end effector unit

---

for the endoscopic creation of scalable anastomoses, a focus is set on this kind of application and respective procedures.

### 3.2.1 Form-fit based compression anastomosis devices

Form-fit based systems rely on plug-in mechanisms to connect the two compression implant halves, which are inserted into the intestinal endings after resection. The **AKA-2** (Seidel Medipool, Friedrichsthal, Germany) [37, 38] is an early example, not being clinically available any more. The implant was applied in open or laparoscopic intervention, piercing through the tissue to prevent it from slipping out of the compression zone, forming an inverting end-to-end anastomosis. A circular blade cut a lumen within the implant rings for immediate intestinal patency and stool passage [37]. The **Valtrac™ BAR** (invented by Sherwood-Davis & Geck, St. Louis, MO, USA) is a biodegradable compression anastomosis system which is currently still available on the market at Medtronic Principal Executive Office, Minimally Invasive Therapy Group, Minneapolis, MN, USA [39, 40]. Introducing one ring into the aboral and the other one into the oral open bowel residual, the implant halves are fixed to the bowel wall via purse-string sutures [39]. The implantation can either be conducted in laparoscopic incisions or transanally with a rigid 20 cm long applicator [41]. The **CARP®** method (Carponovum AB, Halmstad, Sweden) using the compression implant RapAn® enables seamless end-to-end, side-to-side and end-to-side anastomoses, as well as the possibilities for measuring the compression pressure between the connected intestinal endings during the surgical intervention and the examination of the anastomosis integrity in the postoperative course [21, 42]. Depending on the configuration type and anastomosis location, there are different application devices available, all of them requiring free access to the intestinal endings [21, 42].

### 3.2.2 Shape-memory based compression anastomosis devices

Shape-memory based devices exploit the temperature-dependent behavior of the Nitinol alloy, made from nickel and titanium, for pressure application. The metal is formed at high temperatures into the shape it is supposed to adopt when it is inserted into the body and reaches body temperature. By cooling the system below 0°C the alloy changes into the martensitic phase and becomes supple [43, 44].

The **CAC™** (NiTi Alloys Technologies, Ltd., Netanya, Israel) [45], formerly clinically available, consisted of two elliptical coil windings forming an opening angle of approximately 30° in the initial state at 0 °C. The implant allowed the formation of side-to-side anastomoses [38]. The implant was inserted in open configuration, through the abdomen and laterally into the bowel limbs at the operation situs, with a pincer-shaped device of about 10 cm length [41]. Nudelman et al. demonstrated hand-assisted laparoscopy as application technique for the CAC™ in 2004 [46]. When the body temperature was reached, the alloy changed from the martensitic to the austenitic phase and the implant adopted its predetermined geometry with an opening angle of 0°. By means of the clip applicator, the implant was closed and exposed the

---

tissue to a uniform pressure [41, 43, 44], leading to tissue necrosis after approximately seven days [15].

The **ColonRing™**, also known as CAR™ (novoGI Inc., formerly NiTi Surgical Solutions Ltd., Netanya, Israel), relied on the shape memory alloy Nitinol as well, and, just as the CAC™ is not in clinical use any more. The CAR™ consisted of a polymer ring and a metal ring, the latter containing Nitinol band springs and spikes at equidistant intervals [47]. Due to the limited reach of the rigid applicator, the CAR™ was mainly used for anastomosis after rectal resection (LAR) and was applied in a procedure similar to the formation of an end-to-end anastomosis using a circular stapler or the AKA-2, using an anvil protruding from the oral stump, and a mandrel, punched through the rectal stump. Connecting the mandrel and anvil via a rotation of the turnstile in the handle [44] and closing the implant parts, the bolts penetrated the intermediate tissue and plunged into the polymer ring, fixing the tissue and preventing axial movement with uniform radial and longitudinal compression pressure provided by the Nitinol ring. Simultaneously with the connecting procedure, a circular lumen was achieved by means of an annular blade in order to restore immediate intestinal patency [44, 47].

### **3.2.3 Endoscopic compression anastomosis devices**

Flexible robotics and endoscopic devices have been important drivers in recent research to further reduce trauma in visceral surgery. Flexible endoscopes comprise a long polymer coated shaft, which contains the optical components and image transmission is achieved either by objective lenses, glass fibers or chip on the tip solutions (video endoscope). Bowden wires, which are guided through the endoscope shaft, are controlled by two wheels at the handle, to bend the tip in two axes and navigate the endoscope throughout the curvatures and flexures of the colon. The endoscopes have working channels to insufflate the colon with gas, flush water or insert instruments to perform therapeutic interventions, such as biopsies. [48] Both, length and diameter of flexible endoscopes may vary with respect to the field of application (colon/stomach) [49]. They can have a length between 800-1600 mm and a diameter in the range of 5.9 - 14.8 mm [48–50].

Magnet-based implants, which are the last category of compression implant systems, are the only devices available that already allow endoscopic application.

Two magnet-based compression implants are currently in a pre-clinical market phase. In recent years, numerous magnetic implants for different applications and indications in the entire gastrointestinal tract have been tested in animal and human studies. Magnetic systems are particularly suitable for endoscopic applications due to their mutual attraction of magnetic components allowing for force-saving connection of intestinal endings and to close the implant. In the following, only systems with a certain degree of product-maturity are described, which have been proven to be feasible for the generation of intestinal anastomoses in humans.

---

The self-aligning, ring-shaped **Magnamosis™** implant (Magnamosis, Inc., San Francisco, CA) comprises two neodymium-iron-boron magnet rings, available in two different magnetic strengths, N35 and N50, which are encased by a medical grade polymer e.g. polycarbonate [19, 51–54]. The implant can be inserted by open, laparoscopic or endoscopic surgery via natural orifices [52, 54, 55], primarily intended to create side-to-side anastomoses. The first-in-human pilot study took place in 2017 [19]. The endoscopic application technique for Magnamosis™ is called “rendez-vous technique”, and was conducted in an experimental animal trial in pigs. Two flexible endoscopes are used, one of which is introduced transorally, and the other one transanally. The Magnamosis™ implant halves are held with a snare during transportation, and joined at the anastomosis site due to their mutual attraction force. In the last step, the endoscopes are withdrawn. [56]

**IMAS** (Incisionless Magnetic Anastomosis System, GI Windows, West Bridgewater, MA, USA) is the second magnetic compression anastomosis implant, which was designed for transoral, endoscopic delivery. Machytka et al. performed the pilot clinical evaluation of IMAS in 2017 [20]. Similar to its predecessor SAMSEN (Smart Self-assembling Magnets for Endoscopic Surgery), the implant consists of neodymium-iron-boron magnets, which are encapsulated by a biocompatible shape memory Nitinol exoskeleton. This enables the implant to fold to a predefined configuration at the anastomosis site (IMAS: octagonal [20] and SAMSEN: square shape [57]). For transportation, the magnetic elements are positioned within the working channel of an endoscope, configured as a linear chain, and are delivered to the anastomosis site under fluoroscopic and endoscopic visualization. By means of a specific overtube system, and via two tiny incisions, one in the stomach and the other in the small bowel, the magnets are deployed into the corresponding intestinal lumina. For this, the linearly arranged magnets are pushed out of the channel into the small intestine and self-organize into the predefined configuration upon release. The procedure is repeated for the stomach. The two resulting octagons align to each other to form the anastomosis, compressing tissue in between them [57].

### 3.3 Shortcomings of existing endoscopic anastomosis techniques

Magnamosis™ and IMAS were the first to combine the compression anastomosis approach and technology of flexible endoscopy, to evolve a novel, micro-invasive alternative to conventional procedures. Creating side-to-side anastomoses, they allow for the apposition of the serosal wall layers, which is favorable with respect to the avoidance of anastomotic leakage (*2.3 Influence of bowel wall layers on anastomotic healing*). [11]

However, there are still major concerns and drawbacks for both techniques, which need to be solved. Bilateral access to the anastomosis sites, purely via natural orifices, is complicated and time consuming in humans. The small intestine has a length of 5 - 6 m, which is why it cannot be passed easily with flexible standard endoscopes. Tools such as double balloon or spiral overtubes are needed, requiring high levels of dexterity and experience of the physician.

---

Due to the one-sided access, IMAS offers a solution to this problem. However, side-to-side anastomoses require the permanent closure of intestinal stumps that remain after bowel resection. Closure can either be achieved by suturing or by stapling. While hand suturing is time consuming, leading to prolonged anesthesia times, using staple sutures is expensive and both techniques induce inflammation and scarring due to foreign material reactions [15]. Furthermore, closure of the intestinal stump requires an additional surgical step, which again increases the trauma. In other words, it makes things more complicated than they need to be.

End-to-end adaptation, in contrast, is the most natural configuration type with respect to restoring intestinal function and motility. No additional staple suture material is required to permanently close the remaining endings. However, an end-to-end approximation is usually only considered appropriate if both lumina are approximately comparable in size, and have a sufficiently large diameter to prevent stenosis [16]. In case of large lumen diameter discrepancy, special challenges may arise with respect to endoluminal manipulation, as excess tissue complicates the handling and neat approximation of bowel lumina, increasing the risk of protrusions and leakage. The diameter significantly varies for different segments of the colon (sigmoideum, descendens, transversum, ascendens) [7] and also individually from one patient to the other (depending on factors such as sex, age, pathology) [58]. In very narrow lumina, insertion of anastomosis devices can become even impossible. Thus, size adaptability of the anastomosis system would be desirable, to address both, the requirements during secure instrument navigation throughout the colon [59] and restoring lumen width of appropriate diameter at the anastomosis site [16].

Based on this knowledge, design guidelines and the relevant procedure steps to create an ideal anastomosis were derived. The lack of suitable mechanisms to realize basic, key tasks of endoluminal manipulation was addressed by the development and assessment of respective principles and prototypes. The most promising solutions were then integrated into the scalable, endoscopic manipulator, enabling patient-adaptable, inverting end-to-end anastomosis.

### 3.4 The ideal anastomosis procedure

The overall concept is based on a compression anastomosis implant approach, due to the advantages derived in chapter 3.1 *Comparison of techniques and identification of shortcomings*. The manipulator is required to carry and deliver the implant that supports the restored lumen continuity throughout the healing phase. To endoluminally create an end-to-end anastomosis, starting from two open bowel endings after resection of a colon section, an instrument must be transanally introduced and axially positioned within the oral and aboral lumina, that allows to reliably grab, drag and approximate the two colonic endings. Thus, the device must comprise two applicator entities, which can move relatively to each other, and allow visualization of the navigation path and operation site. To achieve a leakage-proof end-to-end anastomosis, the bowel margins have to be inverted and uniformly folded into the implant compression zone [11].

As large variations in patient constitutions, between individuals as well as between colonic segments may occur with respect to the lumen diameter, an adaptation to different anatomies is desirable to prevent obstructions. Thus, a scaling feature is integrated that enables expansion of the anastomosis implant, supported by the platform. The applicator must allow axially and radially congruent configuration of the implant halves, which means that the implant diameters must be of same size, and mating implant elements must be maintained aligned throughout the closure process. By using an implant with a closure mechanism, that pierces through the bowel wall and form-fittingly protrudes into an opposing arranged implant half, tissue can be prevented from slipping out of the compression zone and the compression gap can be adapted to the tissue thickness to adjust the healing pressure. Respective piercing and coupling forces must be applied by the applicator. In the last step, the implant must be deployed from the applicator, which is collapsed and retracted from the surgical site. Figure 2 shows all relevant procedure steps and indicates corresponding research questions (RQ), which arise from the challenges of endoluminal manipulation.

Of note, the scope of this research project comprised only the manipulator and not the implant, which was to finalize by a research partner. Explicitly, the implant development was conducted in cooperation with the Institute for Medical Materials and Implants and is part of another thesis. However, in the beginning of the project, it was defined that the implant will comprise four rigid and four expanding segments. These central elements were used as precondition for any further applicator design specification, dimensioning and feature integration.

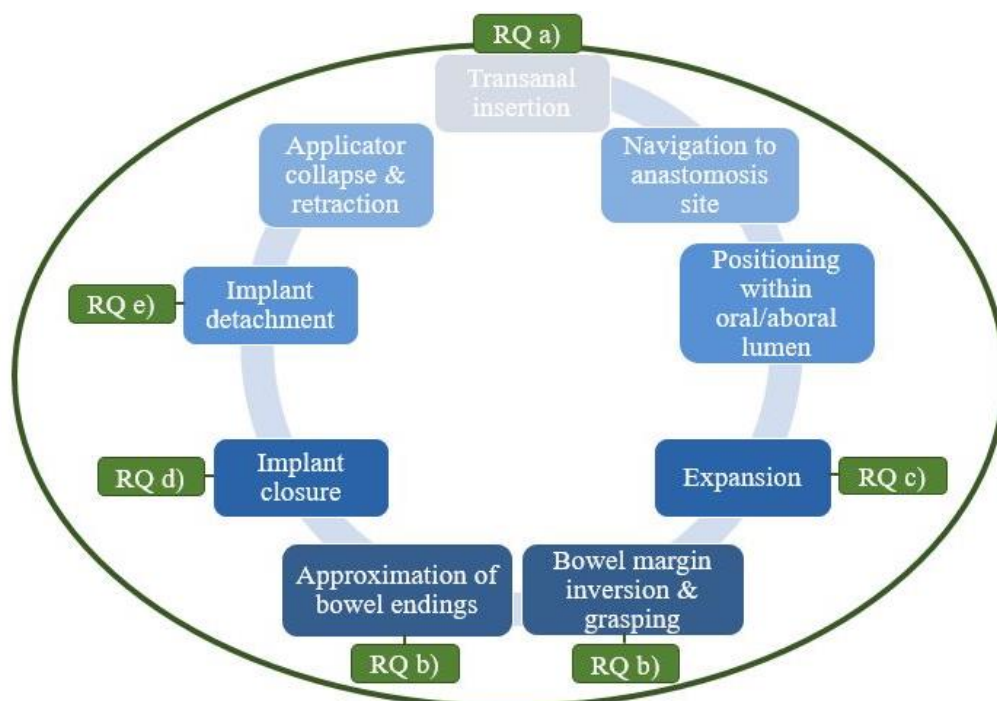


Figure 2 Process diagram of the endoscopic anastomosis procedure with assigned research questions (RQ). Research question a), addresses the (biomechanical) characterization of the anatomical environment (colon), to determine procedure relevant design guidelines. Research question b) focusses on the development of mechanisms to endoluminally grab, manipulate and adjust colon edges in an inverted manner. Research question c) addresses the development of

---

expansion mechanisms to support congruent implant and applicator scaling of oral and aboral units. Research question d) focusses on the development of force application mechanisms to pierce tissue and close an implant while maintaining axial congruence. Research question e) addresses the development of a power-efficient, endoluminal implant detachment mechanism.

In order to enable the formation of the ideal anastomosis, the following technical key issues (research questions) were defined and addressed within the scope of this work.

- a) During endoscopic manipulation, instruments mechanically interact with colon tissue. The occurring forces must be known in order to design and dimension novel devices appropriately. Thus, the biological environment must be characterized with respect to procedure relevant parameters. Questions in focus are: *How powerful the manipulator needs to be, to pierce through two bowel wall layers, which design parameters influence the piercing process and which system dimensions have to be addressed?*
- b) Inverting the intestinal wall to achieve serosa-to-serosa contact has been proven to reduce the risk of leakage [11]. Furthermore, end-to-end anastomosis appears to be the favorable configuration type, as it saves time and material. *So, a solution is needed, to endoluminally grab and manipulate bowel tissue. The principle must allow relative movement between oral and aboral applicator heads to adjust colon edges in an inverted manner.*
- c) The most commonly used technique (stapling) shows increased susceptibility to stenosis formation [23, 24, 29]. By adapting the implant size to the native bowel diameter, the entire lumen can be used for the anastomosis to ensure permanent and unhindered stool passage. *Thus, the applicator must integrate an expanding mechanism, that supports implant scaling by applying radial forces. As the principles of force transmission along the flexible platform shaft in conventional endoscopy are inefficient [59] and may lead to deflections [4, 59–61], mechanisms are examined to enhance abilities of force application at the endoscope tip, where the endoluminal manipulation task needs to be performed. The expansion unit must further allow for congruent scaling of both applicator units, as well as for a complete and controlled collapse after implant delivery. Parallel orientation of the implant compression faces and equivalent distance between implant halves mounted on the applicator arms must be maintained, to distinctively control implant closure in all size configurations.*
- d) An implant supports the reconnection at the anastomosis site during the healing phase. *This implant has to be closed by the applicator, while simultaneously piercing through the tissue. The device must ensure axial congruence of the implant halves throughout the process.*
- e) The implant has to be carried by the applicator during endoscopic navigation. After the implant has been delivered, the applicator must be retracted from the bowel. Therefore, the implant has to be detached from the applicator at the anastomosis zone. *A power-efficient solution is needed, to depose the implant from the manipulator.*

---

With respect to current efforts in flexible endoscopy to provide single-use solutions in order to reliably prevent cross-contamination between patients [62], all prototypes developed within the scope of this work were designed to be producible from polymers, to allow future integration into single-use medical products. Using additive manufacturing allowed to choose from a broad range of task optimized materials, to fabricate complex, miniaturized geometries and to design highly function integrated, monolithic components.

## Material and Methods

### 4.1 Anatomical and mechanical characterization of colon tissue

During abdominal organ manipulation, high forces occur [63]. In endoscopic interventions, applying forces at, or transmitting them to the endoscope tip is challenging, as the flexible shaft is prone to buckling under load [60, 61], and despite the complex colon anatomy and curvatures, force application behavior - efficiency, as well as instrument responsiveness and accuracy - must be consistent and predictable for arbitrary shaft lengths and shapes. Mechanically complex surgical tasks, such as the reconnection of two hollow organs including piercing through tissue layers, therefore present special technological challenges for the development of instruments. Thus, biological and mechanical properties of the colon were assessed, to clarify basic design requirements and dimensioning guidelines for the novel system and force transmission unit.

According to literature, piercing forces are influenced by the type of fixation [64–66], the surface tension of the tissue, the tip geometry [67] and number [68], as well as the trajectory velocity and acceleration [69, 70] of the tissue piercing bodies. In the study presented, piercing force data was collected for different design specifications of future system components (anastomosis manipulator and implant). Thus, the spike amount and configuration of piercing bodies were chosen and altered with respect to the future implant. Furthermore, the influence of closure trajectory variations in velocities and accelerations, and of alterations in tissue fixation point locations were assessed. [5] In addition, colonic lumen diameters and tissue wall thickness were measured. [5]

#### 4.1.1 Setup design

The experimental setup to determine the piercing forces, illustrated in Figure 3, comprised a Sauter FH 100 calibrated force gauge (Kern & Sohn GmbH, Sauter, Balingen, Germany), which was fixed onto a slide, translationally (1 DOF) movable along a guide rail. The movement was actuated by a wedge toothed belt, tensioned onto two gears, of which one was driven by a stepper motor (StepSyn Type 103H7126-0740, Sanyo Denki Co., LTD., Japan). Two identical tissue fixation entities (applicator dummies) were mounted on the centering rail, facing each other in 4 mm distance. A disc with spikes, arranged symmetrically in segments (implant dummy), was attached to the force gauge. Motor speed and acceleration were controlled by an Arduino CPU (Arduino Uno) with a motorshield (Arduino Motor shield Rev3)

in terms of  $\frac{\text{steps}}{\text{min}}$ . To ensure sufficient power supply, an external power source was connected and powered with 5 V. [5]

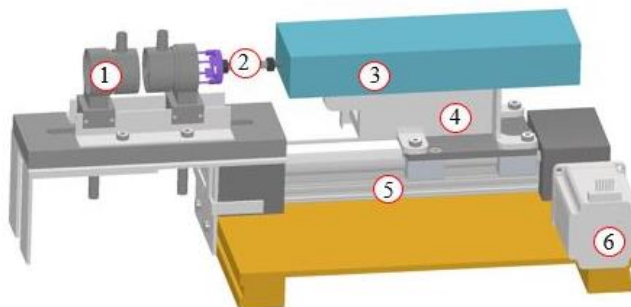


Figure 3 Experimental setup to measure forces required to pierce colonic tissue. A force measurement gauge (3) was mounted on an axially moving sleigh (4), that glides within a square ITEM profile (25 x 25 mm) (5). The movement was actuated by a wedge toothed belt, tensioned onto two gears, of which one was driven by a stepper motor (6). Two opposing assembled specimen holders (1) were mounted on a centering rail. A disc with spikes (2) was attached to the force gauge. (Figure adapted from Steger et al. [5])

**Design variations and parameters:** In the following, all tissue fixing and piercing entities, including their variations in design are described. Furthermore, the assessed piercing body velocities and accelerations are specified. These were investigated to find out whether and to what extent the way of axially approximating two implant halves has an influence on the required closing forces and device stability. Findings were transferred to the design and selection of possible force transmission mechanisms (e.g. abrupt/smooth closing process).

The fixing entities were designed with respect to the central task of grabbing and manipulating bowel tissue endoluminally. Using suction to atraumatically fix tissue to an endoscopic device showed promising results in prior research projects [71]. Thus, the approach was transferred to the endoscopic anastomosis device and different fixation point arrangements were investigated to determine the effect of tissue tensioning on piercing forces.

The design of piercing bodies and locations of spikes were chosen with respect to the future implant design, comprising four *closing segments* with spikes, as well as four *expanding segments* without. The goal was to determine whether the amount of spikes has an influence on the required piercing forces. For the anastomosis implant, the sweet-spot between a sufficient tissue fixation and implant retention force, and minimized piercing force must be achieved.

Figure 4 provides an overview over all parameter sets assessed within the study. For each parameter set, experiments with n=5 samples were performed. [5]

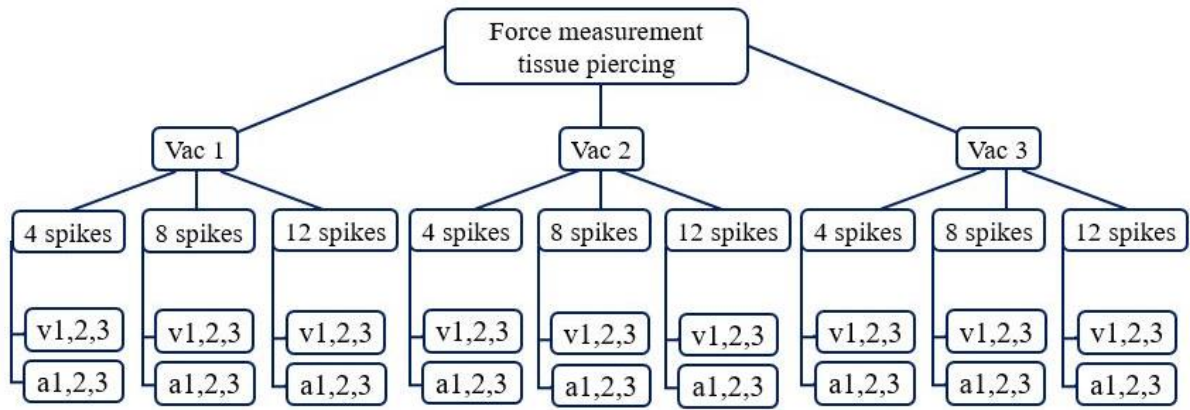


Figure 4 Overview of 54 tested parameter sets, which were tested with a sample size each of  $n=5$  ( $n_{total}=270$ ). A total of three tissue mounting entities with different fixation point configurations (Vac 1, Vac 2, Vac 3), three piercing bodies with different amounts of spikes (4, 8, 12 spikes), and six trajectories with constant velocities ( $5, 10, 15 \frac{mm}{s}$ ) and accelerations ( $5, 10, 15 \frac{mm}{s^2}$ ) were tested. (Figure adapted from Steger et al. [5])

In addition, colonic lumen diameters were measured to determine the required applicator dimensions and the extent of device expandability. Furthermore, the variation in tissue wall thickness was determined to approximate an adaptation range of the implant gap. [5]

## 4.1.2 Investigated design parameters

### 4.1.2.1 Tissue fixation

Each specimen holder featured openings through which the implant tips were passed and suction surfaces to atraumatically fix the tissue [72].

The sample holder was designed mimicking the way of how the implant would be mounted onto the applicator device. This configuration determined the relative position of spikes and fixation points to each other. One holding entity had an outer diameter of 35 mm (chosen in orientation to other colonoscopy devices [73]) with a total suction area for all entities of  $\sim 130 \text{ mm}^2$ , which was chosen with respect to space requirements of a preliminary implant dummy. A fixation force per side of  $F_{fixation} = \Delta p * A = 10.4 \text{ N}$  ( $\Delta p$ : Difference between atmospheric and system pressure; A: surface of suction area) could be achieved, by connecting a suction pump to each of the specimen holders (maximum pressure: - 80 kPa related to atmospheric pressure). Three variations of suction surface configurations (Figure 5) were investigated to assess whether number and arrangement of tissue fixation points effect the penetration process/force to deduce information for the design of the implant holders in the future applicator. Fixation point configuration1 (Vac1I) comprised suction surfaces exclusively in the center of the specimen holder (respectively implant). For fixation point configuration2 (Vac2I) they were split and located on both sides of the frontal spike apertures (respectively the closing segments of the implant) and for configuration3 (Vac2A) they were located towards the lumen center at the frontal face and on the sheath. [5] All fixation entities assessed are illustrated in Figure 5.

---

#### **4.1.2.2 Spikes**

The piercing bodies, with a diameter of 26.5 mm (to fit through the apertures of the holding entities), comprised four equidistant segments arranged symmetrically on a plate. Each segment engaged 36° of the ring body. This resulted in an arc length segment of approx. 8.3 mm. The piercing bodies were dimensioned with respect to the future implant design, of which the closing segments must be minimized to provide sufficient space for the intermittent expanding segments. These must allow for a multiplication of the initial diameter. Every segment comprised one to three spikes, resulting in piercing body configurations of four, eight and twelve tips in total.

For configurations with four spikes, one needle was applied centrally on each segment. For eight spikes, two tips were positioned on one segment with an offset to the center and a distance of 18° in between. For twelve needles, one spike was located in the segment center and two others in 14° distance to both sides. The tip geometry was designed according to Okamura et al., who detected lowest penetration forces for a triangular/tetrahedral tip shape [67]. Accordingly, the resulting needles had a tip angle of 15°, a length of 20 mm and a diameter of 1.7 mm. The needles had to be of sufficient length to compensate for indentation typically occurring in viscoelastic biological tissue. All piercing bodies and specimen holders were 3D-printed using a Formlabs2 (Formlabs GmbH, Berlin, Germany) printer from standard White<sup>1</sup> or Clear resin.<sup>2</sup>[5] All piercing bodies assessed are illustrated in Figure 5.

---

<sup>1</sup> Formlabs; <https://formlabs-media.formlabs.com/datasheets/1801089-TDS-ENUS-0P.pdf>; last accessed May 7, 2022.

<sup>2</sup> Formlabs; [https://formlabs-media.formlabs.com/datasheets/Clear\\_Resin\\_Technical.pdf](https://formlabs-media.formlabs.com/datasheets/Clear_Resin_Technical.pdf); last accessed May 7, 2022.

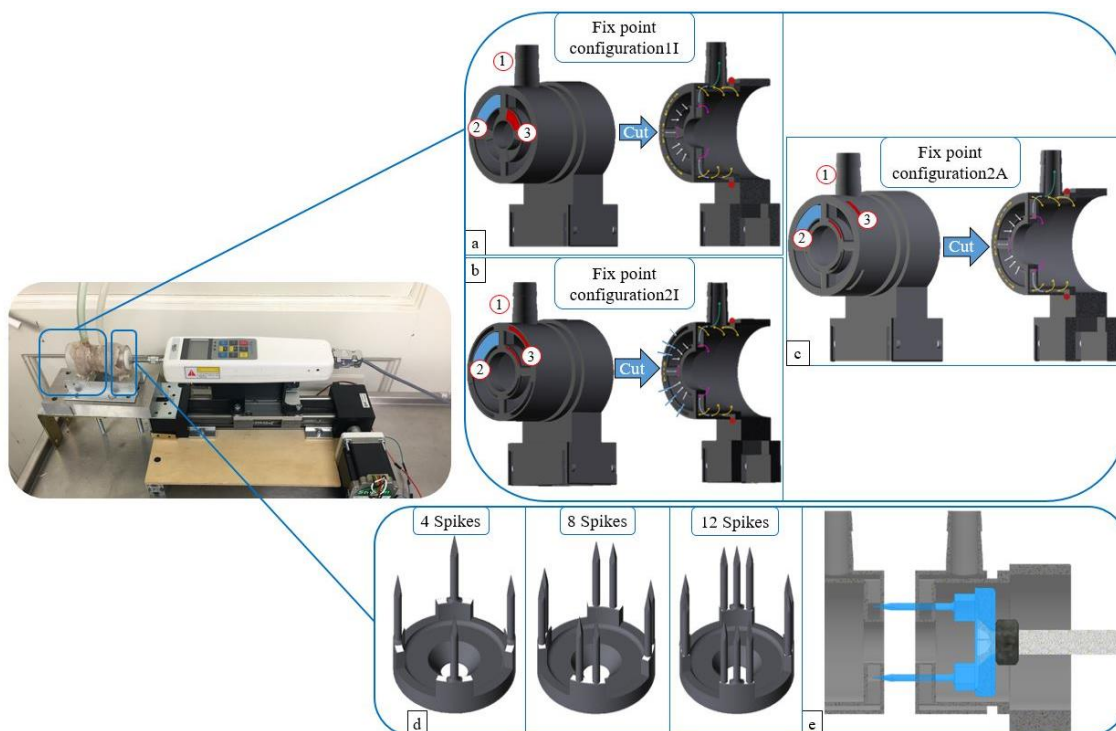


Figure 5 Image of the piercing force measurement setup with detailed specification of specimen holder designs and piercing bodies. Illustrations a) - c) show the fixation point configurations: configuration1I comprised suction surfaces (3) exclusively in the center of the specimen holder, for configuration2I they were located on both sides of the frontal spike apertures (2) and for configuration2A they were located towards the lumen center at the frontal face and on the sheath. To all specimen mounts, the suction pump was connected via the tube nozzle (1). Image d) shows three piercing bodies with 4, 8 and 12 spikes, and e) illustrates a cross sectional view of the piercing bodies protruding through the holding entities. (Figure adapted from Steger et al. [5])

#### 4.1.2.3 Trajectory

The selection of trajectory velocities and accelerations was specified in orientation to related examples from the literature [69], technical feasibility for the integration into the applicator and patient safety. By variation of motor velocity and acceleration, three constant axial velocities of  $v_1 = 5 \text{ mms}^{-1}$ ,  $v_2 = 10 \text{ mms}^{-1}$  and  $v_3 = 15 \text{ mms}^{-1}$  and three constant axial accelerations of  $a_1 = 5 \text{ mms}^{-2}$ ,  $a_2 = 10 \text{ mms}^{-2}$ ,  $a_3 = 15 \text{ mms}^{-2}$  were examined, for which final velocities of  $12.5 \text{ mms}^{-1}$ ,  $17.7 \text{ mms}^{-1}$  and  $21.6 \text{ mms}^{-1}$  were achieved when reaching the piercing plane. The corresponding Arduino script motor velocities were  $4 \text{ rpms}^{-1}$ ,  $8 \text{ rpms}^{-1}$  and  $12 \text{ rpms}^{-1}$ , and the motor accelerations  $10 \text{ rpms}^{-2}$ ,  $100 \text{ rpms}^{-2}$  and  $150 \text{ rpms}^{-2}$ .

#### 4.1.3 Sample preparation

Pig colon samples were obtained day-fresh from the local butcher, cooled and kept moist during the day until use. Fat tissue was removed and the colon was cut perpendicular to the taenia libera into tubular segments of approximately 30 mm length. For each parameter set, five sample pairs were prepared and stored in two kidney shells, covered with bandages soaked with saline (NaCl 0.9) [66] and numbered according to the sequence in the experimental procedure. The remaining specimens prepared were stored in a cooled box. [5]

---

Before the experiment, each specimen was draped flat on a base plate to measure half of the circumference,  $u_{0.5} = \frac{U}{2}$ , in the center of each probe. The respective diameters were calculated by  $D = 2 * \frac{u_{0.5}}{\pi}$ , subsequently. The pierced tissue thickness of each specimen pair was assessed by means of indirect optical measurement. [5]

#### 4.1.4 Experimental preparation

The script specifying the trajectory was uploaded to the Arduino board prior to each parameter set. One of the prepared bowel segments was mounted onto each of the specimen holders, so that the fixation surfaces were inside the sample lumen. The open bowel endings were adjusted along the circumference until all channel apertures were fully covered and a stable suction force could be established. The compression forces occurring during tissue piercing were recorded over time with the FH 100 (Kern & Sohn GmbH, Sauter, Balingen, Germany) calibrated force gauge, using Matlab. After each trial, the specimens were replaced. [5]

#### 4.1.5 Statistical analysis

To investigate the influence of the number of spikes, of different fixation point arrangements and trajectories, the received results were statistically analyzed. Therefore, the Gaussian distribution of each parametric set was checked with the Shapiro-Wilk test based on a significance level of  $\alpha_N = 0.05$ . A parametric three-way ANOVA (A) as well as the non-parametric KRUSKAL-WALLIS (KW) test were used, whereby the  $H_0$  hypotheses were rejected with respect to a significance level of  $\alpha_{A/KW} = 0.01667$  for both tests. [5]

### 4.2 Development and evaluation of solutions to enable basic endoluminal manipulation tasks

The development process of the patient-adaptable, endoscopic single-use anastomosis device followed the VDI 2221 guideline for the “Design of technical products and systems”. Based on the definition of the overall procedure/task of the device and basic requirements, the process was split up into the required key functions with respect to endoluminal manipulation, that have to be fulfilled or executed by the system. Competing *solution principles* to realize the defined functions were developed (shown in "morphological boxes") and their feasibility was comparatively examined with respect to the requirements based on literature and experiments. In the next process phase, all selected modules were refined, integrated into the final product architecture and the results were evaluated with respect to the goals defined at the beginning. This included calculations, simulations and tests.

In order to enable visualization of the navigation path and intervention site in a cost effective way, an over-the-tube design, which can be mounted on conventional flexible endoscopes, was chosen. This allowed to avoid integration of high-priced modules such as fiber optics, imaging units, related electronics, and components for insufflation or aspiration.

Figure 6 shows the morphological box for the research questions addressed concerning endoluminal manipulation (RQs b) – e) from *chapter 3.4 The ideal anastomosis procedure*), with the developed solution concepts.

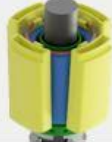
Principles of endoscopic manipulation			
Tissue grasping, inversion and applicator expansion	Bowel lumen expansion without vacuum channel expansion	Bowel lumen expansion by vacuum channel expansion	
			Balloon
Applicator closing unit	Springs 	Hydraulics 	
Implant detachment	Electromagnets 		

Figure 6 The morphological box includes the basic research questions of endoscopic tissue manipulation and shows the solution principles assessed within the scope of this thesis. Prototypes to realize tissue inversion, manipulation, applicator expansion, tissue piercing, implant closure and implant detachment were tested. All approaches were developed and designed for the integration into endoscopic overtube manipulator platforms.

All system components were manufactured by 3D printing using the SLA printer Formlabs (Formlabs GmbH, Berlin, Germany) Form2 or Form3B. The material was chosen with respect to the functional requirements.

The functionality of the prototypes was investigated and comparatively evaluated in interaction with porcine colon tissue, which was obtained day-fresh from the local butcher and prepared in pieces of comparable size (~ 50 mm length, ~ 45 mm diameter). For all samples, adipose tissue was largely removed to provide comparable conditions to mobilized bowel endings during state of the art anastomosis procedure.

#### 4.2.1 Design and test methods: Grasping/ inversion of colonic margins and patient adaptation (*Theses b, c*)

In flexible endoscopy, limited space and lack of direct access pose special challenges for the physician with respect to endoscopic bowel manipulation. Significant variations in lumen diameters between colonic segments and patients make this even more difficult. To support the dissemination of interventions conducted endoscopically and simplify the performance for

---

physicians, it is necessary to find ways how to conveniently and reliably capture and manipulate bowel endoluminally and adapt the platform size to the patient individual lumen diameter. With respect to the task of anastomosing, additional challenges arise such as inverting bowel margins over the implant edges into the compression zone, adapting bowel diameter for congruent apposition and approximating endings in end-to-end configuration.

As it was observed during prototypic testing and in prior research projects, the use of suction forces allowed atraumatic fixation and did show promising results for grabbing and manipulating bowel [71]. It was further observed that the intestinal endings turned inwards, to the lumen center, when the tissue was expanded. By positioning suction surfaces in the center of an implant, arranged around the entire circumference of the endoscope, it was possible to completely cover the compression zone with tissue.

However, the question remained, whether these holding entities need to be expandable together with the implant to approximate them to the colon wall, or whether the inverted intestinal endings reach far enough into the center to cover the channel outlets.

Two types of prototypes were designed and tested:

- a. Expanding the colon to dilate and invert colonic endings to the suction surface, *without adjusting* the suction channels to the bowel wall.
- b. Expanding the colon to dilate and invert colonic endings to the suction surface, *by adjusting* the suction surfaces towards the bowel wall.

The respective approaches are illustrated in Figure 7.

The expansion was driven either by balloon dilatation or by the actuation of a hydraulic unit. The stereolithographic process allowed to produce units with integrated air channels. Clear and White Resin were utilized, which are two of the standard materials of Formlabs (Formlabs GmbH, Berlin, Germany), used for parts free of critical loads. Due to its transparent design, Clear Resin allowed to ensure that suction channels are free of resin for an unhindered flow of air [74]. White resin captured smooth surfaces, being especially suited for low-force applications [75].

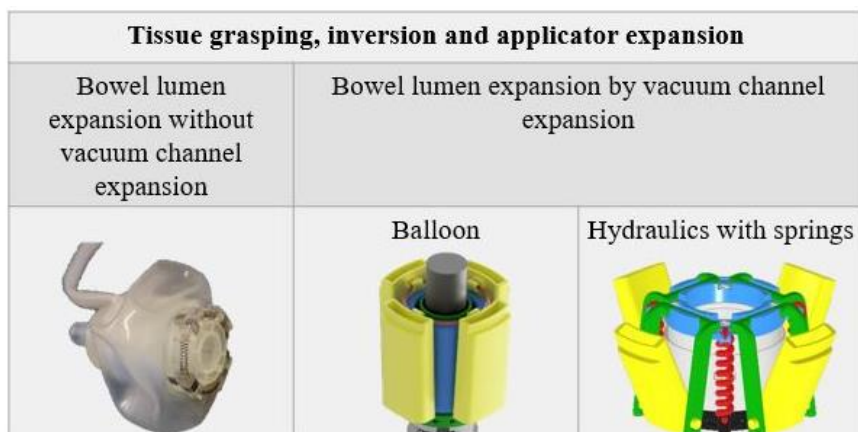


Figure 7 Extract of the morphological box showing approaches to realize tissue grasping and inversion of intestinal edges to uniformly prepare the tissue in the implant compression zone. The expansion was driven either by balloon dilatation or hydraulic actuation.

**Test setup:** The experimental setup consisted of a Poly(methyl methacrylate) (PMMA) tube bisected along the longitudinal axis, which was fixed to a PMMA plate via a threaded rod. The tube was held in a horizontal configuration by a pipe clamp and the prototypes with mounted intestinal samples were inserted. The intestine was positioned to protrude beyond the applicator arm edges by approximately ~1.5 cm. By this means, the orientation and conformation of the intestinal tissue within the abdominal cavity was simulated. This was particularly important in order to investigate whether gravity can be overcome without further auxiliary means, for the gut segments hanging down towards the base plate (resp. within the abdominal cavity towards the dorsal wall).

All concepts were compared with respect to their potential to invert colon margins over the implant edges into the compression zone, enable uniform apposition of the bowel margins along the entire circumference of applicator and implant, and provide sufficient grip to drag and manipulate tissue. The bowel had to be inverted and draped over the implant face without wrinkles or bulges. Comparable tissue portions with respect to the amount and weight of overlapping tissue were ensured by determining the specimen diameter.

Secondary assessment criteria to compare the expansion mechanisms were the feasibility to allow a controlled dilatation, congruent configuration of the oral and aboral components, and a complete collapse. Crucial features were the integration of feedback about the degree of expansion, as well as locking the expansion state.

#### **4.2.1.1 Expansion of colon *without adjusting* the suction channels to the bowel wall**

**Prototype 1** (see Figure 8) was designed to assess, whether the colonic margins can be folded inward, to the lumen center, where the suction channel outlets were positioned. The expansion to achieve the sleeve effect, was realized by balloon dilatation, but could also be achieved by an alternative technique.

The prototype (see Figure 8) comprised a hollow cylinder of 25 mm diameter to account for the tubular geometry restrictions of the overtube design. It further included a circularly running

offset, proximate to the vacuum channel outlets, where the implant dummy was mounted. Four outlets at the front face of the prototype body ran inside the cylinder and merged into a common port on the opposite side, where a suction pump was connected. To allow for uniform expansion, a medical grade balloon (conventionally used for fecal drainage (ConvaTech FlexiSeal Signal, ConvaTech Inc., Greensboro, USA)) was mounted centrally to the prototype. The balloon was expanded using a syringe, inflating a maximum infill volume of 45 ml and resulting in a maximum diameter of ~55 mm.

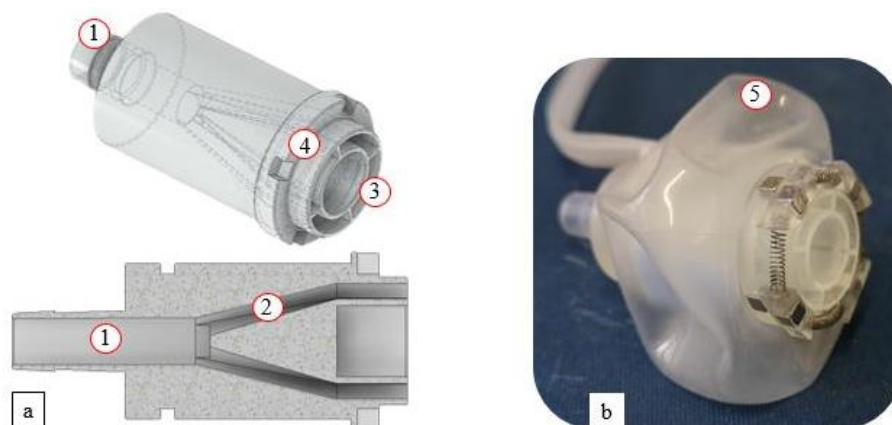


Figure 8 Detailed description of the prototype used to assess the concept of expanding colon to invert bowel margins towards the suction channel outlets in the center, without adjusting the suction channels to the bowel wall. Illustration a) shows the CAD graphics with the central suction port (1) that connects the prototype to the pump. The inflow splits into four channels which form suction surfaces at the front side (3). The front surface contains an offset (4) on which the implant can be mounted. Illustration b) shows the additively manufactured prototype with the balloon (5), which was inflated to invert the colon margins.

#### **4.2.1.2 Expansion of colon by adjusting the suction channels to the bowel wall**

For the second approach, the applicator entity was designed, to expand the lumen by dilating implant mounts with integrated suction channels, towards the bowel wall. It was investigated, whether decreasing the distance between the channel outlets and the tissue, would simplify inversion of the bowel margins and allow to uniformly cover the suction surfaces. Expansion units based on different actuation principles were designed and examined with respect to implant scaling capabilities. All components were developed to position the force application feature directly at the endoscope tip.

#### **Design of a platform expansion unit to support implant scaling (Thesis c):**

Two different mechanisms to realize a controlled expansion of the applicator platform were developed (see Figure 9).

The application of forces is one of the biggest challenges for the development of endoscopic platforms [59, 61, 76–78], as the endoscope shaft is too flexible to effectively establish abutment [61].

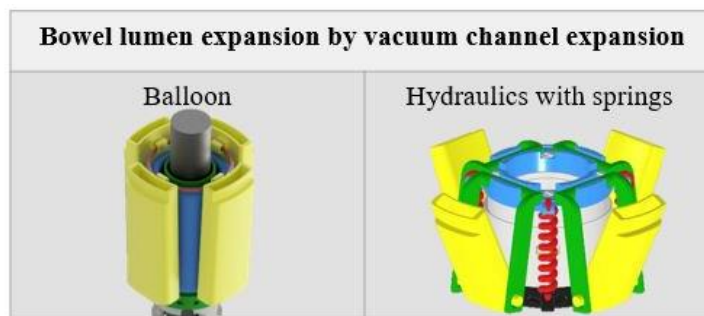


Figure 9 Extract of morphological box, showing approaches of different applicator expansion mechanisms tested and compared.

### Applicator expansion based on balloon dilatation:

**Prototype 1:** The first expansion mechanism was based on an inverse umbrella approach, allowing to unfold four hollow applicator arms (see Figure 10). These were suspended from a ring via hinge joints. A balloon (Enteroscope Balloon BS-4 from Fujifilm (FUJIFILM Holdings Corporation, Tokyo, Japan)) was positioned in the center of the applicator arms, pushing them radially outwards during expansion. To retract the dilatation, a rebounding element (rubber band/springs) was integrated into eyelets at the upper edges of the applicator arms, connecting and contracting the arms. Due to the lack of standard balloon systems in smaller dimensions (required: 25 x 25 mm), the prototype was adapted to the available balloon size (35 x 35 mm instead of 25 x 25 mm), for a preliminary proof of concept. In maximally expanded configuration, the prototype had an outer diameter of ~50 mm (circumference along the implant mounts).

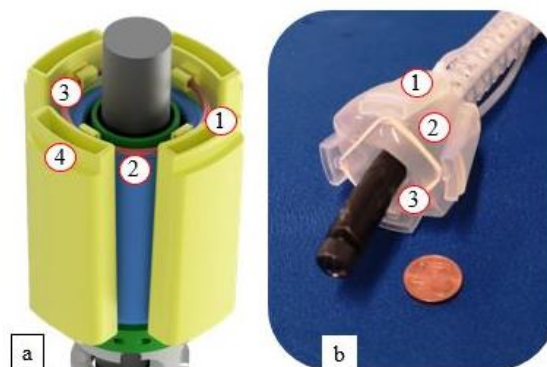


Figure 10 Detailed description of the prototype used to assess the concept of expanding the applicator blades with integrated suction surfaces (1) by a balloon (2) to the colon wall. The blades contained a recess (4) to mount the implant. Applicator collapse was achieved by an integrated elastic retraction band (3). Illustration a) shows the CAD graphics and b) the assembled prototype.

### Applicator expansion based on hydraulics:

**Prototype 2** (see Figure 11): The second prototype comprised a single-acting telescopic hydraulics [79], for which the axial piston displacement was converted into a radial expansion via articulated lever arms.

One mounting ring each was fixed to the bottom of the hollow cylinder and to the cover of the piston. The applicator arms were attached to the lower mounting ring and the lever arms were suspended from the piston. The applicator arms were configured to realize a maximum expansion for non-actuated piston (hub = 0 mm (i.e. negative relative internal pressure)), whereas the arms were attached to the cylinder wall when the pressure was maximized (hub = max. expansion).

The ring-shaped telescopic hydraulics had a total diameter of ~30 mm (including applicator arms) in the minimized state and a diameter of ~49 mm in the maximized configuration. To seal the piston against the cylinder wall, O-rings with a diameter of 12.5 mm and a rope thickness of 1.5 mm were used on the inside and O-rings with a diameter of 18.5 mm and a rope thickness of 1.5 mm were used on the outside. Liqui Moly Silicone Fat (LIQUI MOLY GmbH, Ulm-Lehr, Deutschland) was used to improve the gliding properties of the 3D printed hydraulic partners.

Four tension springs were mounted between the piston and base plate of the hydraulic cylinder. The springs were maximally elongated for the maximum hub, thus when the applicator diameter was minimal. The springs' contraction forces supported the expansion process.

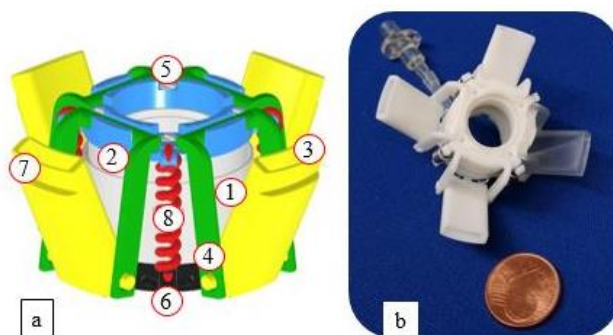


Figure 11 Detailed description of the prototype used to assess the concept of expanding the applicator blades with integrated suction surfaces by hydraulic actuation to the colon wall. Illustration a) shows the CAD graphics of the hydraulic expansion unit, comprising a cylinder (1) and a piston (2). Applicator blades with suction surfaces (3) and a recess (7) to mount the implant were assembled by lever arms (4) in two mounting rings, one at the bottom of the cylinder (6) and one at the top of the piston (5). Springs (8) were integrated to support a smooth expansion process. Illustration b) shows the assembled prototype.

To ensure smooth operation of the hydraulic units without air related disturbance [80], bleeding valves were integrated into all hydraulic units. A M2 thread was cut into the socket of a core hole in the cylinder and sealing was achieved by means of an O-ring (1.5 x 1 mm, NBR, 70A) (Landefeld Druckluft & Hydraulik GmbH, Kassel, Germany), which was pressed against the flange by screwing in a flat head screw (M2 x 5 mm, stainless steel). Feasibility of the vent valves was assessed by applying a pressure of 3 bar and testing the cylinders for water tightness.

## 4.2.2 Design and test methods: Applicator integrated implant closing unit (Thesis d)

In anastomosis procedures, the implant supports the restored intestinal continuity during the healing phase, it ensures leakage free connection and establishes uniform tissue compression. An implant, which is closed by locking one half into the other, simultaneously piercing through the tissue located in the compression zone, allows to reliably fix the bowel between the implant halves and to adapt the compression gap to the tissue thickness. Therefore, two actuation principles were assessed.

- Actuation via springs (prototype 1)
- Actuation via hydraulics (prototype 2)

The endoscopic closing unit (see Figure 12) must further ensure axial congruence of mating implant parts throughout the closing process. To axially align the implant coupling elements and realize an abutment for the closing forces, a snap mechanism, connecting oral and aboral applicator units, was developed.

An estimation of the required piercing forces, and an evaluation of parameters mechanically influencing the process, was performed in chapter 4.1 *Anatomical and mechanical characterization of colon tissue*.

The force transmission units including the connector were manufactured from White Standard Resin with the Form2, due to its smooth surfaces properties and to enhance gliding properties of the relatively moving parts [75].



Figure 12 Extract of morphological box, showing approaches tested and compared for the applicator closing unit, including tissue piercing with the compression anastomosis implant. Prototypes with a spring-based and a hydraulic-based mechanism were investigated and compared.

**Test setup:** Both mechanisms were evaluated with respect to their capabilities to pierce through two layers of tissue. To axially align the implant coupling elements and realize an abutment for the implant closing forces, one implant dummy half was mounted on each side of the applicator unit, one on the male and one on the female unit of a snap-fit connector.

The aboral implant comprised 12 color-marked tips, arranged in four groups of three directly adjacent peaks. The oral implant half was a ring with holes to receive these spikes. A colon sample was pulled over each applicator unit, the snap-fit was connected and the implant halves were closed.

Assessment criteria for the closing mechanism were:

1. The ability to keep the implant halves aligned in axial congruence during the closing process
2. The ability to provide enough power to pierce through two layers of colon tissue

Secondary assessment criteria were the mechanisms' feasibility to allow for an adaptable and controlled closure process.

The implant was made of Clear Standard Resin, to verify whether the spikes have entirely pierced through the tissue.

#### **4.2.2.1 Actuation via springs**

**Prototype 1:** For the first mechanism the axial force was applied by releasing a precompressed spring (Figure 13). The core of the assembly was a hollow cylinder, which ended with the male part of a snap-lock. The spring, with a spring constant of  $k= 4.7 \frac{N}{mm}$ , was precompressed between a disc that was fixed to the core (initial length:  $L_0= 15.8$  mm, compressed length:  $L_n= 8.1$  mm) and a retainer clamp. The retainer consisted of a ring and two opposing arranged cantilevers with small hooks at the ends. These cantilevers were radially pressed to the disc by a safety ring. The female counterpart, with the mounted oral implant half, was fixed to the endoscope.

For the experiment, male and female connector parts were assembled. The securing ring was pulled back via attached wires. Upon release, the retainer with mounted aboral implant half, snapped forward being axially guided along the core shaft by a groove nose guidance to prevent torsion and tilting. For this mechanism, the transmissible force depended on the maximum spring force and its initial compression. This was derived from the spring constant  $k$ , the initial length  $L_0$  and the maximum compressed length  $L_n$ .

$$(I): F_{Spring} = k (L_0 - L_n)$$

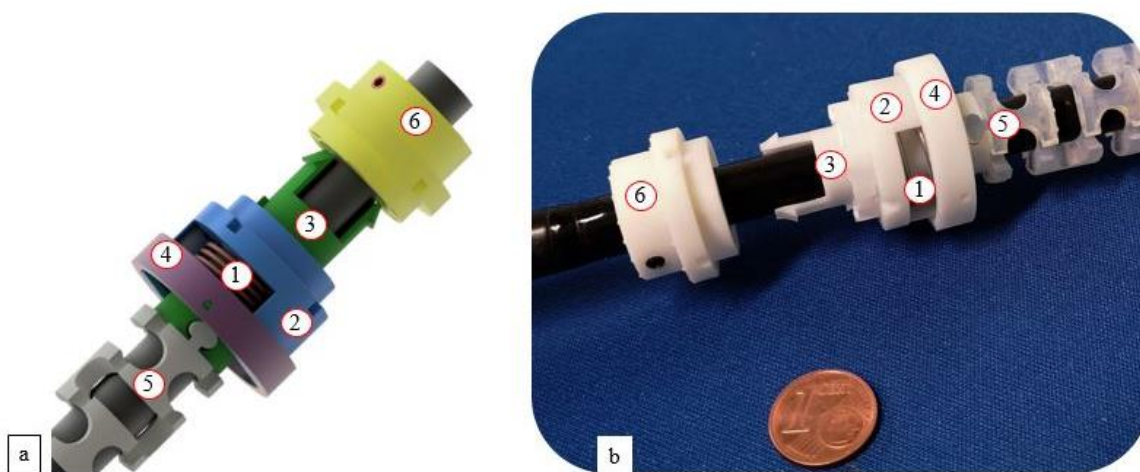


Figure 13 Detailed description of the prototype used to assess the concept of closing a compression anastomosis implant by releasing a spring (1) that is precompressed between a retainer clamp

(2) and the core (3). The retainer, with a recess to mount the aboral implant, is released by pulling the safety ring (4) back. The aboral unit is connected to an overtube (5), while the oral counterpart (6) is attached to the endoscope. Illustration a) shows the CAD graphics and b) the assembled prototype.

#### **4.2.2.2 Actuation via hydraulics**

**Prototype 2:** The second approach was based on hydraulic actuation (Figure 14). A hollow cylinder was designed, closing with the male connector. A piston was assembled to move axially within this cylinder, carrying the aboral implant half. The hydraulic unit had a pressure active surface area of  $\sim 146 \text{ mm}^2$ . Piston and cylinder were sealed by O-rings with a diameter of 12.5 mm and a rope thickness of 1.5 mm on the inside and O-rings with a diameter of 18.5 mm and a rope thickness of 1.5 mm on the outside, using Liqui Moly Silicone Fat (LIQUI MOLY GmbH, Ulm-Lehr, Deutschland) to enhance the gliding properties between the 3D printed hydraulic partners. The female counterpart with the oral implant half was fixed to the endoscope.

The experiments were performed by actuation of the hydraulic unit with water, pushing the aboral implant mount towards the oral one. Based on the pressure active surface area and the pressure applied ( $\sim 2 \text{ bar}$ ), neglecting frictional forces and losses, the maximum realizable force was derived by equation (II).

$$(II): F_{hydraulics} = \Delta p_{hydraulics} * A_{hydraulics}$$

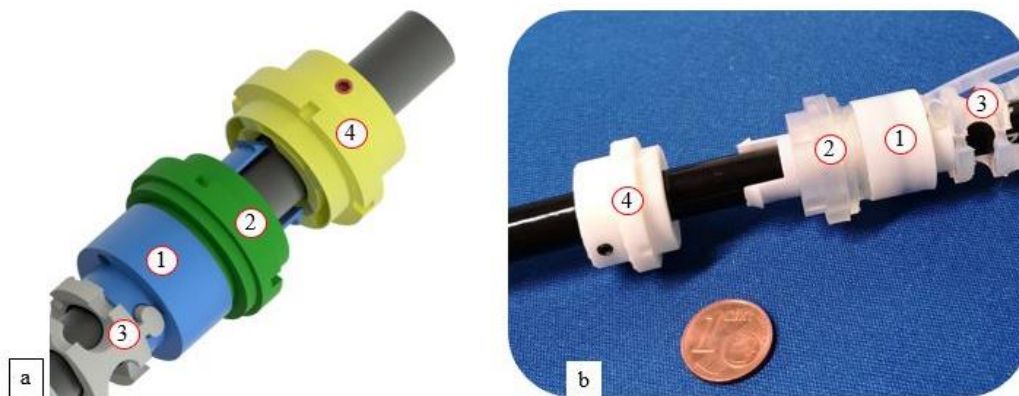


Figure 14 Detailed description of the prototype used to assess the concept of closing a compression anastomosis implant by the actuation of a hydraulic unit, which consists of a cylinder (1) and piston (2) with a recess to mount the aboral implant. The aboral unit is connected to an overtube (3), while the oral counterpart (4) is attached to the endoscope. Illustration a) shows the CAD graphics and b) the assembled prototype.

#### **4.2.2.3 Snap connector for axial congruence of applicator units**

Before the closing unit is actuated, the axially congruent positioning of the applicator heads and implant halves must be secured. Since there is only a limited range of motion available due to the endoluminal access route, and the handling, as well as transmission of movements pose great challenges for physicians in terms of dexterity [81], platform features must be kept as simple as possible. For this reason, a snap connector interface between oral and aboral applicator units was integrated. This was closed by feeding the aboral applicator head with the

male connector axially forward, into the opposing positioned female part. As axial force transmission around flexures and due to large surface contact between endoscope and bowel wall might be challenging, the snap connection design was optimized with respect to smooth/force-minimized closure on the one hand, and providing sufficient abutment (holding force) to pierce two layers of colon tissue during implant closure on the other hand.

**Test setup:** Thus, the joining and holding forces of the snap connection design were determined experimentally. A FH500 digital force gauge (Kern & Sohn GmbH, Balingen, Germany) with a cylindrical force transducer plate was fixed to a square ITEM profile (25 x 25 mm) and mountings, holding the male and female connector geometries, were axially guided within the ITEM profile.

Maximum values of the joining force were measured while pushing the male connector into the female counterpart, pressing it against the force transducer (see Figure 15 a). For the determination of the holding forces, the mount was clamped between the measurement gauge and the transducer (see Figure 15 b). The male connector was pulled back and the retraction force was measured until release or failure of the snap fit occurred.

The connector was manufactured from Standard Clear Resin. The printing orientation was orthogonal to the load direction. The closing and holding forces for the connector pair were measured in  $n = 3$  trials. Each trial was performed with a novel sample.

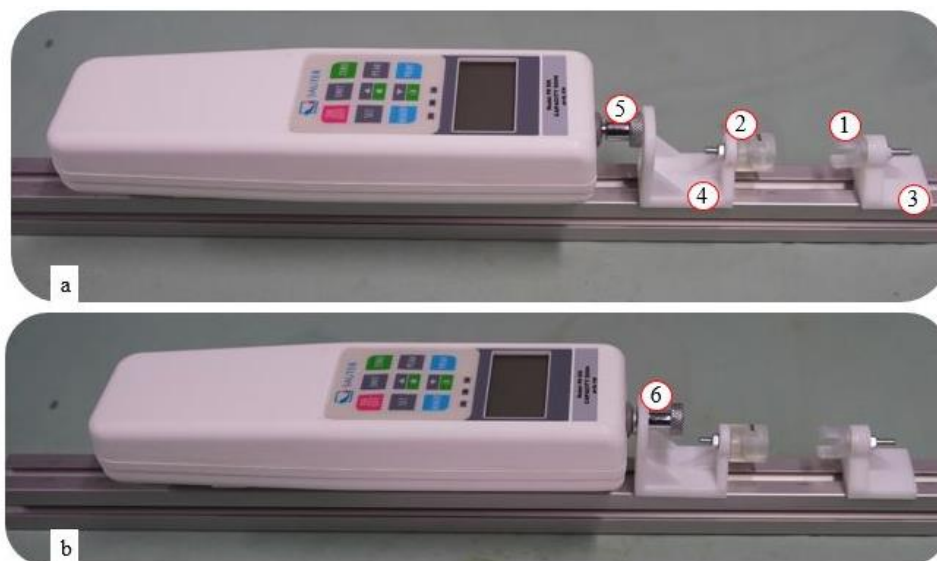


Figure 15 Illustration of the test setup to determine the a) closure and b) holding forces of a snap connector design, which is required to ensure axial congruence between applicator units during implant closure. A FH500 digital force gauge is fixed to a X-shaped ITEM profile. It comprises two holding units (3, 4), to which male and female snap connector parts (1, 2) are attached and axially guided on the profile. A cylindrical force transducer is attached to the measurement gauge. The measurement gauge is pushed forward (5) (locking male and female connector units) or pulled back (6) (unlocking male and female connector units) to measure closure and holding forces.

**Prototype:** The snap connector was designed according to rules given by Bonenberger [82].

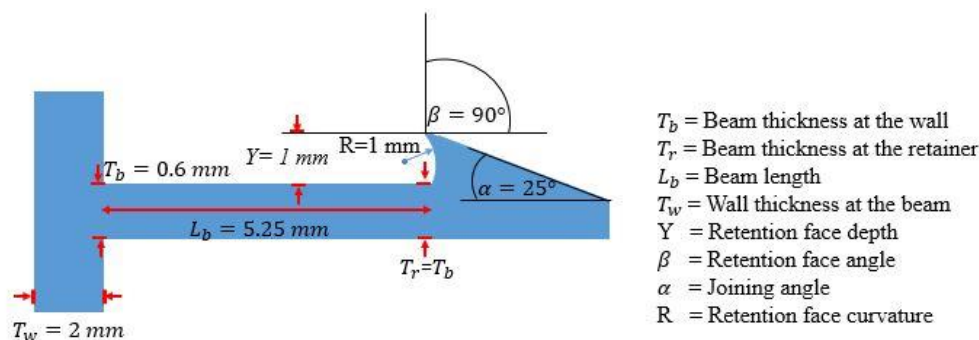


Figure 16 Schematic drawing of the basic snap design, respective adjusted parameters and the chosen dimensions. The design was adapted according to the rules of Bonenberger [82].

Holding forces (force that must be applied to loosen the connection) were maximized by choosing a retention face angle of  $\beta = 90^\circ$  and adding a concave profile beneath the hook ( $R = 1\text{ mm}$ ). To minimize the joining force, joining angle alpha was selected as pointed angle of  $\alpha = 25^\circ$ . For the ratios between beam length, thickness, depth and the retention face depth, the rule  $5 \cdot T_b \leq L_b \leq 10 \cdot T_b$  was applied, while for stiff materials the ratio  $\frac{L_b}{T_b}$  must reach a multiplier of 10. Accordingly, we chose  $L_b = 5.3\text{ mm}$  and  $T_b = 0.6\text{ mm}$  to achieve the desired effects. The beam width was  $T_d = 7.5\text{ mm}$  and the retention depth length, following the rule  $\frac{L_b}{T_b} \approx 5 \leftrightarrow Y < T_b$  or  $\frac{L_b}{T_b} \approx 10 \leftrightarrow Y = T_b$ , was determined to be  $Y = 1\text{ mm}$ . The female connector was designed as the negative counterpart of the male part. [82]

#### 4.2.3 Design and test methods: Endoscopic implant detachment using electromagnets (*Thesis e*)

In endoscopic procedures, implants are often used to close defects within the bowel wall or on other organs of the abdominal cavity. While the implants have to reliably attach to the endoscope during endoluminal navigation, they must be released on demand at the site of application. For the anastomosis device, the applicator must be collapsed and retracted from the bowel after the anastomosis has been formed. A force- and space- saving mechanism has to be identified, that allows to keep the implant reliably attached during navigation, and detach it from the applicator after delivery.

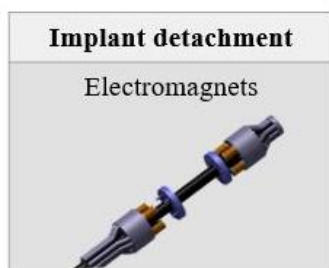


Figure 17 Extract of morphological box, showing the approach investigated to detach an implant at the anastomosis site, integrating electromagnets into an endoscopic device.

A concept based on electromagnetic interaction of applicator and implant was developed. Experiments were conducted with a prototype that comprised two applicator units, including each four electromagnetic coils, which were used to carry the magnetic implant halves.

**Test setup: *Implant detachment:*** The goal of this experiment was to assess, whether it is possible to create electromagnets in a magnitude that can be integrated into an endoscopic device, but strong enough, to detach an implant despite the counteracting forces resulting from mechanical interaction between the components and with the colon tissue.

To conduct the experiments, an applicator prototype was built, which comprised two units, each of which included four electromagnetic coils and carried one implant half. The prototype was mounted onto a horizontally running axis, which was fixed to a PMMA plate by means of a threaded rod. The experimental setup is shown in Figure 18.

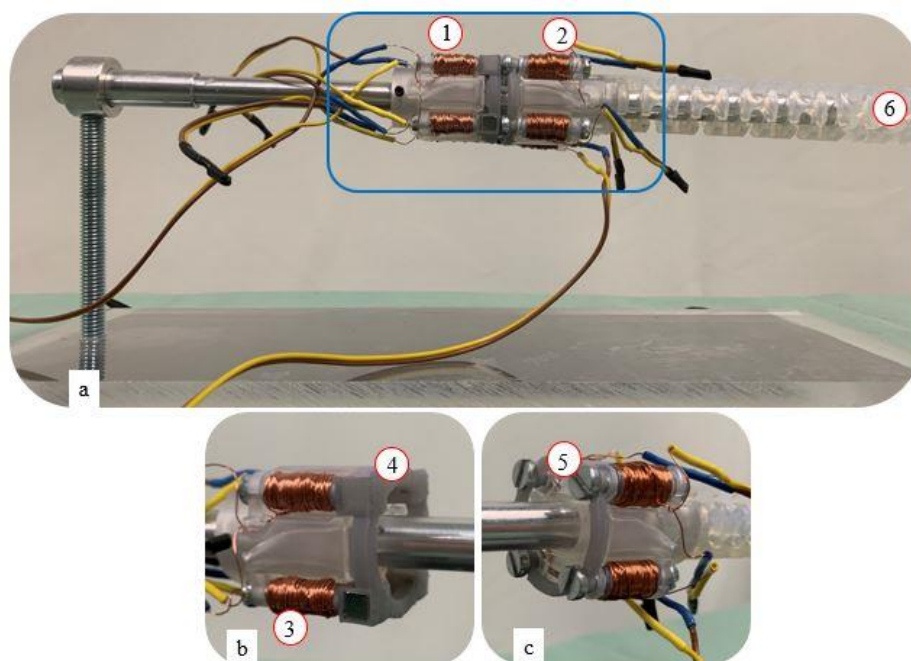


Figure 18 Illustration of the experimental setup to assess functionality of an electromagnetic implant detachment mechanism. Illustration a) shows an applicator prototype consisting of an oral (1) and an aboral (2) unit with electromagnetic coils (3). An overtube (6) is connected to the aboral unit to facilitate the handling. The mounted implant prototype comprises an oral half with permanent magnets (4) and an aboral half with soft magnetic elements (5). Illustration b) shows the oral applicator and implant unit with permanent magnets. Illustration c) shows the aboral applicator and implant unit with soft magnets.

Tissue segments of approximately 6 cm length with closed endings (to fully cover the implant compression faces) were pulled over each of the applicator heads (see Figure 19). Under these conditions, the oral and aboral implant halves were connected across the clamped tissue by pushing oral and aboral applicator units together. The closure was performed only by magnetic attraction of integrated elements here.

The oral implant half was decoupled from the oral applicator by means of a pulsed current. Subsequently the same procedure was performed for ejecting the aboral implant.

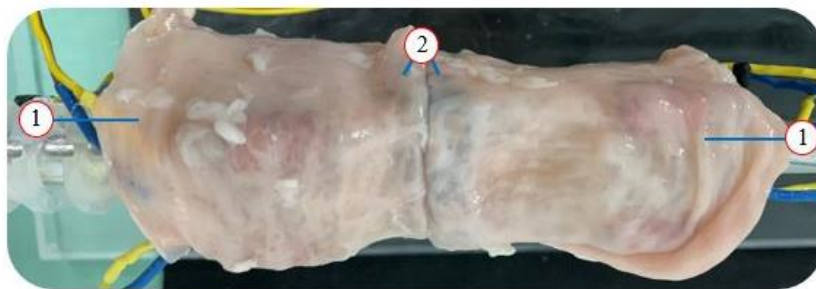


Figure 19 Illustration of the test setup comprising the applicator (1) with electromagnets and with the magnetic compression implant (2). Two samples of colon tissue are pulled over the prototype to assess tissue induced interaction forces during the detachment process.

*Electromagnetic heating assessment:* Even though electromagnets are an increasingly recognized tool in visceral surgery, their integration in minimally invasive instruments is still considered critical, especially for intracorporeal use. Concern has to be given in respect to electric and electromagnetic compatibility with surrounding organs and in regard to temperature increase which results from resistance-based heating of the coils [76, 83] during operation of the electric components. Typical operation modes were defined with respect to different application scenarios during endoscopic procedures [84] and for the special case of anastomosis formation. These comprised either short repellent impulses (i.e. for the detachment of magnetic implants/ maximum amount of admissible de-/reattachment cycles), or a continuous operation (i.e. for traction of tissue portions/ exposure of dissection site) [84].

The corresponding experimental setup is shown in Figure 20. Temperature measurements were taken only on the electromagnets of the aboral side, due to their higher resistance (larger coil  $\rightarrow$  longer wire) and therefore more critical heating characteristics. For this means, the tip of a thermometer (CP011A, Habor, Shenzhen Xintuo Supply Chain Ltd., Shenzhen, China), with a measuring range between  $-50^{\circ}\text{C}$  to  $300^{\circ}\text{C}$  and an accuracy of  $0.1^{\circ}\text{C}$ , was brought into contact with the shell surface of one of the electromagnets. The position was fixed using a tape (Durapore™, 3M™, Saint Paul, USA) to ensure permanent contact between the prototype and the thermometer throughout the entire experiment duration.

Electromagnets were operated in two different modes, including pulsed as well as continuous current supply modes. The resulting temperature rise of the coils was measured.

- **Impulses - Temperature development for pulsed coil powering:** The heat development of the coils was investigated for automatically switching on and off the electromagnets. The coils were powered six times for one second each, to simulate the short repellent impulse for implant detachment and to investigate the system behavior for repeating pick-up and disconnection cycles. A three-second pause was maintained between each pulse. The initial ( $T_{init}$ ) and the maximum temperatures ( $T_{max}$ ) were recorded, as well as after each individual impulse  $X$  ( $T_{x \in [0;7]}$ ). The experiment was performed with an initial coil temperature equal to room ( $T_{init} = T_{room} \sim 23.0^{\circ}\text{C}$ ) or body temperature (about  $T_{init} = T_{body} \sim 37.0^{\circ}\text{C}$ ). Both sets of experiments were repeated  $n = 5$  times.
- **Continuous operation – Measurement of powering duration and maximum temperature:** The temperature development of the coils was investigated in consequence to continuous power supply, starting from the coil temperature  $T_{init} = T_{body} = 37.0^{\circ}\text{C}$ , to define threshold values for tissue manipulation durations or automated system shutdown functions. Subsequently, the coils were powered until the

thermometer indicated a rise in temperature of  $1^{\circ}\text{C}$  ( $T_{stop}=38.0^{\circ}\text{C}$ ). The electromagnets were switched off and the power supply duration was measured, as well as the maximum temperature ( $T_{max}$ ) reached. The experiment was repeated  $n = 10$  times.

Between all test sets, it was ensured that the coils cooled down until they reached to their respective initial temperature ( $T_{room}$  or  $T_{body}$ ) to provide equal and comparable preconditions. The results from the heating assessment were used to calculate design guidelines with respect to the wall thickness of a heat shielding encapsulation.

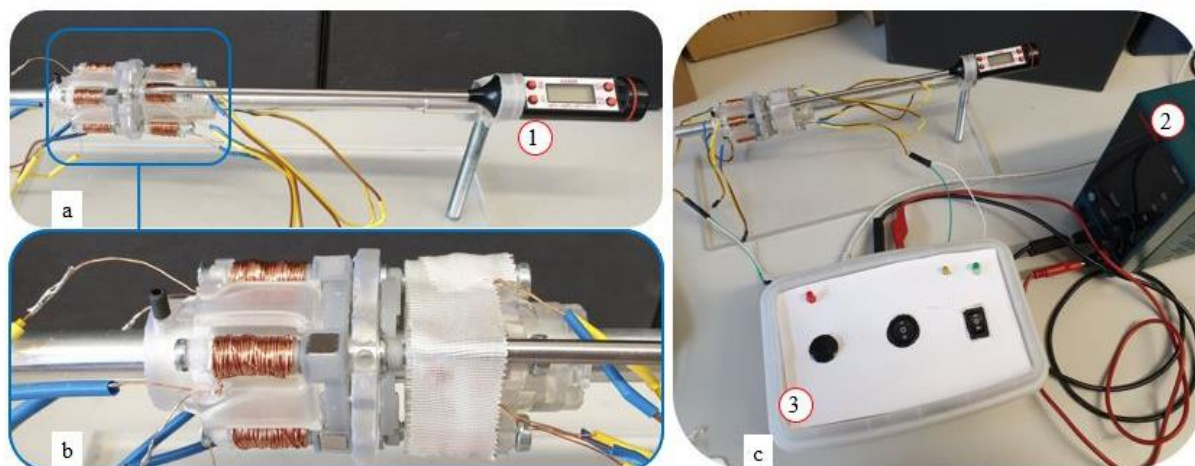


Figure 20 a) Overview and b) detailed zoom of the experimental setup to measure the heat generation of the electromagnetic coils using a thermometer (1). c) Current is provided by an external power supply (2), controlled and triggered by a control unit (3).

**Prototype:** In the following, the prototype is described, which comprises an applicator (consisting of two separate units) and a two-part implant. The implant on the oral side comprised four cubic N52 magnetized neodym magnets<sup>3</sup> (EarthMag GmbH, Dortmund, Germany) with a side length of 5 mm, being encapsulated in a polymeric sheath of 0.6 mm wall width. Four mild steel screws<sup>4</sup> with a standard M4 thread were used as soft magnetic elements on the aboral side.

In the oral applicator unit, the electromagnetic coils included a monolithic core, whilst in the aboral applicator head, the cores were split in two parts. One of these two elements was anchored in the coil, and the other one protruded from the implant into the electromagnet (see Figure 21 (6)). This hull like structure supported the reliable attachment of the implant to the applicator during navigation through the colon.

<sup>3</sup> Magnet shop Neodym Magnets 5x5x5 mm NdFeB N52; <https://www.magnethandel.de/neodym-magnete-5-5-5-mm-n52#tab-description>; last accessed May 7, 2022.

<sup>4</sup> Re-In Retail International GmbH 803588 Combi-Screw-Sortiment 3000 parts; <https://www.voelkner.de/products/74881/803588-Kombi-Schrauben-Sortiment-3000-Teile.html>; Product sheet: [https://asset.re-in.de/add/160267/c1/-/de/000803588IN01/IN\\_803588-Kombi-Schrauben-Sortiment-3000-Teile.pdf](https://asset.re-in.de/add/160267/c1/-/de/000803588IN01/IN_803588-Kombi-Schrauben-Sortiment-3000-Teile.pdf); last accessed May 7, 2022

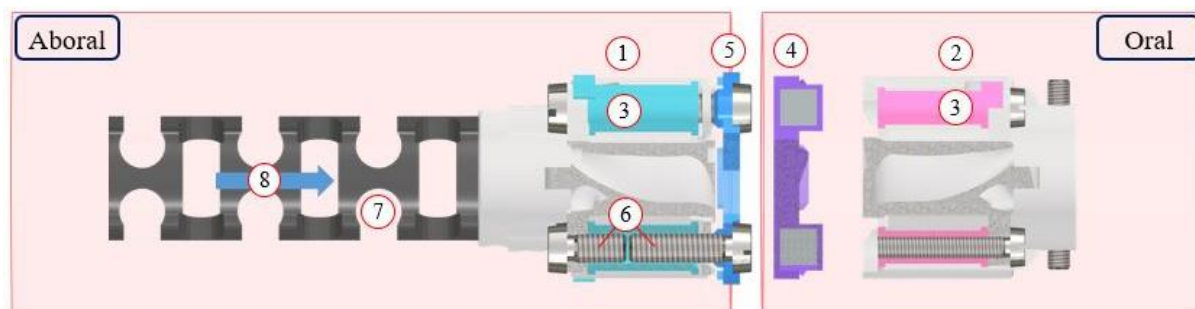


Figure 21 Schematic illustration of the electromagnet-based anastomosis device, comprising applicator units (1, 2), implant dummy halves with magnetic elements (4, 5), endoscope overtube (7), electromagnets (3) to control implant de- and attachment, as well as split electromagnetic cores (aboral applicator) (6), positioned within aboral and oral colon lumina. (8) indicates the insertion direction.

The coil bodies of the oral and the aboral implant carrier units had a maximum length of  $l_{coil}=15.0$  mm (winding length of 13.0 mm). The diameter of the oral polymeric coil bodies was  $\varnothing_{oral}^{coil} = 4.6$  mm and of the aboral coils  $\varnothing_{aboral}^{coil} = 6.4$  mm. For the electromagnetic cores, soft magnetic mild steel screws<sup>4</sup> with a standard M3 thread in the oral applicator and standard M4 thread in the aboral applicator (magnetic permeability range  $\mu_{r_{min}} = 100$ ;  $\mu_{r_{max}} = 800 - 2000$ ) [85] were used. On the aboral side, one third of the entire core length protruded from the implant, and two third were integrated in the electromagnetic coil.

All coils were spooled clockwise from bottom to top with an enameled, 0.3 mm diameter copper wire (Conrad Electronic SE, Hirschau, Germany). The coils comprised 100 windings and were operated at 24 V direct current (3 A). All coils of each of the two applicator heads were connected in series. A control unit was designed with the help of an Arduino<sup>TM</sup> micro-controller board circuit (Arduino<sup>TM</sup> Uno SMD R3, Italy) and a laboratory power supply (HM305, Hanmatek, Shenzhen, China) unit. By these means the electromagnetic coils of the oral and aboral applicator heads were switched on separately for accurately adjustable time periods. Furthermore, the electrical current flow was inverted for the aboral side, attracting or repelling the respective implant half.

The implant halves and coil bodies were manufactured with the Formlabs2 stereolithographic process (Formlabs GmbH, Berlin, Germany) from the material “Tough 1500“. This resin was used for filigree components of the prototype, due to its lower tensile modulus compared to standard resins, and therefore higher flexibility and decreased risk of breakage [86]. The implant carrier units were printed with the Formlabs3B (Formlabs GmbH, Berlin, Germany), using “Clear standard resin”, which is a material designated for components affected by low mechanical loads, but high accuracy requirements [74].

### 4.3 Final design approach and mechanical assessment

Finally, a comprehensive approach for the final applicator system was derived from the results of the subsolution testing. In addition to the basic investigations with respect to endoscopic

---

manipulation, a mechanism to fix the oral applicator unit to the endoscope shaft was developed. Furthermore, a concept to keep implant compression faces of both halves aligned in parallel in all size configurations of the applicator was derived.

Holding, closing and expansion forces were evaluated for the manipulator concept and compared to the requirements defined for the creation of the ideal anastomosis.

### **4.3.1 Design and test methods: Handling concept of final applicator prototype**

#### **4.3.1.1 Fixation of oral applicator unit to the endoscope**

For the task of endoscopically anastomosing two colonic lumina, the bowel edges have to be approximated. Therefore, relative movement between both applicator units must be enabled. While the aboral entity is pushed, pulled and rotated by the physician via a handling platform (i.e. overtube structure, which is not further specified within the scope of this work), the opposing entity must be fixed to the endoscope, so its position can be controlled by manipulating the endoscope. Axial forces during endoscopic navigation can be high due to friction between tissue and endoscopes, or with respect to obstacles such as flexures, haustres, etc. The fixation mechanism must withstand these forces to maintain the position of the oral applicator unit during endoscopic navigation.

**Test-setup:** Thus, the holding force of the developed mechanism was experimentally determined, by a FH500 digital force gauge (Kern & Sohn GmbH, Sauter, Balingen, Germany), mounted on a square ITEM profile (25 x 25 mm), which was fixed on a workbench to prevent slipping. A prototype of the locking mechanism with two eyelets that were symmetrically arranged around the central endoscope axis was positioned on a 13801PKS gastroscope (Karl Storz, Tuttlingen, Germany) about 10 cm behind the flexible endoscope tip. A surgical suture material was threaded through the eyelets of the cap and the resulting loop was connected to the hook-shaped force transducer of the measurement gauge (Glyconate monofil 5/0 70 cm, AESCULAP AG & Co. KG, Tuttlingen, Germany).

The endoscope was pulled back along its longitudinal axis, away from the force measurement gauge until slippage occurred between the adapter and the endoscope, or the sewing material was torn. The maximum force measured in each trial (n=5) was recorded.

**Prototype:** The friction lock principle, chosen to attach the oral applicator head to the endoscope, comprised eight symmetrically arranged cantilevers that were flexibly connected to a threaded body via pliable film joints [87, 88] (see Figure 22 a). The droplet-shaped cap was designed to support transanal insertion and navigation, and comprised the mating counterpart to the corpus. The inclination angles of the outer cantilever surfaces and the inner cap surface were identical with 80.0°. The film joints were compressed towards the endoscope by means of a screwed on cap (see Figure 22 b). By mounting the cap onto the corpus with film joints, the axial tensile force introduced by means of the thread, was converted into a radial clamping force.

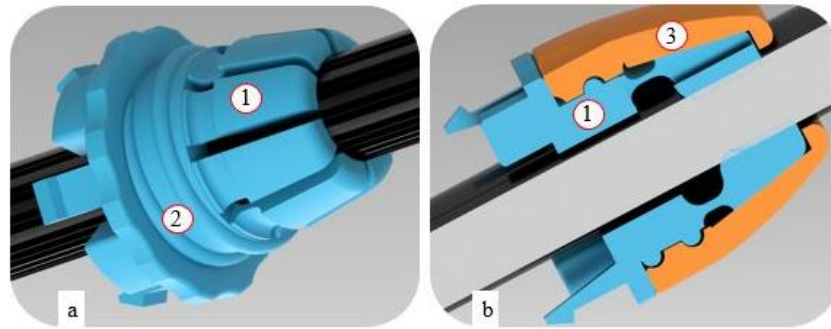


Figure 22 Mechanism to fixate the oral unit to the endoscope. The unit comprises film joints (1), which are compressed to the shaft by a screwed (2) on cap (3) a) Core with symmetrically arranged pliable film joints b) Cross sectional view through the core with the mounted cap.

### Film joints

For the film joints, used in the oral screw fixation cap a standard geometry according to Kunz et al. was chosen [88].

As film joints require materials with high ductility, easy deformability and high flexural fatigue strength [87], polypropylene (PP) is commonly recommended in literature [89]. As an equivalent to this thermoplast, Tough1500 Resin was selected, as it provides similar mechanical material properties [86].

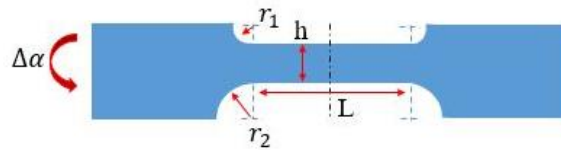


Figure 23 Schematic drawing of the film joint, modified from Kunz et al. [88], used for the screw attachment of the oral applicator unit, with corresponding measures to calculate dimensions.

The film joint was dimensioned according to Erhard, who gave a correlation for the required tapered section length  $L$  [mm], depending on the tapered section thickness  $h$  [mm] [89].

$$(III): L = \frac{h \cdot \Delta\alpha \cdot S}{2 \cdot \varepsilon_\alpha}$$

The geometry specific maximum elongation  $\varepsilon_\alpha$  [%] of bent Polypropylene joints was used, as no respective values for Tough1500 exist up to today ( $\varepsilon_\alpha = 60\%$  after  $10^4$  load cycles). [89] The film thickness  $h = 0.7$  mm was chosen with respect to accuracy limitations of the printing process and to achieve a maximum bending angle of  $\Delta\alpha = 90^\circ$ . Since the number of bending cycles for the application was assumed to be less than 100 cycles, a safety factor of  $S \leq 1$  was used [88].

$$L = \frac{0.7 \text{ mm} \cdot \frac{\pi}{180^\circ} \cdot 90^\circ \cdot 1}{2 \cdot 0.6} = 0.9 \text{ mm}$$

The length  $L$  of the tapered cross-section was dimensioned to 1 mm. To minimize notch stresses, the transition to the middle segment was formed with a radius  $r_1 = 1.0$  mm on one side, and of  $r_2 = 1.5$  mm [89] on the other side. The bending of the joint was performed in the direction of the larger radius [88].

## **Thread**

The thread design was optimized according to recommendations of Formlabs 3D-printing guidelines. Using Standard Resins and a semicircular thread profile (screw and nut), engagement and wear properties were enhanced. Tough1500 Resin was used due to its decreased tensile modulus compared to standard resins, allowing higher flexibility and optimized bending properties of the film joints [86].

### **4.3.1.2 Manipulation of tissue with final applicator prototype**

To approximate the tissue, it must be grabbed by the applicator and adhesion must be sufficient to drag the tissue.

Establishing a suction force between applicator and the bowel wall allowed to invert, grab and manipulate colon lumina in preliminary experiments.

Thus, the approach was integrated into the final device design and channel geometry was adapted to provide enough space for the latest implant geometry. Channel outlets of the applicator claws, protruding from the center, were arranged in an interdigitating sequence.

Each applicator blade of the final prototype comprised two vacuum channels, which were connected via Polyurethan tubes (outer  $\varnothing = 3.0$  mm; inner-  $\varnothing = 2.0$  mm) (ESSKA.de GmbH, Hamburg, Germany) to a suction pump (Medela Basic Absaugpumpe, Medela Medizintechnik GmbH & Co. Handels KG, Dietersheim, Deutschland). The planes of the channel outlets were aligned with the front surface of the respective implant half, to establish a stable suction and adhesion of the intestinal tissue.

The realizable total suction force was calculated for every applicator blade to estimate realizable forces for pulling, pushing and manipulating tissue.

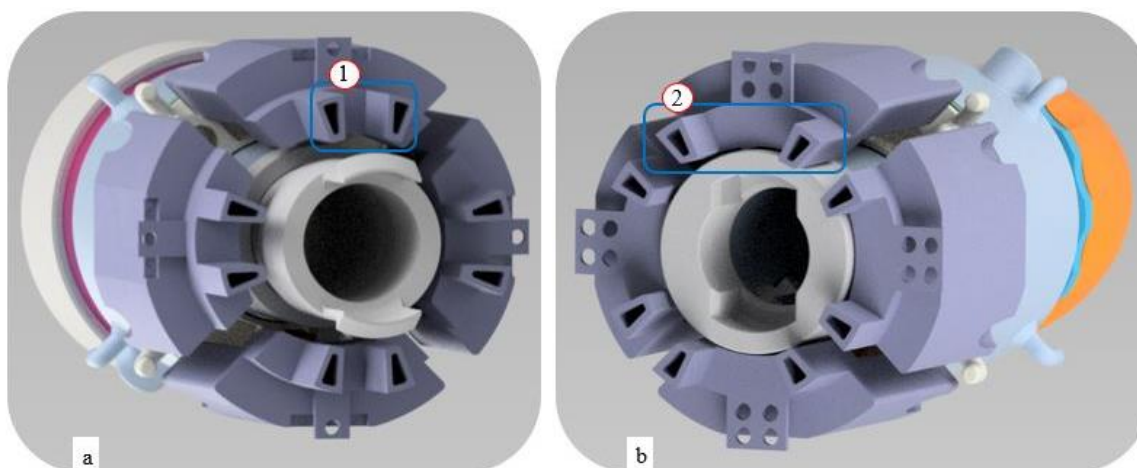


Figure 24 Suction channel outlets (1, 2) of aboral (a) and oral (b) applicator arms protruding from the center are arranged in an interdigitating sequence to provide sufficient space for the latest implant geometry and respective features.

### 4.3.2 Design and test method: Patient adaptation of final applicator prototype

Patient adaptation comprises both, the platform expansion to adjust to the lumen diameter, and the adjustment of the implant compression gap to the tissue thickness, which influences the compression pressure and determines the anastomosis formation with respect to tissue healing and necrosis. In order to be able to close the implant in a controlled manner, it is crucial to maintain parallel implant compression faces and an equal distance between them for all size configurations.

#### 4.3.2.1 Implant mounting by scissor kinematics

The implants were mounted on the applicator blades, which were assembled to the hydraulic units by means of scissor joints. The mechanism comprised two opposing arranged fixed bearings, and two loose ones, being X-wise connected via rigid struts. On the endoscope side, the fixed bearings were attached to the applicator's cylinder core wall, oriented towards the upper applicator blade edge, as well as on the blade side, where the eyelet was fixed close to the implant suspension. The loose bearings were oriented away from the implant (see Figure 25 a), one eyelet being attached to the hydraulic piston and one eyelet to a trapezoidal slide, axially gliding within the groove of the applicator arm (see Figure 25 b, c). When the expansion hydraulics were actuated and the floating bearing was pushed towards the respective fixed point on the same side, the opposing loose bearing in the applicator arm moved accordingly by the same distance. Both applicator heads had an outer diameter of 33.1 mm in the unexpanded configuration, of  $d_1 = 46.8$  mm in first expansion stage and  $d_2 = 51.5$  mm in second expansion stage.

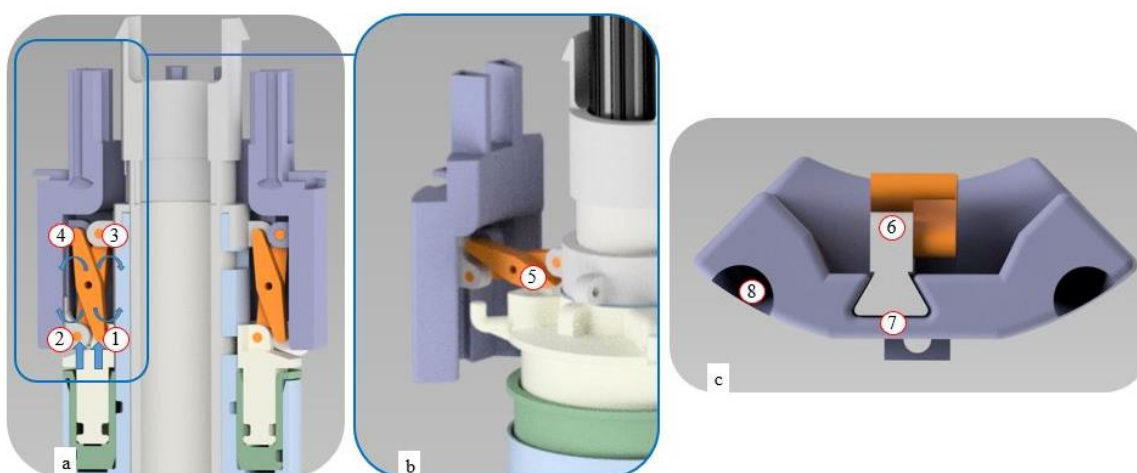


Figure 25 Illustration of the X-kinematics, mounting the applicator arms (with suction channels) onto the applicator unit. a) Minimized configuration of the aboral applicator unit: Connection of applicator blades to the hydraulic expansion unit via scissor joints. The mechanism comprises two loose bearings (1, 2) and two fixed bearings (3, 4). b) Expanded configuration: The joints are cross-wise connected by struts (5). By actuation of the hydraulic piston, the loose bearing at the endoscope moves upwards, towards the respective fixed bearing. Due to the geometrical constraint, the opposite loose bearing moves upwards by the same distance. c) Detailed illustration of the loose bearing in the applicator blade (2), which comprises a trapezoidal slide (6) gliding in a groove (7). Tube holes (8) enable the connection of the blade to a suction pump.

### 4.3.2.2 Modeling expansion & bearing forces

The expansion forces were modeled for these kinematics, to determine the feasibility of the approach with respect to the task of expanding an implant.

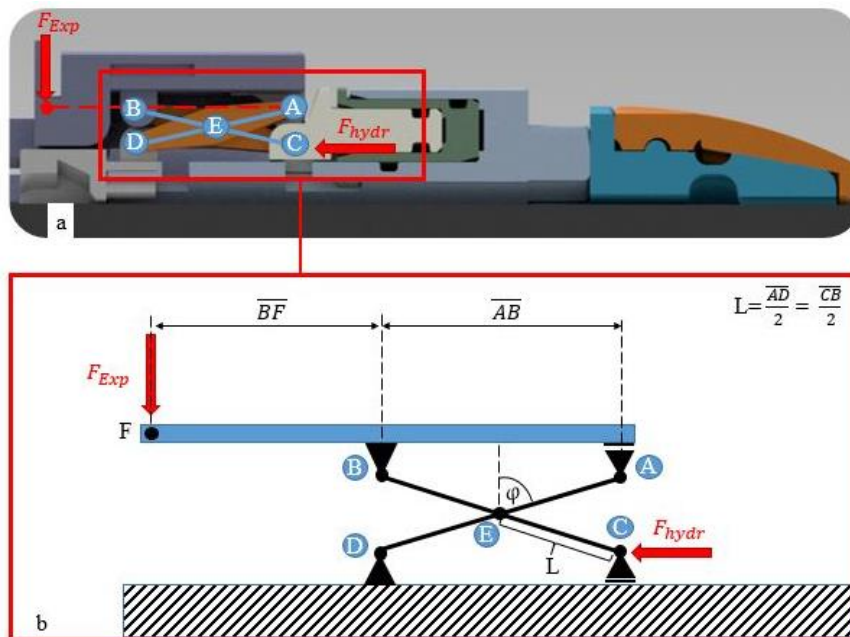


Figure 26 Mechanical model of one applicator arm and X-kinematics. a) Illustration of one applicator arm in the CAD model and designation of joints b) Simplified model representing mechanics of X-kinematics and respective joints.

The maximum force per hydraulic entity was calculated by equation (II).

One applicator arm suspension was modeled (see Figure 26) by reducing the expansion hydraulics to the bearing points and externally exerted forces. A and C are loose, and B and D are fixed joints, facing each other respectively and being X-wise connected by struts of length  $L = \frac{\overline{AD}}{2} = \frac{\overline{CB}}{2}$ .  $F_{exp}$  represents the force acting on the applicator blade at the implant mount position during dilatation, which is located in distance  $\overline{BF}$  from bearing B.  $\overline{AB}$  describes the distance between the fixed joint B and the floating bearing A. While the length of section  $\overline{BF}$  remains constant, length  $\overline{AB}$  is shortened during the expansion process ( $\overline{AB} = max$  for unexpanded applicator,  $\overline{AB} = min$  for maximally expanded applicator).  $\varphi$  describes the angle between the strut and the axis running through the joint, orthogonally to the stroke direction. The angle  $\varphi$  is maximal, when the applicator is not expanded and vice versa minimal, if the scissor joint is maximally expanded. The angular range of  $\varphi$  is measured in the CAD model for both expansion stages.

For the first hydraulic cylinder (1<sup>st</sup> expansion state)  $\varphi_1$  runs between  $\varphi_1 = [39.6^\circ, 77.4^\circ]$ .

For the second hydraulic cylinder (2<sup>nd</sup> expansion state)  $\varphi_2$  runs between  $\varphi_2 = [15.9^\circ, 39.6^\circ]$ .

Complementary to this, leverage effects and respectively occurring bearing forces in A were assessed to evaluate the suitability of the implant mounting position.

For the calculations of this chapter, the weight force, as well as dynamic effects of acceleration and inertia were neglected with respect to the low mass and velocities of motion. As the oral and aboral hydraulic units had identical dimensions, with arms symmetrically arranged around the circumference and identical bearings, it was assumed that the resulting hydraulic force is equally distributed on all four applicator arms. Thus, modeling was performed on a single applicator blade unit and transferred to the remaining arms thereafter. In the mechanical model, it was assumed that the actuating hydraulic force  $F_{Hydr}$  results in a well aligned elevation of the joint points A and B and that the expansion force  $F_{Exp}$  acts perfectly perpendicular to the stroke direction of the expansion hydraulics. Friction forces between the gliding partners in the expansion hydraulics were neglected.

#### 4.3.3 Design and test method: Anastomosis formation unit of final applicator prototype

To form the anastomosis, the applicator must approximate the two bowel endings and allow to apply forces high enough, to pierce through the compressed tissue layers and connect the mounted implant halves.

Therefore, another hydraulic entity was designed. To assess whether this approach is feasible to realize the required forces [5], which were determined in the preliminary biomechanical investigations, the capacity of the hydraulic closing unit was modeled and calculated.

Modeling the closing process, it was assumed that forces of equal magnitude apply on each of the four arms, acting along the joint axis  $\overline{AB}$ . As the arms are symmetrically arranged on the applicator, it was assumed that the hydraulic force is also distributed uniformly over all arms, respectively contact points. Friction forces between the gliding partners in the closing unit hydraulics were neglected.

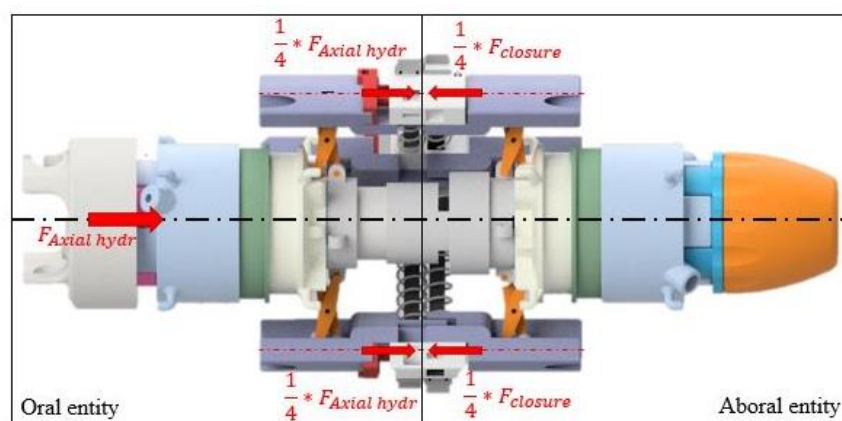


Figure 27 Model of the implant closing forces applied by the final applicator.

## Results

### 5.1 Biological and mechanical characterization of colon tissue: Derivations for an endoscopic applicator closure unit

In the following, the results of the biomechanical investigations are described. One aspect was, to determine the influence of piercing trajectory velocity and acceleration.

For the three different velocities  $v = 5, 10, 15 \text{ mms}^{-1}$  and accelerations  $a = 5, 10, 15 \text{ mms}^{-2}$  investigated, the original assumption according to  $F = m \cdot a$  and  $F \delta t = m \cdot \delta v$  was that higher forces occur at higher velocities and accelerations. This in turn would lead to stricter stability requirements, for mechanisms with increased closure velocity/acceleration. Thus,  $H_0$  postulated that there is no difference in occurring insertion forces for groups  $v_1, v_2, v_3, a_1, a_2$  and  $a_3$ .  $H_0$  was approved with a  $p\text{-value}_A$  of 0.513 and a  $p\text{-value}_{KW}$  of 0.236, which means that there was no significant variation in piercing forces observed with respect to the assessed velocity and acceleration groups.

As suction forces established to be a valuable tool to grab and tract tissue [71], the influence of the way how tissue is attached to the applicator was investigated. Thus, the suction channel outlet surfaces were arranged in three different design configurations, to stretch tissue across the spike openings in different ways. It was assumed that with increasing the specimen tension of spanned tissue, the indentation of the specimen can be reduced, allowing to puncture the colonic tissue in the compression zone. Based on the available literature it was further assumed that an increased surface tension would lead to an increase in piercing force [90, 91]. The second  $H_0$  was therefore: There is no difference in occurring insertion forces depending on the arrangement of fixation points (different vacuum configurations used). The ANOVA test revealed a  $p\text{-value}_A$  of 0.501 and the KRUSKAL–WALLIS test a  $p\text{-value}_{KW}$  of 0.845, which means that among the groups compared, the fixation point arrangement did not show a statistically significant effect on the forces required to pierce the tissue.

Finally, increasing the amount of spikes, a more secure fixation of tissue in the compression zone can be achieved and the holding forces between implant halves can be increased. At the same time it was assumed that this would lead to increased piercing forces. The third  $H_0$  was: There is no difference in occurring insertion forces depending on the amount of spikes (4, 8, 12 spikes). With  $p\text{-values}_{A/KW}$  of  $< 2e-16$  for ANOVA and the KRUSKAL-WALLIS test, this hypothesis was rejected with respect to  $\alpha_{A/KW}=0.01667$ . The results showed a statistically significant increase in piercing forces with an increasing number of tips. Average forces of about  $6.4 \pm 1.5 \text{ N}$ ,  $13.6 \pm 1.4 \text{ N}$ ,  $21.7 \pm 5.8 \text{ N}$  for 4, 8, 12 tips were measured.[5]

The 5th and 95th percentiles of the sample diameters were deduced to be in a range between 24.1 mm to 40.1 mm ( $n=540$  samples) and the 5th and 95th percentiles of tissue thickness of

two layers, as compressed between the implant halves, were in a range between 2.8 mm to 4.8 mm ( $n = 270$  sample pairs). [5]

## 5.2 Results of task specific solutions to enable endoluminal manipulation

### 5.2.1 Results: Grasping/ inversion of colonic margins and patient adaptation (Theses b, c)

#### 5.2.1.1 Expansion of colon *without adjusting* the suction channels to the bowel wall

**Prototype 1 (balloon expansion):** Figure 28 displays the deflated and expanded balloon covered with tissue. In the inflated configuration three regions were identified (see Figure 28 b). In area 1, the maximum diameter of the balloon in expanded state can be observed. The bowel was stretched and followed the geometry of the expanding device. In area 2, the bowel detached from the balloon, but folded towards the lumen center anyway. In region 3, the contraction dissolved. At the lowest point, tissue was hanging downward, as expansion of the intestine did not cause sufficient inversion to adjust the colon to the suction surfaces along the entire applicator circumference.

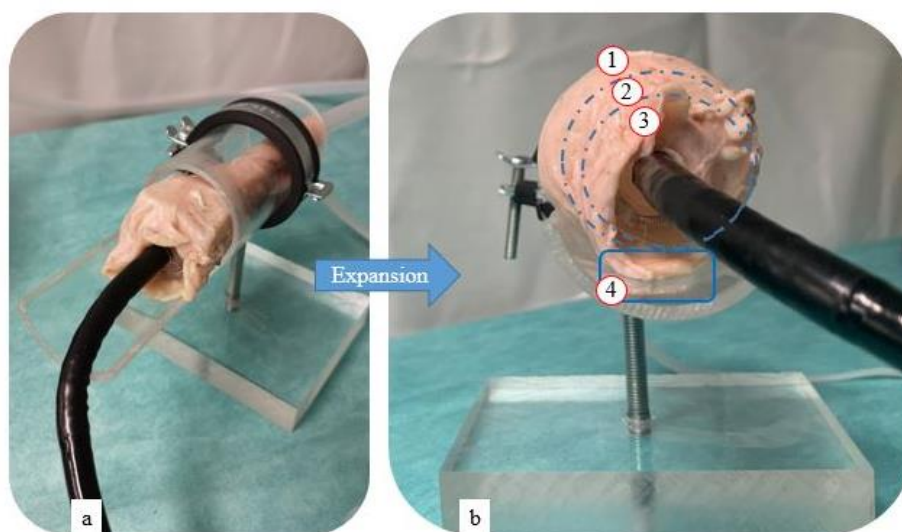


Figure 28 Images showing the results gained by balloon expansion, to assess the concept of expanding the colon to invert bowel margins without adjusting the suction outlets towards the wall. While image a) shows the situation with the deflated balloon, image b) corresponds to the expanded situation. In the inflated configuration, three regions are identified. In area (1), the balloon is maximally expanded. The bowel is stretched and follows the geometry of the balloon. In area (2) the bowel is detached from the balloon, but still folds towards the lumen center. In region (3) the contraction dissolves. At the lowest point, tissue is hanging downward (4), as expansion of the intestine does not cause sufficient inversion to adjust the colon to the suction surfaces along the entire applicator circumference.

Although the desired effect of shaping the bowel by expansion was achieved, some negative aspects were noticed. First, and although the balloon expanded uniformly, the bowel margins could not be turned sufficiently towards the center, so that no stable suction force and no reliable connection to the applicator was established. This holds specifically true for the tissue at the lowest point of the balloon (lower border), for which the expansion of the intestine did not cause

sufficient inverting force to overcome gravity. When the margins were adjusted to the frontal face manually, the excess of tissue still led to significant folding and protrusions, resulting in an heterogeneous coverage of the implant by tissue (see Figure 29).

### **5.2.1.2 Expansion of colon by adjusting the suction channels to the bowel wall**

#### **Design of a platform expansion unit to support implant scaling (Thesis c):**

In comparison to the latter prototype, expanding the vacuum channel outlets towards the intestinal wall allowed to fully cover open spaces with tissue, establish stable suction and adherence, and to reliably grab and manipulate the bowel (balloon and hydraulics) (see Figure 29). It was most efficient in avoiding folding and protrusions of the tissue in the implant compression zone to reduce the risk of anastomosis leakage.

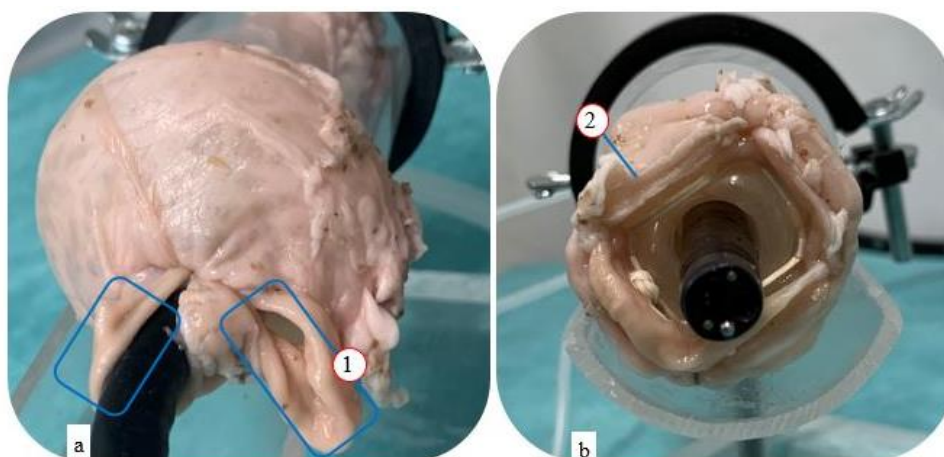


Figure 29 The illustration shows the results gained by expanding colon without adjusting the suction channels to the bowel wall (image a) vs. expanding colon by adjusting the channels to the wall (balloon and hydraulics) (image b). While large protrusions (1) occur in the first approach, the second approach allows to fully cover open spaces with tissue (2), establish stable suction and adherence, and to reliably grab and manipulate the bowel.

For the applicator arm expansion mechanism, both approaches (balloon and hydraulics) allowed isolation of the force application to the applicator end-effector unit. With respect to the future integration of the unit into endoscopic devices, this holds the potential to avoid power losses along transmission paths.

**Prototype 1 (Balloon mediated expansion mechanism):** The filling volume of the balloon allowed to determine the degree of expansion, which is required to enable congruent dilatation of two units. However, this was less accurate than a fixed end stop, as the balloon's material flexibility also allowed over-expansion beyond the targeted diameter. The flexibility of the balloon further restricted the maximum transmissible forces to expand an implant, and showed susceptibility to a varying elasticity of the colon, resulting in expansion irregularities.

**Prototype 2 (Hydraulic unit with springs):** For the hydraulically driven unit the expansion was controlled and distinctively constrained by the maximum hub. Hydraulic actuation allowed to lock the expansion stages and to completely collapse the expanded configuration after dilatation.

However, operating the hydraulic unit in an inverted mode, i.e. expanding the applicator by drawing negative pressure, reduced efficiency of the unit. Integrated springs, which were maximally tensioned in minimized applicator head configuration, supported to smoothen the expansion process, but increased the forces required for collapsing the system.

The integration of vent valves allowed to significantly enhance the efficiency of the hydraulically actuated prototype [80], which allowed smooth and reproducible actuation and retraction of the piston to collapse expanded configuration. They were tight up to a pressure of 3 bar.

## 5.2.2 Results: Applicator integrated implant closing unit (*Thesis d*)

### 5.2.2.1 Actuation via a precompressed spring vs. hydraulics

By actuating the mechanism, the implants were advanced with the spikes penetrating the tissue. Subsequently and with completion of closure, the spikes were sunk into the receiving counterpart on the oral applicator unit. The success of closure and a complete penetration of spikes was visually verified.

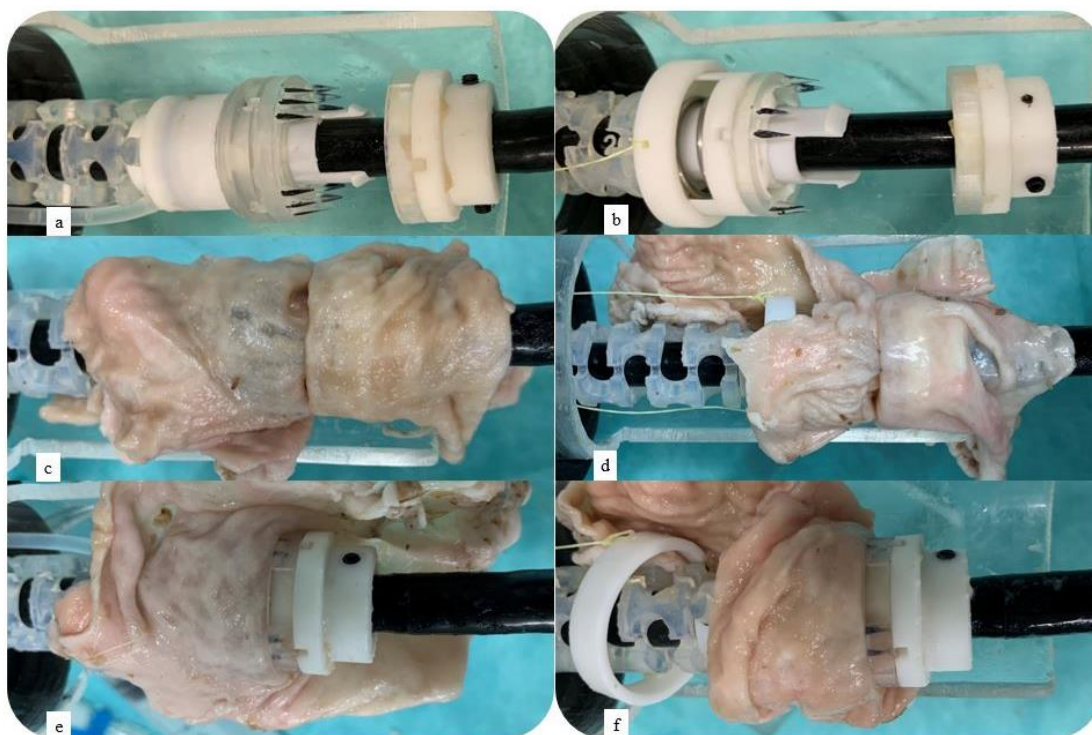


Figure 30 Experimental evaluation of force application mechanisms to close the implant. Left column: Hydraulic implant closure mechanism, Right: Spring based implant closure mechanism. a) & b) The applicator prototypes with mounted implant dummies (black marked spikes) are shown. c) & d) One colon sample each is pulled over the implant halves. e) & f) The pierced colon samples are pulled back to control entire immersion of the piercing bodies in the receiving implant half.

The spring and hydraulic based mechanisms were able to apply closure forces of:

$$F_{spring}^{prototype} = 4.7 \frac{N}{mm} (15.8 \text{ mm} - 8.1 \text{ mm}) = 36.2 \text{ N}$$

$$F_{hydraulics}^{prototype} = 0.2 \frac{N}{mm^2} * 146.0 mm^2 = 29.2 N$$

Both mechanisms, allowed to successfully pierce through two layers of colon tissue (see Figure 30).

### **5.2.2.2 Snap connection of applicator units**

For the closing forces of the snap connector a mean value of  $F_{snap\ closure}^{mean} = 15.2 \pm 1.0 N$ , and holding forces of  $F_{snap\ holding}^{mean} = 43.6 \pm 3.9 N$  were measured.

## **5.2.3 Results: Endoscopic implant detachment using electromagnets (Thesis e)**

### **Implant detachment**

The use of electromagnets in endoscopic procedures, to deliver implants to defects within the abdominal cavity or bowel, was investigated with respect to its feasibility (size, power) for integration into novel platforms. The implant dummy halves were connected while being mounted to the applicator. The oral and aboral implant halves were subsequently decoupled from the applicator by consecutively actuating the electromagnets with a pulsed current, resulting in a magnetic repulsion force. The detachment of the closed implant from the oral and the aboral applicator units was reproducibly successful.

### **Electromagnetic heating assessment**

Special concern was given to the resistance-based heating of the coils.

*Impulses - Temperature development for pulsed coil powering:* The development of the absolute coil temperature (Figure 31) was evaluated with respect to the number of impulses. A continuous increase in coil temperature with increasing number of pulses was observed. Temperature recording time step  $x = 0$  corresponded to the initial coil temperature ( $T_0 = T_{init}$ ), which was either room ( $T_{room}^{1s} = 22.9 \pm 0.5^\circ C$ ) or body temperature ( $T_{body}^{1s} = 37.0 \pm 0.0^\circ C$ ). Temperature measurements ( $T_x^{1s}$ ) were repeated every 4 seconds, thus after 1, 5, 9, 13, 17, 21 s. Furthermore, the maximum coil temperatures ( $T_7 = T_{max}$ ) reached with a certain time delay ( $\sim 2$  s) after switching off the coils were recorded. Averaged over all 5 trials per single set, coils heated up to a maximum temperature of  $T_{max\ room}^{1s} = 28.4 \pm 0.8^\circ C$  starting from room temperature ( $T_{room}$ ), and of  $T_{max\ body}^{1s} = 41.6 \pm 0.1^\circ C$  for starting at body temperature ( $T_{body}$ ).

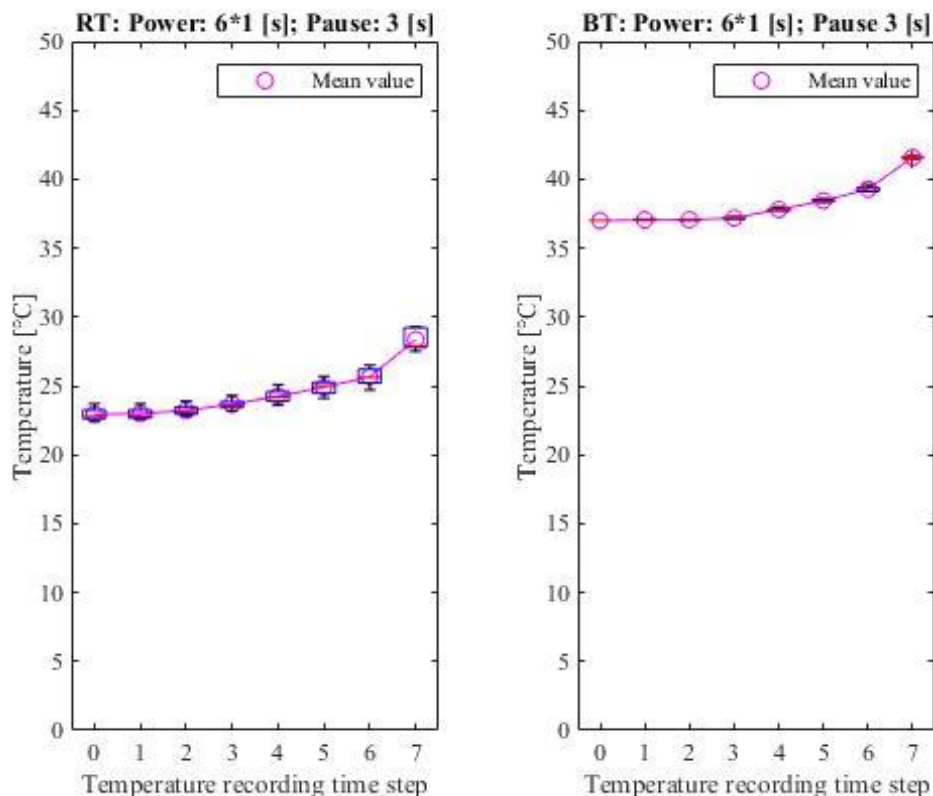


Figure 31 Illustration of electromagnetic coil temperature evolution with respect to an increasing number of implant detachment cycles (= power supply impulses). Measurements at eight time-steps ( $T_{x \in [0;7]}$ ) were performed: initial coil temperature ( $T_0$ ), temperature after each of 6 pulses, and the maximum coil temperature reached after a time delay of  $\sim 2$  s ( $T_7 = T_{max}$ ) (time steps for measurements  $T_{x \in [0;6]} \neq$  time steps to measurement  $T_7$ ). For each protocol,  $n = 5$  trials were performed. Magenta circles and linking line indicate mean values of all measurement sets at temperature recording time  $x$ . Left: starting from room temperature  $T_{room} = 22.9 \pm 0.5^\circ\text{C}$ , right: starting from body temperature  $T_{body} = 37.0 \pm 0.0^\circ\text{C}$ .

*Continuous operation – Measurement of powering duration and maximum temperature:* To derive permanent operation related effects (such as for proper traction of tissue portions and clear exposure of dissection site), the admissible duration of power supply to rise the coil temperature by  $1.0^\circ\text{C}$  (starting from the body temperature ( $T_{body} = 37.0^\circ\text{C}$ )) was assessed. A mean operation duration of  $8123.6 \pm 1427.6$  ms was measured to heat up the coils by  $1^\circ\text{C}$ , while a mean maximum final temperature of  $T_{max}^{continuous} = 44.1 \pm 1.5^\circ\text{C}$  was determined over all test cycles  $n = 10$ .

*Thermal shielding:* The results from the heating assessment were used to calculate the required isolation width of a heat shielding encapsulation. Therefore, the admissible inner and outer wall temperatures had to be defined. With respect to safety-critical dimensioning, the maximum mean measured coil temperature  $T_{max}^{continuous} = 44.1 \pm 1.5^\circ\text{C}$  was rounded up to  $T_{inner\ wall} = \sim 46.0^\circ\text{C}$ . The admissible outer wall temperature of the application device was set to  $T_{outer\ wall} = \sim 37.0^\circ\text{C}$  (to obviate tissue damage also in case of direct applicator wall contact).

During heat transfer through a wall, different phenomena, namely convection, radiation and conduction, occur [92]. For a first approximation, the problem was simplified assuming direct contact between coil and encapsulation wall. Convection, radiation, and interfacial heat transfer phenomena were neglected for the time being. Furthermore, the polymer wall was assumed to be isotropic with respect to heat conduction properties. A current-carrying conductor, supplied by a continuously uniform energy, reaches a state of equilibrium at an elevated temperature, in which the heat transfer rate ( $\dot{Q}$ ) corresponds to the electrical power ( $P_{el}$ ) absorbed [equation V]. Although the maximum temperature was measured directly after the coil had been deactivated, thus  $P_{el}$  being 0 W, an enduring, continuous power of  $P_{el} = 3 [A] * 24 [V]$  at 46.0°C was assumed for the calculations. This approach was chosen to avoid under dimensioning of the heat shielding entity. Furthermore  $\dot{Q}$  was assumed to be steady. By using the equation for heat transfer through a cylindrical wall [equation VI] [93] derived from Fourier's heat equation [equation IV] [93], a required wall thickness  $\Delta r = r_2 - r_1$  was calculated, with  $\dot{Q}$  representing the amount of heat transferred over a certain time,  $A_Q$  being the cross-sectional area and  $k$  the material specific conductivity, with  $k \in [0.1 \frac{W}{m \cdot K}; 0.5 \frac{W}{m \cdot K}]$  for most polymers [93]. For the calculations, the upper limit value for safety reasons  $k = 0.5 \frac{W}{m \cdot K}$  was used.  $L$  is the cylinder length active for heat conduction with  $L = 15.0$  mm,  $\Delta T$  the temperature gradient over wall thickness with  $T_1 = 46.0^\circ C$  and  $T_2 = 37.0^\circ C$ ,  $r_1 = \frac{6.4 [mm] + 0.3 [mm] * 6}{2} = 4.1 [mm]$  the outer coil radius (including 3 layers of windings with a wire diameter of 0.3 mm) and  $r_2$  the outer encapsulation wall radius. Inserting all variables into the equations yields:

$$(IV): \dot{Q} = \frac{Q}{\Delta t} = -k * A_Q * \frac{\Delta T}{dr} = -2 * k \pi r L \frac{\Delta T}{dr}$$

$$\dot{Q} \int_{r_1}^{r_2} \frac{1}{r} dr = -2k\pi L \int_{T_1}^{T_2} dT$$

$$\dot{Q} * (\ln(r_2) - \ln(r_1)) = -2k\pi L (T_2 - T_1)$$

$$(V): \dot{Q} = P_{el} = U * I$$

$$(VI): P_{el} = \dot{Q} = \frac{2k\pi L (T_1 - T_2)}{\ln(\frac{r_2}{r_1})}$$

Solving for  $r_2$  led to the following equation and a required shielding wall thickness of 0.024 mm.

$$r_2 = r_1 * e^{\frac{2k\pi l (T_1 - T_2)}{P_{el}}} = 4.1 [mm] * e^{\frac{2 * 0.5 [\frac{W}{m \cdot K}] * \pi * 15 [mm] * (9.0 [K])}{24 [V] * 3 [A]}} =$$

$$4.1 [mm] * e^{5.89 * 10^{-3}} = 4.124 [mm]$$

$$\Delta r = r_2 - r_1 = 4.124 [mm] - 4.1 [mm] = 0.024 [mm]$$

## 5.2.4 Resumé

The following findings emerged from the research for suitable mechanisms to realize basic, key tasks of endoluminal manipulation (see Table 1). The most promising solutions were applied to the development of a novel patient-adaptable, single-use, endoscopic device to allow the creation of inverting end-to-end anastomosis.

Thesis	Result
<b>Characterization of the biological environment with respect to procedure related tasks:</b>	
<ul style="list-style-type: none"> <li>How powerful needs the manipulator to be, to allow for closing a bowel piercing anastomosis implant?</li> </ul>	<ul style="list-style-type: none"> <li>Piercing colon tissue with implants of 4, 8, 12 spikes required average forces of about <math>6.4 \pm 1.5</math> N, <math>13.6 \pm 1.4</math> N, <math>21.7 \pm 5.8</math> N. Thus, a minimum force of 28 N should be feasible.</li> </ul>
<ul style="list-style-type: none"> <li>Looking at the required piercing forces, which design parameters influence the implant closing process?</li> </ul>	<ul style="list-style-type: none"> <li>Among the groups compared within the scope of this work, the variations in piercing velocities <math>v = 5, 10, 15 \text{ mms}^{-1}</math> and accelerations of <math>a = 5, 10, 15 \text{ mms}^{-2}</math> did not show a statistically significant difference in piercing forces.</li> <li>Between the groups compared within the scope of this work, there was no statistically significant difference of piercing forces observed with respect to variations in the fixation point arrangement.</li> <li>The piercing forces increased statistically significantly with increasing number of implant spikes.</li> </ul>
<ul style="list-style-type: none"> <li>Which order of magnitude should be considered for the development of the endoscopic system components?</li> </ul>	<ul style="list-style-type: none"> <li>The outer device diameter should cover a range between 24.1 mm to 40.1 mm.</li> <li>The implant compression gap should cover a range between 2.8 mm to 4.8 mm.</li> </ul>
<b>Finding a mechanism to endoluminally grab, manipulate and to adjust colon edges in an inverted manner:</b>	
	<ul style="list-style-type: none"> <li>Using suction forces allowed to reliably grab and manipulate bowel.</li> <li>Adjusting vacuum channel outlets, integrated into the implant mounts of the applicator, towards the intestinal wall, allowed to invert, and grab tissue margins, by covering air channel outlets with the bowel wall.</li> </ul>

<p><b>Finding a mechanism to adjust the manipulator platform to a patient individual lumen diameter considering the following features:</b></p>	
<ul style="list-style-type: none"> <li>• <i>Apply radial forces at the endoscope tip to support implant scaling</i></li> <li>• <i>Allow congruent expansion of both applicator units</i></li> <li>• <i>Enable a complete and controlled collapse after implant delivery</i></li> </ul>	<ul style="list-style-type: none"> <li>• Hydraulic units allowed consistent behavior in terms of force application for arbitrary shaft lengths and shapes, as well as controlled and distinctively constrained actuation and expansion by limiting the maximum hub.</li> <li>• Hydraulics were less susceptible to local variations in tissue compliance (affecting the expansion behavior of the intestine), than the balloon based expansion mechanisms.</li> <li>• The integration of bleeding valves into the hydraulic units, fabricated by additive manufacturing, allowed to avoid air related disturbance of operation (smoother and enhanced actuation and retraction response).</li> </ul>
<ul style="list-style-type: none"> <li>• <i>Ensure parallel orientation of the implant compression faces and equivalent distance between implant halves in unexpanded state, and for both expansion configurations</i></li> </ul>	<ul style="list-style-type: none"> <li>• Assembling applicator arms by scissor joints to the hydraulics, allowed to realize parallel orientation of the mounted implant compression faces and to maintain a fixed distance between the implant halves for both expansion states.</li> </ul>
<p><b>Finding a mechanism to close an implant considering the following features:</b></p>	
<ul style="list-style-type: none"> <li>• <i>Enable the application of forces at the endoscope tip to pierce tissue</i></li> </ul>	<ul style="list-style-type: none"> <li>• Hydraulics and spring based approaches, both allowed to successfully pierce through two layers of colon tissue and close a dummy implant with twelve spikes</li> <li>• Hydraulics allowed more distinctive control and application of axial forces during the closing process, encouraging the use of an implant with a compression gap that is adjustable to the patient specific tissue thickness.</li> </ul>
<ul style="list-style-type: none"> <li>• <i>Ensure axial congruence of the implant halves</i></li> </ul>	<ul style="list-style-type: none"> <li>• A snap connection between the oral and aboral endoscopic applicator units can be a space and force saving mechanism to freeze relative orientation to one another and support axial congruence during the implant closure process.</li> </ul>
<p><b>Finding a power-efficient mechanism to detach an implant from the manipulator:</b></p>	
	<ul style="list-style-type: none"> <li>• The integration of electromagnets into an endoscopic anastomosis device allowed to</li> </ul>

	<p>reproducibly detach an implant from the oral and the aboral applicator units.</p> <ul style="list-style-type: none"> <li>• Risk assessment revealed that heating effects related to continuous and pulsed operation scenarios may be shielded effectively by polymeric isolation to avoid tissue damage.</li> </ul>
--	--

Table 1 The table summarizes the findings focusing on the realization of basic key issues of endoluminal manipulation, related to the task of endoscopically anastomosing two colon endings.

### 5.3 Design of a scalable, single-use endoscopic device for the creation of inverting, end-to-end anastomoses

A concept for a 3D-printed endoscopic, scalable end-to-end anastomosis device was derived, prototypically realized and mechanically evaluated with respect to relevant tasks of endoscopic anastomosis formation (see Figure 32). The prototype is illustrated in Figure 33.

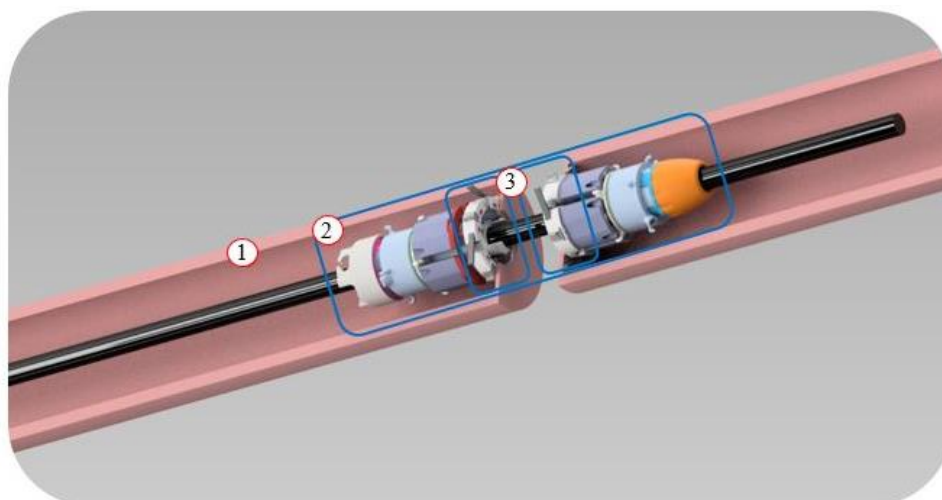


Figure 32 Schematics of the final concept of a single-use, scalable, endoscopic anastomosis applicator unit for single-side access, inserted in the bowel (1). The system comprises an oral and an aboral applicator unit (2) with mounted implants (3) and can adopt three size configurations.

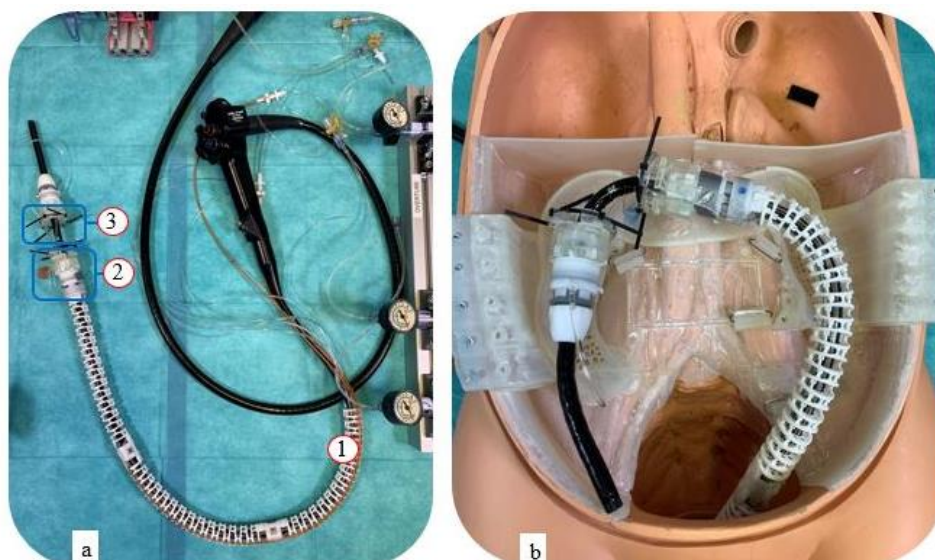


Figure 33 a) Illustration of the final prototype mounted onto an endoscope. An overtube (1) was manufactured from SLS (which is not further specified within the scope of this thesis). The applicator head (2) and implant (3) were manufactured from SLA. b) Illustration of the final prototype within a colon model.

In the following, device specifications are explained in detail with reference to the respective procedure tasks.

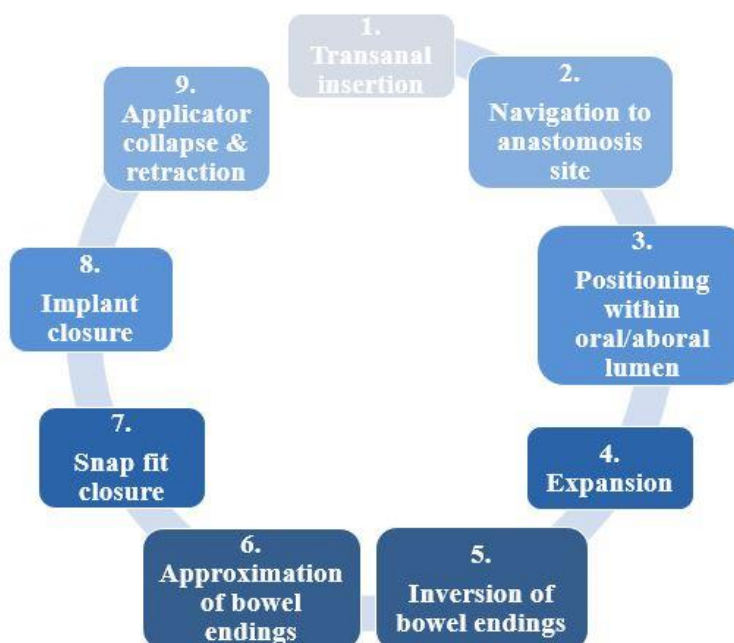


Figure 34 Diagram of the endoscopic anastomosis procedure.

The anastomosis device was designed to be inserted transanally (see Figure 34 procedure step 1), navigated to the anastomotic site (see Figure 34 procedure step 2) and be positioned within the oral and aboral bowel lumina (see Figure 34 procedure step 3). The system comprised two units that can move independently of each other. The components were realized according to an over-the-tube design, to fit on a 11 mm diameter measuring shaft, so it can be used with conventional gastroscopes and small size colonoscopes. While the aboral entity had to provide

linkage to the handling unit (i.e. by an overtube) and be axially movable with respect to the endoscope, the oral applicator head was fixed to the shaft just below the steerable tip. Choosing this position, any restriction of the endoscope tip range of motion, which determines unhindered navigation through the colon [94], had to be avoided. Fixation of the oral component to the endoscope was realized by the friction-locked mechanism (Figure 35), which was profoundly assessed in *chapter 4.3.1.1 Fixation of oral applicator unit to the endoscope*. A mechanical snap connection interface, locking against rotation and axial displacement, was used to attach the hydraulic cylinder unit of expansion stage 1 to the fixation screw cap (see Figure 35).

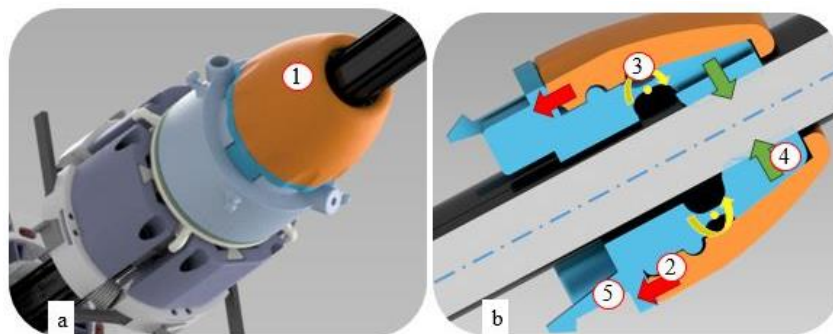


Figure 35 Friction-based fixation (1) of the oral applicator head to the endoscope shaft by using eight cantilevers symmetrically arranged around the circumference. The cap converges conically on the inside and by locking the thread connection (2) between core and compression cap, the cantilevers bend to the center (3) acting with a clamping force radially on the endoscope (4). The oral expansion hydraulics are assembled to the cap via a snap fit connection (5).

The expansion units were the core elements of the device. They had to congruently expand the two implant halves, from their collapsed minimal diameter (during navigation), to a larger diameter at the anastomotic site. To address a range of variations in patient individual colon lumen diameters, the mechanism was supposed to provide three different configurations (unexpanded state, expansion state 1 and expansion state 2). Precise actuation independently of the endoscope shaft shape was an essential requirement, to use the device at arbitrary points within the colon. Thus, the applicator units were designed as single-acting, double telescopic hydraulics (see Figure 36) with two cylinder shells being nested inside each other. While the first stage of expansion was supplied via the cylinder base, the feed line to the second stage was routed through its respective piston to maintain tightness of the first expansion unit. Polyurethane hoses (Polyurethan tube, mm, 10 bar, 50 m Rolle ESSKA.de GmbH, Hamburg, Germany) with an inner- $\emptyset$  of 2 mm, an outer- $\emptyset$  of 3 mm and a maximum operating pressure of 10 bar [95] were used as hydraulic supply lines. For the first expansion stage, the green cylinder was actuated, and for the second stage the beige piston was levered (see Figure 36).

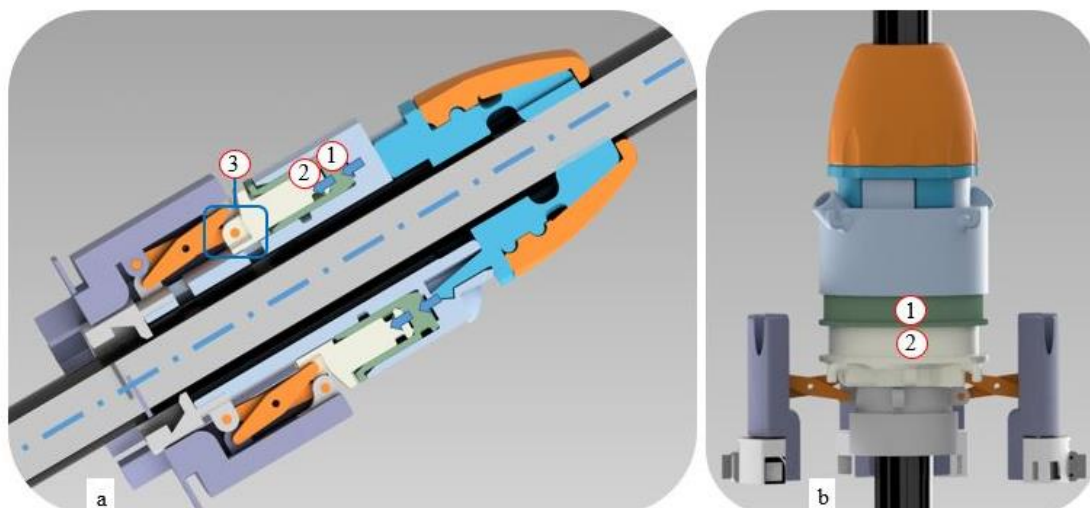


Figure 36 a) Longitudinal cut through the oral expansion unit, which comprises two hydraulic cylinders and pistons. Actuating the hydraulic pistons (1, 2) pushes the joint (3) upwards and allows to expand the applicator arm. b) Illustration of the oral two-stage telescope hydraulics in expanded configuration.

The applicator blades with integrated air channels were assembled to the hydraulic units by means of scissor joints. They carried the rigid segments of the implant. By this means, the orientation, the angulation and the distance between implant compression faces remained constant for unexpanded state and all expansion configurations (see Figure 37).

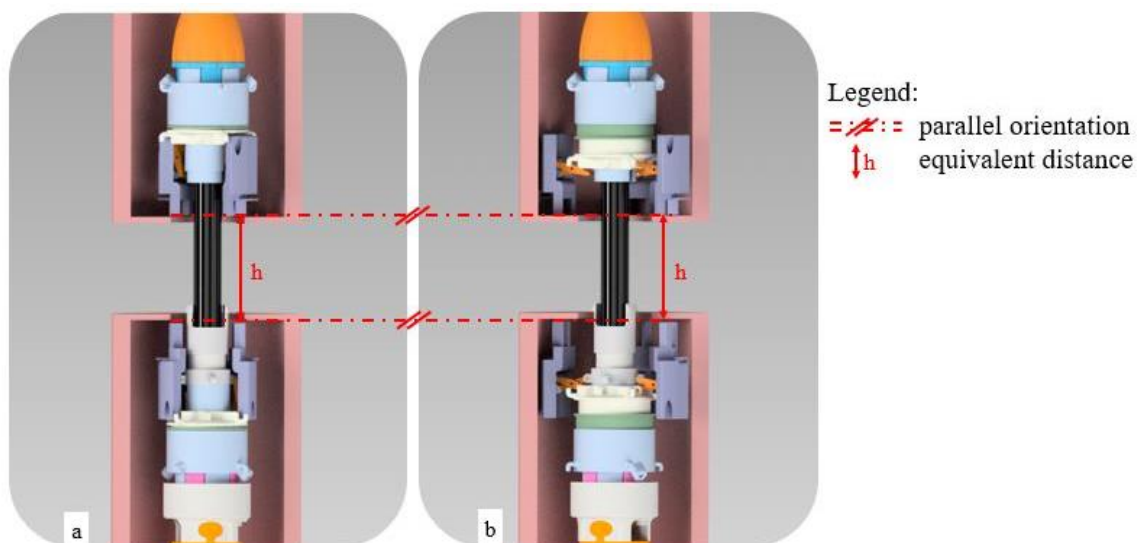


Figure 37 X-kinematics attaching applicator arms to the hydraulics to ensure parallel orientation of the mounted implant compression faces and maintain a fixed distance between the implant halves for all size configurations. a) Unexpanded device, b) Expanded applicator.

This feature was furthermore implemented to expand the applicator arms to the bowel wall and tension, invert and fold the tissue over the implant to the suction channel outlets (see Figure 34 procedure step 4 & 5).

End stops were integrated into the hydraulic cylinders to ensure a controlled and congruent maximum expansion for both configurations, as well as to prevent the gliding bodies from slipping out of the respective cylinder shells. Therefore, the expansion cylinders and piston

were engaged by a pin running in a meander-shaped groove, which consisted of alternating vertical and horizontal sections (see Figure 38). While the vertical sections provided guidance during relative axial displacement and prevented from rotation between the hydraulic elements, the horizontal sections limited the maximum displacement, which was 4.2 mm for the first expansion state and 4.5 mm for the second state (total displacement of the expansion hydraulics: 8.7 mm). The expansion states had to be actuated in the correct sequence (1<sup>st</sup> stage: cylinder into cylinder; 2<sup>nd</sup> stage: piston into cylinder), and had to be retracted vice versa.

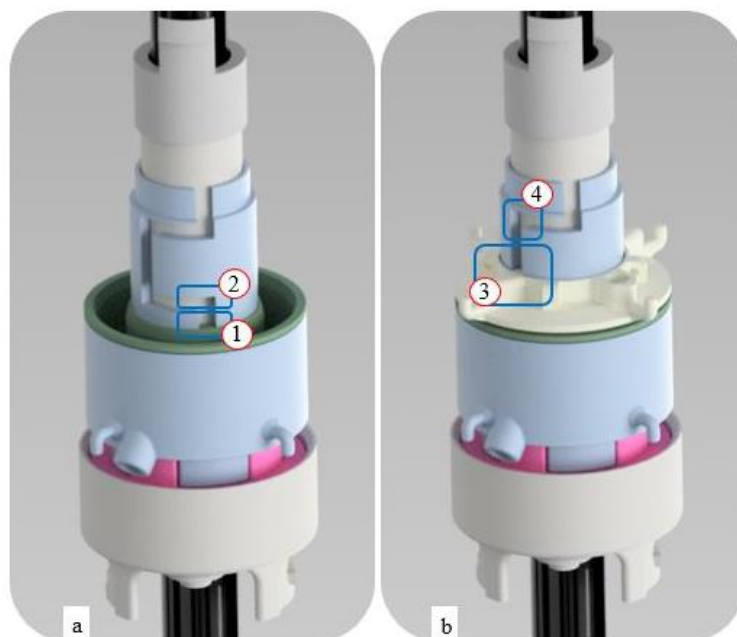


Figure 38 Illustration of the axially running nose-groove (1, 3) pairing between hydraulic cylinder and piston to avoid rotation. Horizontal segments (2, 4) of the grooves serve as end stops limiting the maximum hub and thus maximum expansion. a) Illustration of engaged nose-groove guidance of the hydraulic cylinder and piston of expansion state 1, and b) Illustration of engaged nose-groove guidance of the hydraulic cylinder and piston of expansion state 2.

In order to enable smooth and accurate actuation, as well as to provide the possibility to collapse the expanded applicator head after the implant has been delivered, bleeding valves were integrated into all hydraulic units via a core hole with a diameter of 1.6 mm. A M2 thread was cut into the socket and sealing was achieved by means of an O-ring (1.5 x 1 mm, NBR, 70A) (Landefeld Druckluft & Hydraulik GmbH, Kassel, Germany), which was pressed against the flange by screwing in a flat head screw (M2 x 5 mm, stainless steel).

To approach the two lumen endings and form the anastomosis, the oral and aboral applicator units are brought together, by pulling the endoscope back and pushing the overtube forward (see Figure 34 procedure step 3 and step 6). The connecting element (see Figure 40) described in chapter 4.2.2.3 *Snap connector for axial congruence of applicator units* was integrated into the applicator units and closed (see Figure 34 procedure step 7) to ensure axial congruence between the entities during implant closure. The male part, integrated into the aboral applicator entity, served as an end stop for the actuation of another hydraulic unit, that was used to pierce the tissue and close the implant (see Figure 34 procedure step 8). To the piston of this hydraulic

closing unit, the cylinder bottom of the aboral expansion unit 1 (blue cylinder in Figure 39) was fixed by means of a mechanical snap connection interface. The connector was designed to lock against rotation and axial displacement.

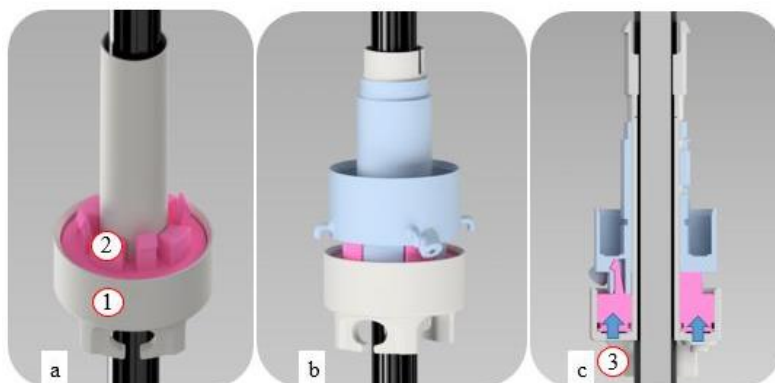


Figure 39 Hydraulic unit of the aboral applicator head used to close an implant, comprising a cylinder (1) and a piston (2). The unit is dimensioned to transmit an axial force of 93.5 N with a pressure of 2 bar to lift (3) the piston. a) Cylinder and piston of hydraulic closing unit, with attached cantilevers, to connect the expansion hydraulics of the aboral applicator unit. b) Illustration of the hydraulic closing unit attached to the cylinder of expansion stage 1 and c) axial cut through the configuration.

A puzzle clip was positioned at the bottom of the axial hydraulic cylinder (in orientation to a system developed by Dr. Daniel Roppenecker [96]), to enable modular connection to an overtube handling unit.

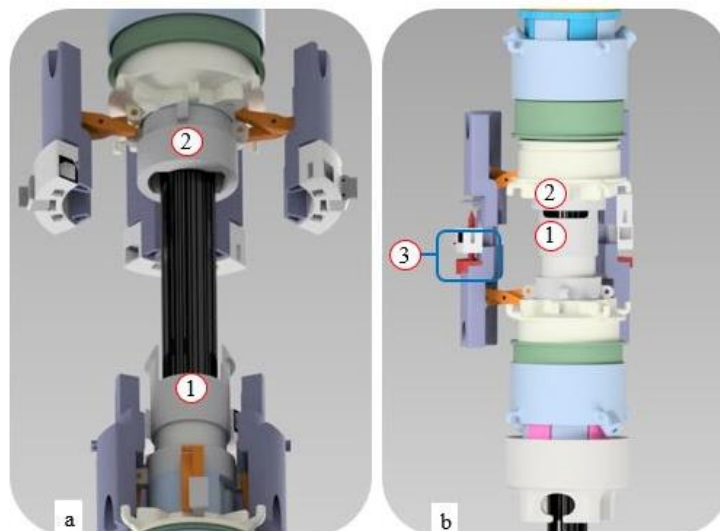


Figure 40 Illustration of the snap fit closure between oral and aboral applicator heads to achieve axial alignment between the implant's coupling elements. Illustration a) shows the open, and b) the closed connection. The male connector part is attached to the aboral applicator unit (1) and the female, receiving unit (2) is part of the oral applicator. The implant is mounted on the applicator blade by a form-fit interface (3).

Despite the promising results observed for implant detachment by means of electromagnets, this approach was not integrated in the present applicator concept. Instead, a form-fit connection between applicator blade and implant was designed to decouple by collapsing the expansion unit after anastomosis formation (see Figure 34 procedure step 9). Adjacent to the vacuum

channels, a carrier was positioned projecting radially to the outwards, that engaged into a pocket in each of the implant closing segments (see Figure 25).

*Manufacturing:* The assembly parts of the applicator were manufactured using Formlabs' stereolithographic process. Thin-walled hydraulic components were printed with Rigid4000, which is especially characterized by its smooth, polished finish, stiffness, and strength. It is recommended for general load-bearing applications [97]. Compliant structures, such as snap connections (i.e. the connector between applicator units to ensure axial congruence, the connecting element between hydraulic cylinders and the fixation cap (oral) or the connecting element between the hydraulic expansion cylinder and the hydraulic implant closing unit (aboral)) etc. were manufactured from Tough1500 and components with particularly critical accuracy requirements (e.g. threads) with Standard Resins. The gliding partners of the applicator arms (blade and slide) were printed with the Formlabs Standard White Resin, due to its favorable surface finish and gliding properties [75]. The connecting struts were printed from Tough1500 to reduce the risk of breakage of the filigree pins [86]. All components were printed with the highest accuracy possible using  $50 \mu\text{m}$  layer thickness. For any cylinder, the vertical axis was arranged orthogonal to the building platform, keeping functional surfaces free of support structures. Eyelets, bore holes and openings were manually rinsed after washing and, if necessary, reamed. In the final step, the components were post-hardened [98, 99].

## 5.4 Results of mechanical assessment

### 5.4.1 Results: Handling concept of final applicator prototype

#### 5.4.1.1 Friction based fixation of oral applicator unit to the endoscope

The design of the fixation cap allowed to attach the oral applicator unit to the endoscope. The cap did not slip in any of the tests. Instead, the suture material failed first (plastic deformation/tearing). Thus, a minimum mean measured attachment force over all samples of  $F_{oral\ fixation}^{mean} = 54.8 \pm 2.0 \text{ N}$  was determined.

#### 5.4.1.2 Grasping tissue using suction

Each applicator blade comprised two vacuum channels, which were connected to a suction pump (Medela Basic suction pump, Medela Medizintechnik GmbH & Co. Handels KG, Dietersheim, Deutschland). The holding forces realizable by the suction mechanism were calculated. The total suction surface of every applicator blade on the oral side was  $5.7 \text{ mm}^2$  and on the aboral side  $5.4 \text{ mm}^2$ , with  $p_{suction} = -80 \text{ kPa}$  (rel. to atm). The force was related to the pressure and respective surface area,

$$\text{(VII): } F_{grasp} = p_{suction} * A_{suction}$$

resulting in a grasping force per blade of

$$F_{grasp}^{oral\ blade} = 0.08 \frac{\text{N}}{\text{mm}^2} * 5.7 \text{ mm}^2 = 0.5 \text{ N and}$$

$$F_{grasp}^{aboral\ blade} = 0.08 \frac{N}{mm^2} * 5.4 mm^2 = 0.4 N$$

and per applicator head (with four blades) of 2.0 N and 1.6 N respectively.

## 5.4.2 Results: Patient adaptation of final applicator prototype

### 5.4.2.1 Modeling expansion forces

The expansion forces for the developed hydraulic units were modeled in order to determine the feasible forces for an implant expansion and to evaluate the suitability of the scissor kinematics for this application. Furthermore, it allowed to derive design specifications for the implant expansion mechanism. The aboral and oral expansion units were designed and dimensioned identically, which is why results were transferred from one unit to the other. For the hydraulic piston of the first expansion state, pressure acts on a surface of  $340.1 mm^2$  and for the second piston on a surface of  $237.5 mm^2$ . A syringe pressure of 2 bar was measured with the Olympus MAJ-1381 (Olympus MaxPass Inflation Device, Single Use, MAJ-1381, Olympus, Tokyo, Japan). The actuation force  $F$  of an hydraulic unit results from the multiplication of the hydraulic medium pressure  $p$  acting on the surface area  $A$  ( $F = p * A$ ) [100].

This resulted in total “expansion (exp) hydraulics (hydr)” actuation forces for both cylinder units of  $F_{exp\ hydr}^{total\ stage\ z}$  (stage  $z=1$  or stage  $z=2$ ). These were identical for the oral and aboral applicator heads, due to the symmetrical design.

$$F_{exp\ hydr}^{total\ stage\ 1} = p_{hydraulics} * A_{exp\ hydr}^{stage\ 1} = 0.2 \frac{N}{mm^2} * 340.1 mm^2 = 68.0 N$$

$$F_{exp\ hydr}^{total\ stage\ 2} = p_{hydraulics} * A_{exp\ hydr}^{stage\ 2} = 0.2 \frac{N}{mm^2} * 237.5 mm^2 = 47.5 N$$

A hydraulic force of 68.0 N was derived for the first cylinder, and a force of 47.5 N for the second cylinder.

For the first hydraulic cylinder (1<sup>st</sup> expansion state) the angle  $\varphi_1$  ran between  $\varphi_1 = [39.6^\circ, 77.4^\circ]$ .

For the second hydraulic cylinder (2<sup>nd</sup> expansion state)  $\varphi_2$  ran between  $\varphi_2 = [15.9^\circ, 39.6^\circ]$ .

In the following image all bearing and externally acting forces are illustrated. Fixed bearings transmit forces in x- and y- direction, while floating bearings only transmit forces perpendicular

to the free movement direction. The applicator arm was divided into three subunits (see Figure 41), for which forces and momentum equilibria were established.

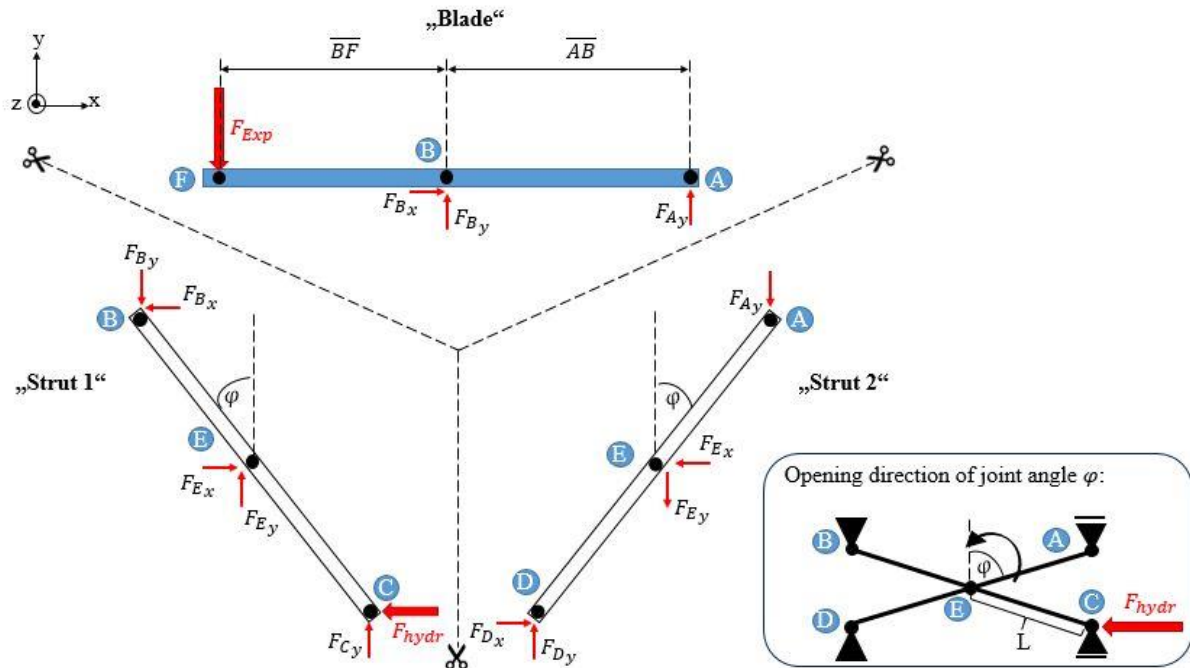


Figure 41 Illustration of all bearing and externally acting forces. The system is composed of three parts: strut 1, strut 2 and the blade, for which force and momentum equilibria are defined. Furthermore, the opening direction of the joint angle is indicated by  $\varphi$ .

$F_{hydr}$  was given and  $F_{exp}$  was sought. The equation system was solved by means of the forces and moment equilibria.

“Blade”

$$(VIII): \rightarrow \sum F_{i,x} = 0; F_{Bx} = 0$$

$$(IX): \uparrow \sum F_{i,y} = 0; F_{By} + F_{Ay} - F_{exp} = 0 \leftrightarrow F_{exp} = F_{Ay} + F_{By}$$

$$(X): \curvearrow \sum M_{i,z}^F = 0; F_{Ay} * (\overline{BF} + \overline{AB}) + F_{By} * \overline{BF} = 0$$

$$\leftrightarrow F_{By} = -F_{Ay} * \left(1 + \frac{\overline{AB}}{\overline{BF}}\right)$$

“Strut 1”

$$(XI): \rightarrow \sum F_{i,x} = 0; F_{Bx} + F_{Ex} - F_{hydr} = 0 \leftrightarrow F_{Ex} = F_{hydr}$$

$$(XII): \uparrow \sum F_{i,y} = 0; -F_{By} + F_{Ey} + F_{Cy} = 0 \leftrightarrow F_{By} = F_{Ey} + F_{Cy}$$

$$(XIII): \curvearrow \sum M_{i,z}^C = 0; -F_{Ey} \sin \varphi L - F_{Ex} \cos \varphi L + F_{By} 2 \sin \varphi L = 0$$

$$\leftrightarrow F_{Ey} = 2F_{By} - \frac{F_{hydr}}{\tan \varphi}$$

“Strut 2”

$$(XIV): \rightarrow \sum F_{i,x} = 0; F_{D_x} - F_{E_x} = 0 \leftrightarrow F_{E_x} = F_{D_x} = F_{hydr}$$

$$(XV): \uparrow \sum F_{i,y} = 0; F_{D_y} - F_{E_y} - F_{A_y} = 0 \leftrightarrow F_{D_y} = F_{E_y} + F_{A_y}$$

$$(XVI): \cup \sum M_{i,z}^D = 0; -F_{E_y} \sin \varphi L + F_{E_x} \cos \varphi L - F_{A_y} 2 \sin \varphi L = 0$$

$$\leftrightarrow F_{E_y} = \frac{F_{hydr}}{\tan \varphi} - 2F_{A_y}$$

The expressions for  $F_{E_y}$  were equated: (XIII) = (XVI)

$$2F_{B_y} - \frac{F_{hydr}}{\tan \varphi} = \frac{F_{hydr}}{\tan \varphi} - 2F_{A_y}$$

Finally, equation (IX) was substituted into this transformed term, giving an expression for the expansion force  $F_{exp}$ .

$$F_{exp} = F_{B_y} + F_{A_y} = \frac{F_{hydr}}{\tan \varphi}$$

The expansion force  $F_{exp}$  was a function of the hydraulic actuation force (for expansion stage 1:  $F_{exp hydr}^{total stage 1}$  or stage 2:  $F_{exp hydr}^{total stage 2}$ ) and the changing dilatation angle  $\varphi$  (with  $\varphi_{initial}$  for minimal expansion and  $\varphi_{end}$  for maximal expansion of the respective hydraulic units 1 and 2).

According to the simplifications, the hydraulic actuation force distributed on one applicator arm corresponded to one fourth of the total hydraulic force of the cylinder unit ( $F_{exp hydr}^{arm} = \frac{1}{4} * F_{exp hydr}^{total}$ ).

For the hydraulic expansion stage 1 the realized force of one arm to expand the implant ( $F_{exp}^{initial/end stage 1}$ ) was calculated for the initial joint angle ( $F_{exp}^{initial stage 1}$  ( $\varphi_{initial}=77.4^\circ$ )) and the final joint angle ( $F_{exp}^{end stage 1}$  ( $\varphi_{end}=36.9^\circ$ )) by:

$$(XVII): F_{exp}^{initial/end stage 1} = F_{B_y} + F_{A_y} = \frac{\frac{1}{4} * F_{exp hydr}^{total stage 1}}{\tan(\varphi_{initial/end})}$$

For the hydraulic expansion stage 2 the realized force of one arm to expand the implant ( $F_{exp}^{initial/end stage 2}$ ) was calculated for the initial joint angle ( $F_{exp}^{initial stage 2}$  ( $\varphi_{initial}=36.9^\circ$ )) and the final ( $F_{exp}^{end stage 2}$  ( $\varphi_{end}=15.9^\circ$ )) joint angle by:

$$(XVIII): F_{exp}^{initial/end stage 2} = F_{B_y} + F_{A_y} = \frac{\frac{1}{4} * F_{exp hydr}^{total stage 2}}{\tan(\varphi_{initial/end}^{stage 2})}$$

The initial and final expansion forces are given for both expansion stages in the following table.

	$F_{exp}^{initial} [N]$	$F_{exp}^{end} [N]$
$\varphi_{initial/end}^{stage 1} = [77.4^\circ, 39.6^\circ]$	3.8	20.5
$\varphi_{initial/end}^{stage 2} = [39.6^\circ, 15.9^\circ]$	14.4	41.7

Table 2 Indication of realizable expansion forces for the initial and final joint angle  $\varphi$  of the applicator arm X-joint, for expansion stage 1 and expansion stage 2.

#### 5.4.2.2 Modeling bearing forces

The suitability of the implant mounting position was assessed by determining the resulting leverage effects on the applicator arm. For this purpose the bearing forces in A were calculated by means of a momentum equilibrium around joint B at the blade.

$$(XIX): \cup \sum M_{i,z}^B = 0; F_{Ay} * \overline{AB} + F_{exp} * \overline{BF} = 0 \leftrightarrow$$

$$\leftrightarrow F_{Ay} = -F_{exp} * \frac{\overline{BF}}{\overline{AB}}$$

While the distance  $\overline{BF}$  remained constant, the distance  $\overline{AB}$  was shortened with increasing degree of expansion. Thus,  $\overline{AB}$  can be expressed as a function of  $\varphi$ .

An axis through the hinge point E, running orthogonal to the endoscope, exactly bisected the distance between the joints A and B ( $\overline{AB}$ ). With this condition, the following relationship was derived to describe the distance  $\overline{AB}$ , depending on the changing angle  $\varphi$ :

$$(XX): \overline{AB} = 2 \sin \varphi L$$

Inserting equation (XX) into equation (XIX), and using the results from Table 2 for the expansion forces (calculated with (XVII) and (XVIII)), the following relationship for the bearing force in A ( $F_{Ay}^{initial/end}^{stage 1}$ ) was derived for expansion hydraulics stage 1 for the initial joint angle ( $F_{exp}^{initial}^{stage 1}(\varphi_{initial}=77.4^\circ)$ ) and the final ( $F_{exp}^{end}^{stage 1}(\varphi_{end}=36.9^\circ)$ ) joint angle by:

$$(XXI): F_{Ay}^{initial/end}^{stage 1} = -F_{exp}^{initial/end}^{stage 1} * \frac{\overline{BF}}{2 \sin(\varphi_{initial/end}^{stage 1})L} =$$

$$-\frac{\frac{1}{4} * F_{exp}^{total}^{stage 1}}{\tan(\varphi_{initial/end}^{stage 1})} * \frac{\overline{BF}}{2 \sin(\varphi_{initial/end}^{stage 1})L}$$

The bearing force  $F_{Ay}^{initial/end}^{stage 2}$  for expansion hydraulics stage 2, for the initial joint angle ( $F_{exp}^{initial}^{stage 2}(\varphi_{initial}=36.9^\circ)$ ) and the final ( $F_{exp}^{end}^{stage 2}(\varphi_{end}=15.9^\circ)$ ) joint angle was calculated by:

$$(XXII): F_{Ay}^{initial/end^{stage 2}} = -F_{exp}^{initial/end^{stage 2}} * \frac{\overline{BF}}{2 \sin(\varphi_{initial/end}^{stage 2})L} =$$

$$-\frac{\frac{1}{4} * F_{hydr}^{total^{stage 2}}}{\tan(\varphi_{initial/end}^{stage 2})} * \frac{\overline{BF}}{2 \sin(\varphi_{initial/end}^{stage 2})L}$$

The length  $\overline{BF}$  was 10.45 mm and L was 6.2 mm. By inserting the boundaries of  $\varphi_{initial/end}^{stage 1}$  and  $\varphi_{initial/end}^{stage 2}$  the following forces in  $F_{Ay}$  were calculated, depending on the expansion force.

	$F_{Ay}^{initial} [N]$	$F_{Ay}^{end} [N]$
$\varphi_{initial/end}^{stage 1} = [77.4^\circ, 39.6^\circ]$	-3.3	-27.1
$\varphi_{initial/end}^{stage 2} = [39.6^\circ, 15.9^\circ]$	-19.0	-128.3

Table 3 Indication of bearing forces in point A for the initial and final joint angle  $\varphi$  of the applicator arm X-joint, for expansion stage 1 and expansion stage 2.

$F_{Ay}$  had a negative value as it acted in opposite direction of the expansion force  $F_{exp}$ . Like the expansion force, the bearing force in A increased with increasing degree of expansion.

### 5.4.3 Results: Anastomosis formation unit of final applicator prototype

The second hydraulic entity was designed to approximate the two applicator heads, pierce the tissue in the compression zone and connect the future implant. To achieve the required forces the hydraulic cylinder had an outer diameter of  $\varnothing = 30.0$  mm and the piston a surface area of  $467.6 \text{ mm}^2$ , resulting in an axial force of 93.5 N for 2 bar filling pressure.

$$F_{closing \text{ hydraulics}} = p_{hydraulics} * A_{closing \text{ hydraulics}} = 0.2 \frac{N}{\text{mm}^2} * 467.6 \text{ mm}^2 = 93.5 \text{ N}$$

For the defined assumptions, the balance of forces in the longitudinal direction of the endoscope axis indicated that the magnitude of the force  $F_{closing \text{ hydraulics}}$  was equal to the implant closure force  $F_{implant \text{ closure}} = 93.5 \text{ N}$ .

$$(XXIII): \rightarrow \sum F_{i,x}; \frac{1}{4} * F_{closing \text{ hydraulics}} - \frac{1}{4} * F_{implant \text{ closure}} = 0 \leftrightarrow$$

$$F_{closing \text{ hydraulics}} = F_{implant \text{ closure}}$$

## Discussion

### 6.1 Feasibility assessment of final concept with respect to procedure related mechanical requirements

The creation of anastomoses following resective interventions is one of the core challenges in abdominal surgery. Surgeons can choose from a considerable range of different techniques and

devices, all of which still show similar complication rates and shortcomings, especially with respect to the intraoperative trauma. For the development of future techniques, standardizing procedure and outcome, as well as minimizing trauma are of special interest. Thus, within this research work, a novel approach for an endoscopic anastomosis device was developed. The concepts were developed using the benefits of additive manufacturing.

To approach the challenging task of developing a novel endoscopic anastomosis instrument, the most relevant design criteria for the ideal procedure were derived from literature. This includes an inverting arrangement of the intestinal lumina to favor tissue healing, the end-to-end arrangement to save time and material, and the implant excretion after completed healing to restore bowel motility, which is why a compression implant based approach was chosen.

In order to provide the appropriate platform to accomplish this procedure, solutions addressing the key challenges of endoluminal manipulation were established within the scope of this thesis.

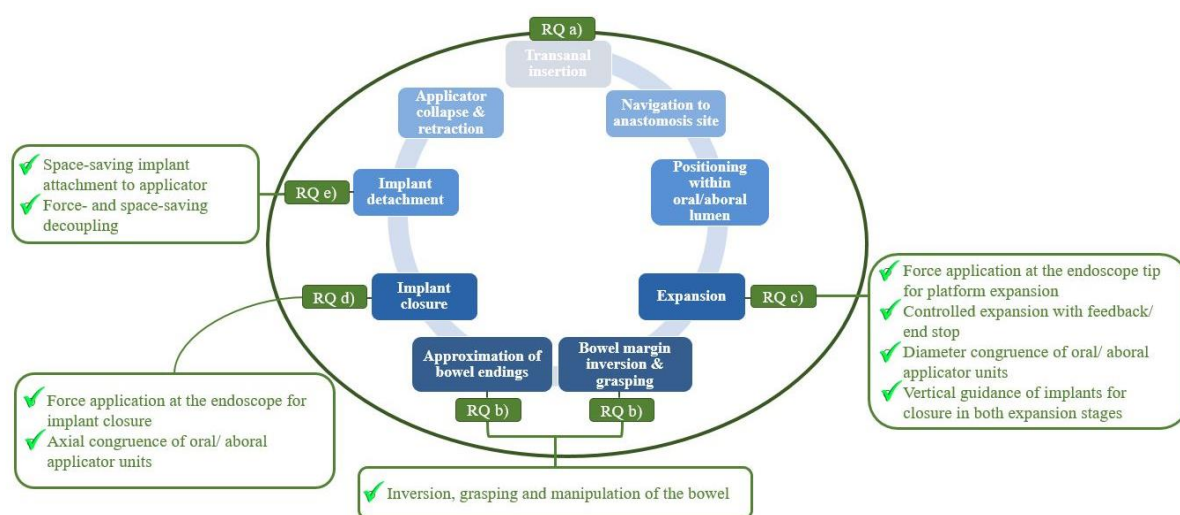


Figure 42 Illustration of procedure steps for the endoscopic anastomosis device. Supplementary, respective research questions that were answered within the scope of this project are indicated.

As it has been shown by others, adequate force application at the endoscope tip/operation situs is one of the biggest challenges during the development of endoscopic platforms [59, 61, 76–78], as their shaft is too flexible to establish high counter-forces [61] and as the endoscope might adopt different shapes during the intervention due to the curvatures and flexures of the colon.

In the following, the concept developed is discussed with regard to its suitability for the task of endoscopic anastomosis formation and its ability to meet the mechanical challenges outlined.

### 6.1.1 Tissue manipulation and handling

The respective manipulator is required to carry and deliver the implant. An essential prerequisite for the endoscopic navigation and manipulation is the visualization of the endoluminal path and surgical site, as well as aspiration and insufflation features of standard endoscopes. Thus, the device is designed as overtube solution to be mounted onto conventional

gastrosopes and small size colonoscopes, as this allows reduction of device complexity, costs and regulatory effort.

For the tasks of accurately positioning the applicator units within the respective lumen and for anastomosing bowel edges relative movement between the platform entities (and mounted implant halves) has to be enabled. Thus, the prototype includes one entity, which is able to move relatively along the endoscope (aboral) and one entity that is fixed to the endoscope (oral). In order to reliably maintain the position of the oral applicator unit during endoscopic navigation, it is crucial that the fixation mechanism withstands the axial forces acting in the context of colonoscopy. Based on the comparison of the holding force measured ( $F_{oral\ fixation}^{mean} = 54.8 \pm 2.0\ N$ ), to those forces derived from literature for axial push ( $\sim 11.6\ N$ ) and pull ( $\sim 10.7\ N$ ) movements occurring during colonoscopies in clinical practice [1], the clamping mechanism proves suitable attachment for endoluminal navigation.

The required ability to grasp and drag tissue is addressed by the integration of suction channels into the applicator arms, which are dilated towards the bowel wall. The surface areas of channel outlets are dimensioned to provide enough space for the implant mountings, but at the same time enough holding force to keep the tissue attached. Thus, they enable a suction force of 2.0 N orally, and 1.6 N aborally. This is set into relation to the forces applicable by state-of-the-art NOTES platforms. For example the instruments of the TransPort System enable a maximum manipulation force of 1 N (0.23 lb) (vs. 0.4 N (0.09 lb) for endoscopes) [61], the Scorpion-overtube robot allows to grab soft tissue with a force of 3 N for each of two grasper arms [101], and the flexible instrument of the ViaCath-System, which is an electronically remotely controlled master-slave system, can generate a tip force of 3 N. [59, 102]

Thus, the order of magnitude of applicable manipulation forces is comparable to that of the anastomosis device, which is why the use of suction forces for endoluminal tissue grasping purposes appears to be a suitable tool.

### 6.1.2 Expansion unit

As large variations in patient constitutions, between individuals as well as between colonic segments may occur, a scaling feature, that enables expansion of the anastomosis implant to approach the patient-individual lumen diameter, is integrated into the platform. The challenges of force application in flexible endoscopy are even increased if the endoscope is shaped around flexures. In order to provide a platform solution that is feasible for application in the entire colon, a space saving principle had to be established, which allows to apply forces directly at the endoscope tip. In the preliminary prototypic studies, the hydraulic units showed most promising results and allowed expansion in a controlled and congruent manner. This accounts for the requirement that the implant diameters must be of same size during the closure process.

By implementing a two-stage telescopic hydraulic entity with nested cylinders to minimize the required construction space, three different expansion stages can be realized.

The attachment of applicator arms to the hydraulics by scissor joints enables parallel orientation of the mounted implant compression faces and a constant distance between the implant halves for all size configurations, which is required to close the implant and adapt the compression gap to the tissue thickness. Modeling the realizable expansion forces with these kinematics shows that the efficiency significantly depends on the degree of expansion, indicated by the angle  $\varphi$ . Although the force of the premier hydraulic expansion cylinder ( $F_{hydr}^{total\ stage\ 1} = 68.0\text{ N}$ ) is significantly higher than the force of the second one ( $F_{hydr}^{total\ stage\ 2} = 47.5\text{ N}$ ), the maximum expansion force (41.7 N) is derived for the second stage and a minimum angle  $\varphi_{end}^{stage\ 2}$  (which corresponds to maximal arm expansion). The minimum realizable expansion force of 3.8 N occurred during actuation of hydraulic unit 1 for the maximum angle  $\varphi_{initial}^{stage\ 1}$  (which corresponds to the minimal arm expansion). This value also restricts the maximum admissible expansion force to dilate an implant and therefore gives guidance for the future implant design and dimensioning.

For the minimal expansion stage ( $\varphi_{initial}^{stage\ 1}$ ), the magnitude of the expansion force is greater than the magnitude of the bearing force in A ( $|F_{Ay}| < |F_{exp}|$ ). Conversely, the bearing force is significantly larger than the expansion force at maximum expansion ( $\varphi_{end}^{stage\ 2} \rightarrow |F_{Ay}| \gg |F_{exp}|$ ). This can be explained by the different lengths of the lever arms. While at minimum expansion, the lever arm  $\overline{AB}$  ( $\sim 12.1\text{ mm}$ ) is slightly longer than the distance  $\overline{BF}$  ( $\sim 10.45\text{ mm}$ ) ( $\overline{AB} > \overline{BF}$ ) and thus  $F_{Ay}$  must be smaller than  $F_{exp}$  for momentum equilibrium, this relationship reverses with increasing expansion (and the inversion of the lever arm length ratio) ( $\overline{AB} \ll \overline{BF} \leftrightarrow |F_{Ay}| \gg |F_{exp}|$ ).

These results provide information on the suitability of the position for the implant mounting (which equals to the point of application of the expansion force in the model). The bearing forces suggest that the implant suspension must be relocated towards the joint B to reduce the momentum and thus the bearing forces. In the model, friction forces between the gliding partners in the expansion hydraulics (cylinder/piston) were neglected. This seems to be a rather strong simplification, as in reality these are assumed to be high due to the manufacturing process inaccuracies [103]. However, since the results were primarily used as a guideline for evaluating the general suitability of the approach and to derive further specifications for the implant design, the simplified model is considered to be sufficiently valid.

### 6.1.3 Closing unit

In order to fit the implant halves together, the corresponding functional segments (expansion/closure) must be aligned with each other. This accounts for the requirements of an axially congruent configuration, which means that the mating implant elements must be maintained aligned throughout the closure process.

---

A snap connection is provided between the oral and aboral applicator unit, which is locked by pushing the aboral applicator unit (male connector) into the oral one (female counterpart) before the hydraulic closing unit is actuated. Since large frictional forces are to be expected during endoscopic interventions due to the extensive surface contact between the intestine and the endoscope, force transmission along the shaft is critical and demands a lot of effort. Thus, the required closing forces for the snap connection must be minimized. These were assessed experimentally for the integrated connector. A mean value of  $F_{snap\ closure}^{mean} = 15.2 \pm 1.0$  N was measured. This is comparable to those forces routinely applied by physicians during colonoscopies for axial push ( $\sim 11.6$  N) and pull ( $\sim 10.7$  N) movements [1]. It is therefore concluded, that the effort and feed force required are still in a reasonable range.

By using an implant, that pierces through the bowel wall and form-fittingly protrudes into an opposing counterpart, tissue can be prevented from slipping out of the compression zone and the compression gap can be adapted to adjust the healing pressure. Respective piercing forces must be applied by the applicator. To design an applicator unit, which is capable to meet these requirements, the colonic environment was biomechanically characterized with respect to procedure relevant parameters. The knowledge gained was translated into the concept and design of prototypes, which were experimentally assessed by evaluating the interaction with porcine colon tissue.

The biomechanical investigations revealed that among the compared parameters – piercing trajectories, tissue fixation point configurations and implant spike amounts – the number of piercing tips of the implant had the most significant impact on the required piercing forces. Variations in trajectory specification among the groups of piercing velocities ( $v = 5, 10, 15$  mms<sup>-1</sup>) and accelerations ( $a = 5, 10, 15$  mms<sup>-2</sup>) tested and compared within the scope of this work, did not lead to increased mechanical stability demands for the closing unit. Furthermore, it was observed that the fixation point arrangement, to grasp tissue with the applicator, did not have a statistically significant effect on the forces required to pierce the tissue. [5]

In contrary, an increase in spikes resulted in a statistically significant increase in piercing forces. This may be due to the fact that with increasing number of insertion bodies, the characteristic spike-tissue interaction force of each single body, occurring due to viscoelastic tissue response and frictional effects, accumulates [5]. Furthermore, since the tips were not distributed evenly over the entire circumference of the piercing body, but only within the segments, the density per segment increased with rising number of tips. Once the spikes contact the tissue surface, micro-injuries in the surface are created [104], which do act as anchor points. As spikes are pushed forward, indentation occurs [67, 69, 105]. Tissue tension is therefore increased between individual tips/attachment points. This pre-tensioning effect may contribute to the increase in insertion force, a correlation, which was also already observed by Frick and Butz [90, 91].

Piercing colon tissue with implants of 4, 8, 12 tips, resulted in average forces of  $6.4 \pm 1.5$  N,  $13.6 \pm 1.4$  N and  $21.7 \pm 5.8$  N, respectively.  $F_{pierce}^{12\ spikes}$  was used as minimal threshold for the design and selection of respective implant closing mechanisms. Comparing the measured holding force of the snap connector  $F_{snap\ holding}^{mean} = 43.6 \pm 3.9$  N to the piercing forces of 28 N reveals that the connection also provides sufficient abutment for the piercing procedure.

Both, the spring and hydraulic concepts, allowed to apply forces high enough to pierce through two layers of tissue ( $F_{hydraulics}^{prototype} = 29.2$  N;  $F_{spring}^{prototype} = 36.1$  N), which was also experimentally proven. However, the spring based closing unit showed limited controllability during axial closure. Once the retainer ring was removed, the spring snapped forward, accelerating the implant according to the spring's dynamics. The hydraulic mechanism, on the contrary, allowed a more controllable and smooth process here, favoring the use of an implant with an adjustable implant gap. Thus, this approach was chosen and modified for the integration into the final endoscopic device.

The closing force of the final unit was dimensioned to achieve forces more than three times higher than  $F_{pierce}^{12\ spikes}$ , to account not only for the tissue piercing task, but also for the forces required to mate the two implant halves, which is to be specified in detail within the further implant development process (depending on spike geometry, closure mechanism etc.).

#### 6.1.4 Device dimensions

However, not only mechanical factors, but also biological parameters were assessed in the biomechanical studies. Colon diameters were measured as an orientation to derive the required device dimensions. Literature shows that the porcine colon morphology has highest similarity to the one of humans [106], comparing the anatomy of commonly used laboratory animals to that of the human gastrointestinal tract. Testing and validation of novel instruments is therefore often performed in pigs or with porcine ex vivo specimens. The realistic tissue environment allows to depict relevant parameters with respect to endoscopic navigation, such as device tissue interaction, impediments during the advancement and gliding behavior. Even though the human intestine generally shows larger lumina, the anatomical parameters of porcine intestine were used as orientation for the initial development of endoscopic anastomosis platform units with respect to system diameters and required expansion scope.

The 5th and 95th percentiles of the sample diameters measured were 24.1 mm and 40.1 mm (n=540 samples) respectively, which implies a required expansion range of 16 mm to cover anatomical variabilities. With the endoscopic hydraulic expansion unit, a total expansion range of about 18.4 mm can be addressed.

While for porcine colon tissue the device diameter of  $\sim 33.1$  mm in unexpanded configuration would be too big to address smaller bowels, the dimension of the developed approach still

seems feasible with respect to human intestine, which tends to show lumina in the range of up to  $\sim 5$  cm and even higher [106].

	<i>Unexpanded</i>	<i>Expansion 1</i>	<i>Expansion 2</i>
<i>Diameter (aboral applicator)</i>	33.1 mm	46.8 mm	51.5 mm
<i>Diameter (oral applicator)</i>	33.1 mm	46.8 mm	51.5 mm

Table 4 Dimensions of the expandable, hydraulic application device, including unexpanded configuration and state 1 and 2.

### 6.1.5 Using electromagnets for implant detachment

Lastly, an interface between implant and applicator is required for implant carrying endoscopic platforms. Here, the respective mechanism must ensure secure fixation of the implant to the applicator during navigation, but must allow on demand deployment at the surgical site. Using electromagnets, which were integrated into an endoscope overtube prototype, enabled to reproducibly detach and resume the anastomosis implant in the experiment. Thus, it was derived that this approach holds high potential for the application in complex endoscopic platforms and improves system controllability and flexibility by providing a distinctively triggered and reusable release mechanism.

However, before electromagnets can be used intracorporeally, any kind of patient hazard must be excluded. If heat is applied to tissue, thermal effects occur in cells that are exposed to temperatures below or above a thermo-neutral zone  $T \in [35^\circ\text{C}; 41.5^\circ\text{C}]$  [107]. Beyond these thresholds, irreversible thermal effects occur, which lead to permanent cell damage. If cellular structures are heated to temperatures between  $41.5^\circ\text{C}$  and  $49.0^\circ\text{C}$ , this leads to invisible devitalization. The affected tissue can subsequently disintegrate, causing life threatening complications, such as delayed perforations and intracorporeal bleeding [107]. While exposure time in this respect is of great importance, immediate devitalization must be expected, if temperature rises even further above  $49.0^\circ\text{C}$  [107].

Thus, heat emission resulting from the electromagnet operation was investigated. The experiments revealed that the maximum temperatures reached critical levels beyond the thermo-neutral zone of  $41.5^\circ\text{C}$  for both, the pulsed ( $T_{max_{body}}^{1s} = 41.6 \pm 0.1^\circ\text{C}$ ) and the continuous operation ( $T_{max_{body}}^{continuous} = 44.1 \pm 1.5^\circ\text{C}$ ). Furthermore, it was observed that an increasing number of pulses led to nonlinear increase in coil temperature. This can be attributed to internal heat accumulation effects, which also occurred for the continuous operation. Here, a final temperature of  $T_{max_{body}}^{continuous} = 44.1 \pm 1.5^\circ\text{C}$  was reached after a certain delay, as the highest temperature first occurs at the innermost winding and then heat propagates towards the outside [93].

---

A polymeric isolation of the hot elements can support preclusion of tissue damage. However, due to the tight size restrictions for endoscopic instruments, the electromagnet encapsulation wall must be restricted in thickness. Based on the experiments conducted and accounting for heat transfer effects, additional preventive design specifications were derived.

A polymeric encapsulation was considered as a shielding safety measure. Heat transfer calculations showed that a wall width of 0.024 mm would already be feasible to effectively shield heat generated by the electromagnets for the assessed scenarios.

Based on these findings, it was derived that for an additively manufactured anastomosis device, which uses an electromagnetic actuation, critical thresholds for the isolating wall are determined rather by stability considerations and machine accuracy limitations, than by heat shielding requirements. Thus, the integration of electromagnets into endoscopic devices seems feasible with respect to resistance related heating, allowing for a safe and force-saving operation.

Electromagnet encapsulation is needed, not only to shield heat but also insulate all active components. The majority of our organs and movements is controlled by electrical impulses originating from the brain. Extraneous current flowing through the body can lead to muscle cramping and may affect organ functions, if it is significantly greater than the body's own. An AC voltage of 50 V and a DC voltage of 120 V can have life-threatening consequences. [108] Thus, special attention should be paid to potential, operating voltage related hazards in further investigations, which is why the approach was not yet included into the device.

### **6.1.6 Using additive manufacturing for the development of novel endoscopic instruments**

Using additive manufacturing for the endoscopic platform development opened up new possibilities, providing a broad range of task optimized materials. It further allowed the fabrication of complex monolithic geometries and the integration of miniaturized components with high degree of functionality, such as filigree plug connections for space saving assembly, thin walled hydraulic components, integrated channels of complex geometries and profiles or integrated groove nose guidance between hydraulic piston and cylinder to determine actuation maximum and direction.

However, the use of stereolithographic additive manufacturing posed challenges with respect to the production of the hydraulic units. Dimensional inaccuracies and staircase effects led to increased surface roughness and friction between the gliding elements. This also deteriorated quality of operation (i.e. unsmooth expansion) and impeded sealing capabilities between hydraulic partners, which is also a well known challenge in literature for related processes (selective laser sintering). [103] Even though it was possible to enhance smoothness of motion by the integration of vent valves, actuation efficiency could benefit significantly from a redesign and optimization of fluid actuation principles, specified for the 3D-printing process.

---

Possible approaches could be to integrate folded bellows structures or concepts that allow to entirely avoid contact between 3D-printed gliding partners. A hermetically sealed system is furthermore desirable with respect to leakage tightness and instrument sterilization.

## 6.2 Using hydraulics vs. Bowden wires in endoscopic platforms: Future potentials

Innovations in this field could open up even greater potentials in robotics and minimally invasive surgery.

The design of endoscopic devices is always subject to the compromise between the limited construction space available (as the system must enable navigation through the colon), and adequate force application at the operation situs (at the endoscope tip) [109], while the endoscope shaft is too flexible to establish relevant abutment [61] and might be positioned in arbitrary shapes around the flexures of the colon.

In the following the proposed platform with hydraulic actuation principle is compared to state of the art endoscopic manipulators, which commonly use Bowden wires, that run along the shaft, to control motion of the platform itself and instrument arms [101]. Those cables are widely used for force actuation in complex and space-constrained environments [110].

Bowden wires comprise a steel wire, which is guided by a flexible sheath and which can withstand compression in the axial direction. The sheath serves as counter-bearing for the transmitted forces. By this means, tensile forces can be transmitted from a remote position to the end-effector. [110]

Traction cables can be easily used for the construction of systems with remote actuation. Using actuators at the site of motion might change dynamic properties of the system due to the mass/moment of inertia of actuators and transmission system, while using Bowden cables allows for displacement of weight away from the end-effector unit and therefore increased power density. Secondly, Bowden wires are highly flexible, in contrast to gear trains, torsion bars and levers, which all restrict the range of motion of the system. [110]

However, a critical disadvantage of Bowden cables is that they exhibit a hysteresis behavior [59] and that cyclic loading results into hysteretic loops [111]. The high friction generated during wire actuation between the inner cable and outer sheath leads to ineffective force transmission, lack of instrument responsiveness and accuracy [59, 110]. A problem, which is even further accentuated during endoscope retroflexion and by long instrument length [59]. Thus, the force application behavior is not consistent for arbitrary platform shapes. Cable elongation may further lead to impaired motion automation and haptic feedback. [59] The latter one is generally problematic for flexible endoscopy due to the long distance between operator and end-effectors. [60] Modelling and thus finding ways of compensation for these losses is difficult, due to the non-linear behavior and multivariable dependencies. [110] This effect

---

makes it difficult to accurately predict structural response of Bowden wires and respective actuated components during cyclic loading [111].

Hydraulic units, which allowed actuation directly where the action is to be performed, enabled consistent force application behavior for arbitrary shaft lengths and shapes (efficiency, responsiveness and accuracy). Lightweight manufacturing from polymers of hydraulic units could also be interesting for other applications in flexible endoscopy or robotics, as it allows to minimize weight force of end-effectors and thus avoid inertia effects. Furthermore, while for Bowden wire based platforms, end-effector and shaft are inseparably connected and thus instrument change is difficult [59], using hydraulically actuated end effector units and a fluid guiding overtube might allow a modularization of the platform and thus a more flexible exchange of instrument.

## Acknowledgement

The system components were verified experimentally in laboratory settings to harmonize subsystems with each other. Some of the experiments were performed in the context of student projects. A comprehensive summary of all student theses is included in the Appendix.

## Appendix

### 8.1 Formula Directory

- (I) Transmissible closure force for spring actuator
- (II) Transmissible closure force for hydraulic actuator
- (III) Equation to dimension a film joint of specific geometry. Correlation for the required tapered section length  $L$  [mm], depending on the tapered section thickness  $h$  [mm].
- (IV) Fourier's heat equation.
- (V) Equation to describe the state of equilibrium of a current-carrying conductor at an elevated temperature, which is supplied by a continuously uniform energy, in which the heat transfer rate ( $\dot{Q}$ ) corresponds to the electrical power ( $P_{el}$ ) absorbed.
- (VI) Equation to calculate heat transfer through a cylindrical wall.
- (VII) Equation to calculate the suction force.
- (VIII) Force equilibrium in x-direction (at the blade).
- (IX) Force equilibrium in y-direction (at the blade).
- (X) Momentum equilibrium around z-axis (at the blade).
- (XI) Force equilibrium in x-direction (at strut 1).
- (XII) Force equilibrium in y-direction (at strut 1).
- (XIII) Momentum equilibrium around z-axis (at strut 1).
- (XIV) Force equilibrium in x-direction (at strut 2).
- (XV) Force equilibrium in y-direction (at strut 2).
- (XVI) Momentum equilibrium around z-axis (at strut 2).
- (XVII) Equation to model the realized expansion force of one applicator arm for the hydraulic expansion cylinder 1 (for both, oral and aboral applicator units), for the initial joint angle ( $F_{exp}^{initial\ stage\ 1}(\varphi_{initial}=77.4^\circ)$ ) and the final ( $F_{exp}^{end\ stage\ 1}(\varphi_{end}=36.9^\circ)$ ) joint angle.
- (XVIII) Equation to model the realized expansion force of one applicator arm for the hydraulic expansion cylinder 2 (for both, oral and aboral applicator units), for the initial joint angle ( $F_{exp}^{initial\ stage\ 2}(\varphi_{initial}=36.9^\circ)$ ) and the final ( $F_{exp}^{end\ stage\ 2}(\varphi_{end}=15.9^\circ)$ ) joint angle.
- (XIX) Momentum equilibrium around joint B at the blade
- (XX) Expression to determine the varying distance between the joints A and B ( $\overline{AB}$ ) of the blade, depending on the changing angle  $\varphi$  during applicator arm expansion.
- (XXI) Equation to calculate the bearing force in joint A, for expansion hydraulics stage 1 for the initial joint angle ( $F_{exp}^{initial\ stage\ 1}(\varphi_{initial}=77.4^\circ)$ ) and the final ( $F_{exp}^{end\ stage\ 1}(\varphi_{end}=36.9^\circ)$ ) joint angle.
- (XXII) Equation to calculate the bearing force in joint A, for expansion hydraulics stage 2 for the initial joint angle ( $F_{exp}^{initial\ stage\ 2}(\varphi_{initial}=36.9^\circ)$ ) and the final ( $F_{exp}^{end\ stage\ 2}(\varphi_{end}=15.9^\circ)$ ) joint angle.
- (XXIII) Equation to describe the implant closure force, derived from the force equilibrium in the longitudinal direction of the endoscope axis.

---

## 8.2 List of publications

J. Steger, C. Kwade, M. Berlet, R. Krumpholz, S. Ficht, D. Wilhelm, P. Mela, "The colonoscopic vacuum model—simulating biomechanical restrictions to provide a realistic colonoscopy training environment.", *International Journal of Computer Assisted Radiology and Surgery*, 18(1), pp. 105-116, 2022, <https://doi.org/10.1007/s11548-022-02792-z>

J. Steger, A. Zimmermann, T. Wittenberg, P. Mela, D. Wilhelm, "Electromagnetic tool for the endoscopic creation of colon anastomoses – Development and feasibility assessment of a novel anastomosis compression implant approach.", *International Journal of Computer Assisted Radiology and Surgery*, 17(12), pp. 2269-2280., 2022, <https://doi.org/10.1007/s11548-022-02722-z>

J. Steger, A. Jell, S. Ficht, D. Ostler, M. Eblenkamp, P. Mela, D. Wilhelm, "Systematic Review and Meta-Analysis on Colorectal Anastomotic Techniques.", *Therapeutics and Clinical Risk Management*, 18, pp. 523-539., 2022, <https://doi.org/10.2147/TCRM.S335102>

J. Steger, A. Zimmermann, T. Wittenberg, D. Wilhelm, "Electromagnets for an endoscopic anastomosis tool in the colon. ", *Current Directions in Biomedical Engineering*, 7(1), pp. 39-42., 2021, <https://doi.org/10.1515/cdbme-2021-1009>

J. Steger, I. Patzke, M. Berlet, S. Ficht, M. Eblenkamp, P. Mela, D. Wilhelm, "Design of a force-measuring setup for colorectal compression anastomosis and first ex-vivo results.", *International Journal of Computer Assisted Radiology and Surgery*, 16(8), pp. 1335-1345., 2021, <https://doi.org/10.1007/s11548-021-02371-8>

J. Steger, S. Ficht, D. Ostler, A. Jell, H. Feußner, P. Mela, M. Eblenkamp, D. Wilhelm, "Anastomoses in visceral surgery—first approach towards a universal transluminal system for micro invasive application.", *International Conference on Computational Science and Computational Intelligence (CSCI), IEEE*, pp. 983-986., 2019

## 8.3 List of patents

J. Steger, D. Ostler, D. Wilhelm, S. Wohlgemuth, S. Ficht, M. Eblenkamp, P. Mela, "Clamping device and applicator for joining flexible tubular walls.", WO 2022/049196 A1., Published: 10/03/2022

J. Steger, D. Ostler, D. Wilhelm, S. Wohlgemuth, S. Ficht, M. Eblenkamp, P. Mela, "Implant and implant applicator for surgical anastomosis.", WO 2022/049197 A1., Published: 10/03/2022

---

## 8.4 List of supervised student theses

I supervised the following student theses during my time as a research associate at the institute MITI. Parts of the gained knowledge and of the results contributed to the successful completion of the DFG project CONNECT (Project number: 386233) and to this work. A summary of the student theses is listed hereafter.

### 2021

- Wahyu Sugiarto (Master Thesis): “Investigation of different force transmission mechanisms to permit rotation and axial translation of NOTES-enabling end-effector units“
- Tim Berndt (Master Thesis): “Development and evaluation of different approaches for an endoscope attachable unit to scale a customizable endoscopic anastomosis implant“
- Amar Cindrak (Master Thesis): “Assessment of different implant expansion and closure mechanisms for an endoscopically applied anastomosis implant“
- Anne Zimmermann (Friedrich-Alexander-University Nuremberg, Erlangen) (Master Thesis): “Investigation and feasibility assessment of electromagnets for NOTES-application“

### 2020

- Alexandra Buchmann (Master Thesis): “Development and evaluation of a hydraulic expansion and implant closure unit to generate transluminal compression anastomoses“
- Christina Kwade (Term Thesis): “Development of a colonic model for realistic validation of different anastomosis methods“
- Isabella Patzke (Bachelor Thesis): “Determination of the maximal force occurring during tissue piercing for a traumatic colon anastomosis approach“
- Sandra Wohlgemuth (Master Thesis): “Development of a cable-based scalable NOTES applicator system for the preparation of end-to-end anastomosis“
- Franziska Jurosch (Term Thesis): “Further development of an intraoperative force sensor including a standardized calibration process for the determination of forces occurring during laparoscopic surgery“
- Moritz Köppenkastrop-Luecker (Term Thesis): “Determination of the forces occurring during the manipulation of tissues throughout laparoscopic and endoscopic surgery“

### 2019

- Johannes Breitsameter (Term Thesis): “Development, design and evaluation of an invagination anastomosis implant“
- Verena Maier (Term Thesis): “Evaluation of compression pressure distribution in porcine intestinal tissue for the development of an anastomosis implant“
- Anqi Peng: (Master Thesis): “Concept development of a minimally invasive, scalable intestinal anastomosis system“

---

## References

- [1] A. R. Ende *et al.*, “Objective Differences in Colonoscopy Technique Between Trainee and Expert Endoscopists Using the Colonoscopy Force Monitor,” *Digestive diseases and sciences*, vol. 63, no. 1, pp. 46–52, 2018, doi: 10.1007/s10620-017-4847-9.
- [2] A. Schneider and H. Feussner, *Biomedical engineering in gastrointestinal surgery: Chapter 1: Surgery and Biomedical Engineering*: Academic Press, 2017.
- [3] O. Schwandner, J. Scheele, and H.-P. Bruch, “Minimal invasive Kolonchirurgie: Welche Vorteile sind evidenzbasiert?,” *Visceral Medicine*, vol. 21, no. 4, pp. 338–346, 2005, doi: 10.1159/000089287.
- [4] D. E. Bowman, “ASGE/SAGES working group on natural orifice transluminal endoscopic surgery: White paper October 2005,” *Gastrointestinal Endoscopy*, vol. 63, no. 2, pp. 199–203, 2006, doi: 10.1016/j.gie.2005.12.007.
- [5] J. Steger *et al.*, “Design of a force-measuring setup for colorectal compression anastomosis and first ex-vivo results,” *International Journal of Computer Assisted Radiology and Surgery*, 2021, doi: 10.1007/s11548-021-02371-8.
- [6] L. M. Ernst, E. D. Ruchelli, and D. S. Huff, *Color atlas of fetal and neonatal histology: Chapter 3: Gastrointestinal Tract*: Springer Science & Business Media, 2011.
- [7] F. Paulsen, Y. Cetin, and R. Hildebrand, Eds., *Organe des Verdauungssystems: Magen-Darm-Trakt*: Springer Medizin Verlag Heidelberg 2010.
- [8] H. Messmann, Ed., *Lehratlas der Koloskopie: Das Referenzwerk zur Untersuchungstechnik und Befundinterpretation: Chapter 1: Allgemeines zur Untersuchung*: Georg Thieme Verlag, 2014.
- [9] N. Chawla, E. N. Butler, J. Lund, J. L. Warren, L. C. Harlan, and K. R. Yabroff, “Patterns of colorectal cancer care in Europe, Australia, and New Zealand,” *Journal of the National Cancer Institute. Monographs*, no. 46, pp. 36–61, 2013, doi: 10.1093/jncimonographs/lgt009.
- [10] D. A. Etzioni, T. M. Mack, R. W. Beart, JR, and A. M. Kaiser, “Diverticulitis in the United States: 1998–2005: Changing Patterns of Disease and Treatment,” *Annals of surgery*, vol. 249, no. 2, pp. 210–217, 2009, doi: 10.1097/SLA.0b013e3181952888.
- [11] F. J. Thornton and A. Barbul, “Healing in the gastrointestinal tract,” *Surgical Clinics of North America*, no. 77, pp. 549–573, 1997.
- [12] M. G. Laukötter and N. Senninger, “Anastomosentechniken am Gastrointestinaltrakt,” (in ger), *Der Chirurg*, vol. 84, no. 12, pp. 1085–1098, 2013, doi: 10.1007/s00104-012-2392-9.
- [13] B. Mann, S. Kleinschmidt, and W. Stremmel, “Prospective study of hand-sutured anastomosis after colorectal resection,” *British journal of surgery*, vol. 83, no. 1, pp. 29–31, 1996, doi: 10.1002/bjs.1800830108.

- 
- [14] J. C. Sliker, F. Daams, I. M. Mulder, J. Jeekel, and J. F. Lange, "Systematic Review of the Technique of Colorectal Anastomosis," *JAMA Surgery*, vol. 148, no. 2, pp. 190–201, 2013, doi: 10.1001/2013.jamasurg.33.
- [15] Y.-H. Ho and M. A. T. Ashour, "Techniques for colorectal anastomosis," *World Journal of Gastroenterology: WJG*, vol. 16, no. 13, pp. 1610–1621, 2010, doi: 10.3748/wjg.v16.i13.1610.
- [16] Z. Mohr and S. Willis, "Intestinale Anastomosen und Techniken im Bereich des unteren Gastrointestinaltraktes," *Der Chirurg*, vol. 82, no. 1, pp. 34–40, 2011, doi: 10.1007/s00104-010-1901-y.
- [17] G. Meyer, R. A. Lang, and F. W. Schildberg, "Einflussfaktoren auf die Anastomosenheilung," *Viszeralchirurgie*, vol. 36, no. 02, pp. 49–68, 2001, doi: 10.1055/s-2001-12711.
- [18] P. Swain, "NOTES and anastomosis," *Gastrointestinal Endoscopy Clinics of North America*, vol. 18, no. 2, pp. 261–277, 2008.
- [19] C. E. Graves *et al.*, "Magnetic Compression Anastomosis (Magnamosis): First-In-Human Trial," *Journal of the American College of Surgeons*, vol. 225, no. 5, 676 - 681.e1, 2017, doi: 10.1016/j.jamcollsurg.2017.07.1062.
- [20] E. Machytka *et al.*, "Partial jejunal diversion using an incisionless magnetic anastomosis system: 1-year interim results in patients with obesity and diabetes," *Gastrointestinal Endoscopy*, vol. 86, no. 5, pp. 904–912, 2017, doi: 10.1016/j.gie.2017.07.009.
- [21] D. Vilhjalmsson *et al.*, "The compression anastomotic ring-locking procedure: a novel technique for creating a sutureless colonic anastomosis," *European Surgical Research*, vol. 54, 3-4, pp. 139–147, 2015, doi: 10.1159/000368354.
- [22] H. Wiesinger, *113 Manuelle Naht versus/sive Maschinennaht (Kompressionsanastomosen)?* [Online]. Available: [http://villach.kabeg2014.t3.world-direct.at/fileadmin/user\\_upload/lkhvillach/allgemeinchirurgie/fachinformationen/publikationen/13\\_Manuelle\\_Naht\\_verseus\\_Klammernaht\\_\\_1996.pdf](http://villach.kabeg2014.t3.world-direct.at/fileadmin/user_upload/lkhvillach/allgemeinchirurgie/fachinformationen/publikationen/13_Manuelle_Naht_verseus_Klammernaht__1996.pdf) (accessed: Jun. 28 2022).
- [23] G. C. Bannura, M. A. G. Cumsille, A. E. Barrera, J. P. Contreras, C. L. Melo, and D. C. Soto, "Predictive Factors of Stenosis after Stapled Colorectal Anastomosis: Prospective Analysis of 179 Consecutive Patients," *World Journal of Surgery*, vol. 28, no. 9, pp. 921–925, 2004, doi: 10.1007/s00268-004-7375-7.
- [24] L. Polese *et al.*, "Risk factors for colorectal anastomotic stenoses and their impact on quality of life: what are the lessons to learn?," *Colorectal Disease*, vol. 14, no. 3, pp. e124–e128, 2012, doi: 10.1111/j.1463-1318.2011.02819.x.
- [25] J. Jähne, "Intestinale Anastomosentechniken," *Der Chirurg*, vol. 82, no. 1, pp. 5–6, 2011, doi: 10.1007/s00104-010-1904-8.

- 
- [26] N. J. Mortensen and S. Ashraf, Eds., *Gastrointestinal Tract and Abdomen (section 5): Intestinal anastomosis (chapter 29)*, 2008.
- [27] J. Steger *et al.*, “Systematic Review and Meta-Analysis on Colorectal Anastomotic Techniques,” *Therapeutics and Clinical Risk Management*, no. 18, pp. 523–539, 2022, doi: 10.2147/TCRM.S335102.
- [28] A. A. P. Slesser *et al.*, “Compression versus hand-sewn and stapled anastomosis in colorectal surgery: a systematic review and meta-analysis of randomized controlled trials,” *Techniques in coloproctology*, vol. 20, no. 10, pp. 667–676, 2016, doi: 10.1007/s10151-016-1521-8.
- [29] H. M. MacRae and R. S. McLeod, “Handsewnvs. stapled anastomoses in colon and rectal surgery,” *Diseases of the Colon & Rectum*, vol. 41, no. 2, pp. 180–189, 1998, doi: 10.1007/BF02238246.
- [30] J. S. Kim, S. Y. Cho, B. S. Min, and N. K. Kim, “Risk factors for anastomotic leakage after laparoscopic intracorporeal colorectal anastomosis with a double stapling technique,” *Journal of the American College of Surgeons*, vol. 209, no. 6, pp. 694–701, 2009, doi: 10.1016/j.jamcollsurg.2009.09.021.
- [31] M. Ito, M. Sugito, A. Kobayashi, Y. Nishizawa, Y. Tsunoda, and N. Saito, “Relationship between multiple numbers of stapler firings during rectal division and anastomotic leakage after laparoscopic rectal resection,” *International journal of colorectal disease*, vol. 23, no. 7, pp. 703–707, 2008, doi: 10.1007/s00384-008-0470-8.
- [32] J. S. Park *et al.*, “Multicenter analysis of risk factors for anastomotic leakage after laparoscopic rectal cancer excision: the Korean laparoscopic colorectal surgery study group,” *Annals of surgery*, vol. 257, no. 4, pp. 665–671, 2013, doi: 10.1097/SLA.0b013e31827b8ed9.
- [33] K. Kawada *et al.*, “Risk factors for anastomotic leakage after laparoscopic low anterior resection with DST anastomosis,” *Surgical endoscopy*, vol. 28, no. 10, pp. 2988–2995, 2014, doi: 10.1007/s00464-014-3564-0.
- [34] C. W. Schell, *Die endoluminale Vollwandresektion im Dickdarm in Klammernahttechnik: Technologische Entwicklung und tierexperimentelle Ergebnisse*. Tübingen, 2005.
- [35] M. Kimura *et al.*, “Evaluation of a new stapler with unique surface gripping technology,” *Journal of Advances in Medicine and Medical Research*, pp. 1–6, 2016, doi: 10.9734/BJMMR/2016/30153.
- [36] P. Rojatkár *et al.*, “A novel powered circular stapler designed for creating secure anastomoses,” *Med Devices Diagn Eng*, vol. 2, no. 2, pp. 94–100, 2017, doi: 10.15761/MDDE.1000123.
- [37] C. Wullstein and E. Gross, “Compression anastomosis (AKA-2) in colorectal surgery: results in 442 consecutive patients // Compression anastomosis (AKA-2) in colorectal

- 
- surgery: results in 442 consecutive patients,” *British journal of surgery*, vol. 87, no. 8, pp. 1071–1075, 2000, doi: 10.1046/j.1365-2168.2000.01489.x.
- [38] R. Aggarwal, A. Darzi, R. Aggarwal, and A. Darzi, “Compression anastomoses revisited,” *Journal of the American College of Surgeons*, vol. 201, no. 6, pp. 965–971, 2005, doi: 10.1016/j.jamcollsurg.2005.06.255.
- [39] T. G. Hardy, W. G. Pace, J. W. Maney, A. R. Katz, and A. L. Kagano, “A biofragmentable ring for sutureless bowel anastomosis,” *Diseases of the Colon & Rectum*, vol. 28, no. 7, pp. 484–490, 1985.
- [40] A. P. Zbar, Y. Nir, A. Weizman, M. Rabau, and A. Senagore, “Compression anastomoses in colorectal surgery: a review,” *Techniques in coloproctology*, vol. 16, no. 3, pp. 187–199, 2012, doi: 10.1007/s10151-012-0825-6.
- [41] O. Kaidar-Person, R. J. Rosenthal, S. D. Wexner, S. Szomstein, and B. Person, “Compression anastomosis: history and clinical considerations,” *The American Journal of Surgery*, vol. 195, no. 6, pp. 818–826, 2008, doi: 10.1016/j.amjsurg.2007.10.006.
- [42] D. Vilhjalmsson *et al.*, “Compression anastomotic ring-locking procedure (CARP) is a safe and effective method for intestinal anastomoses following left-sided colonic resection,” *International journal of colorectal disease*, vol. 30, no. 7, pp. 969–975, 2015, doi: 10.1007/s00384-015-2257-z.
- [43] K. Kusnierz, H. Morawiec, Z. Lekston, D. Zhavoronkov, M. Lucyga, and P. Lampe, “NiTi Shape Memory Compression Anastomosis Clip in Small- and Large-Bowel Anastomoses: First Experience,” *Surgical Innovation*, vol. 20, no. 6, pp. 580–585, 2013, doi: 10.1177/1553350612474494.
- [44] N. Grassi *et al.*, “Validity of shape memory NiTi colon ring BioDynamix ColonRing™ (or NiTi CAR 27™) to prevent anastomotic colorectal strictures. Preliminary results,” *Il Giornale di chirurgia*, vol. 33, no. 5, pp. 194–198, 2012. [Online]. Available: <http://eprints.bice.rm.cnr.it/7933/>
- [45] H. R. Kim *et al.*, “Early surgical outcomes of NiTi endoluminal compression anastomotic clip (NiTi CAC 30) use in patients with gastrointestinal malignancy,” *Journal of Laparoendoscopic & Advanced Surgical Techniques*, vol. 22, no. 5, pp. 472–478, 2012, doi: 10.1089/lap.2011.0406.
- [46] I. Nudelman, V. Fuko, M. Rubin, and S. Lelcuk, “A nickel–titanium memory-shape device for colonic anastomosis in laparoscopic surgery,” *Surgical endoscopy*, vol. 18, no. 7, pp. 1085–1089, 2004.
- [47] H. Masoomi, R. Lou, S. Mills, J. C. Carmichael, A. J. Senagore, and M. J. Stamos, “Compression anastomosis ring device in colorectal anastomosis: a review of 1,180 patients,” *The American Journal of Surgery*, vol. 205, no. 4, pp. 447–451, 2013, doi: 10.1016/j.amjsurg.2012.03.013.

- 
- [48] A. Schneider and H. Feussner, *Biomedical engineering in gastrointestinal surgery: Chapter 5: Diagnostic Procedures*: Academic Press, 2017.
- [49] Karl Storz SE & Co. KG., “Systeme für die Gastroenterologie: 3. Ausgabe 2/2016: Katalog,” no. 3, 2016.
- [50] H. Messmann, Ed., *Lehratlas der Koloskopie: Das Referenzwerk zur Untersuchungstechnik und Befundinterpretation: Chapter 2: Untersuchungstechnik und Koloskopiearbeitsplatz*: Georg Thieme Verlag, 2014.
- [51] R. Jamshidi *et al.*, “Magnamosis: magnetic compression anastomosis with comparison to suture and staple techniques,” *Journal of pediatric surgery*, vol. 44, no. 1, pp. 222–228, 2009, doi: 10.1016/j.jpedsurg.2008.10.044.
- [52] K. D. Gonzales *et al.*, “Magnamosis III: delivery of a magnetic compression anastomosis device using minimally invasive endoscopic techniques,” *Journal of pediatric surgery*, vol. 47, no. 6, pp. 1291–1295, 2012, doi: 10.1016/j.jpedsurg.2012.03.042.
- [53] T. Lambe, M. G. Ó. Ríordáin, R. A. Cahill, and P. Cantillon-Murphy, “Magnetic compression in gastrointestinal and bilioenteric anastomosis: how much force?,” *Surgical Innovation*, vol. 21, no. 1, pp. 65–73, 2014, doi: 10.1177/1553350613484824.
- [54] J. Leroy *et al.*, “An Original Endoluminal Magnetic Anastomotic Device Allowing Pure NOTES Transgastric and Transrectal Sigmoidectomy in a Porcine Model: Proof of Concept,” *Surgical Innovation*, vol. 19, no. 2, pp. 109–116, 2012, doi: 10.1177/1553350611429029.
- [55] C. Graves *et al.*, “V12-02 magnetic bowel anastomosis: first-in-human Magnamosis application s,” *The Journal of Urology*, vol. 195, 4S, e1066, 2016, doi: 10.1016/j.juro.2016.02.2128.
- [56] M. Diana *et al.*, “Totally endoscopic magnetic enteral bypass by external guided rendez-vous technique,” *Surgical Innovation*, vol. 18, no. 4, pp. 317–320, 2011.
- [57] M. Ryou *et al.*, “Smart Self-Assembling Magnets for Endoscopy (SAMSEN) for transoral endoscopic creation of immediate gastrojejunostomy (with video),” *Gastrointestinal Endoscopy*, vol. 73, no. 2, pp. 353–359, 2011, doi: 10.1016/j.gie.2010.10.024.
- [58] B. N.S. Bhatnagar, C. L.N. Sharma, S. N. Gupta, M. M. Mathur, and D. C.S. Reddy, “Study on the anatomical dimensions of the human sigmoid colon,” *Clinical Anatomy: The Official Journal of the American Association of Clinical Anatomists and the British Association of Clinical Anatomists*, vol. 17, no. 3, pp. 236–243, 2004, doi: 10.1002/ca.10204.
- [59] B. P. M. Yeung and T. Gourlay, “A technical review of flexible endoscopic multitasking platforms,” *International journal of surgery*, vol. 10, no. 7, pp. 345–354, 2012, doi: 10.1016/j.ijssu.2012.05.009.
- [60] S. N. Shaikh and C. C. Thompson, “Natural orifice transluminal surgery: Flexible platform review,” *World journal of gastrointestinal surgery*, vol. 2, no. 6, p. 210, 2010.

- 
- [61] L. Swanström, P. Swain, and P. Denk, “Development and validation of a new generation of flexible endoscope for NOTES,” *Surgical Innovation*, vol. 16, no. 2, pp. 104–110, 2009, doi: 10.1177/1553350609334344.
- [62] J. Y. Bang, R. Hawes, and S. Varadarajulu, “Equivalent performance of single-use and reusable duodenoscopes in a randomised trial,” *Gut*, vol. 70, no. 5, pp. 838–844, 2021, doi: 10.1136/gutjnl-2020-321836.
- [63] A. K. Golahmadi, D. Z. Khan, G. P. Mylonas, and H. J. Marcus, “Tool-tissue forces in surgery: A systematic review,” *Annals of Medicine and Surgery*, p. 102268, 2021, doi: 10.1016/j.amsu.2021.102268.
- [64] S. Bourgooin *et al.*, “Biomechanical characterisation of fresh and cadaverous human small intestine: applications for abdominal trauma,” *Medical & biological engineering & computing*, vol. 50, no. 12, pp. 1279–1288, 2012, doi: 10.1007/s11517-012-0964-y.
- [65] K. H. Svendsen and G. Thomson, “A new clamping and stretching procedure for determination of collagen fiber stiffness and strength relations upon maturation,” *Journal of biomechanics*, vol. 17, no. 3, pp. 225–229, 1984, doi: 10.1016/0021-9290(84)90013-7.
- [66] E. L. Carniel *et al.*, “Characterization of the anisotropic mechanical behaviour of colonic tissues: experimental activity and constitutive formulation,” *Experimental physiology*, vol. 99, no. 5, pp. 759–771, 2014, doi: 10.1113/expphysiol.2013.076091.
- [67] A. M. Okamura, C. Simone, and M. D. O’leary, “Force modeling for needle insertion into soft tissue,” *IEEE Transactions on Biomedical Engineering*, vol. 51, no. 10, pp. 1707–1716, 2004, doi: 10.1109/TBME.2004.831542.
- [68] W. Jensen, K. Yoshida, and U. G. Hofmann, “In-vivo implant mechanics of flexible, silicon-based ACREO microelectrode arrays in rat cerebral cortex,” *IEEE Transactions on Biomedical Engineering*, vol. 53, no. 5, pp. 934–940, 2006, doi: 10.1109/TBME.2006.872824.
- [69] N. Abolhassani, R. Patel, and M. Moallem, “Trajectory generation for robotic needle insertion in soft tissue,” 2004, doi: 10.1109/IEMBS.2004.1403782.
- [70] A. A. Sharp, A. M. Ortega, D. Restrepo, D. Curran-Everett, and K. Gall, “In vivo penetration mechanics and mechanical properties of mouse brain tissue at micrometer scales,” *IEEE Transactions on Biomedical Engineering*, vol. 56, no. 1, pp. 45–53, 2008, doi: 10.1109/TBME.2008.2003261.
- [71] D. Wilhelm *et al.*, “MIEO: a micro-invasive endoscopic operation port system for transluminal interventions—an acute and survival porcine study,” *Surgical Endoscopy And Other Interventional Techniques*, vol. 34, no. 6, pp. 2814–2823, 2020, doi: 10.1007/s00464-020-07518-3.
- [72] K. Tachi, K. S. Furukawa, I. Koshima, and T. Ushida, “New microvascular anastomotic ring-coupling device using negative pressure,” *Journal of plastic, reconstructive & aesthetic surgery*, vol. 64, no. 9, pp. 1187–1193, 2011, doi: 10.1016/j.bjps.2011.04.008.

- 
- [73] J. E. Bernth, A. Arezzo, and H. Liu, “A novel robotic meshworm with segment-bending anchoring for colonoscopy,” *IEEE Robotics and Automation Letters*, vol. 2, no. 3, pp. 1718–1724, 2017.
- [74] FORMLABS, *Clear Resin*. [Online]. Available: <https://formlabs.com/store/clear-resin/> (accessed: Jun. 28 2022).
- [75] FORMLABS, *White Resin Material properties*. [Online]. Available: <https://formlabs.com/store/white-resin/> (accessed: Jun. 28 2022).
- [76] J. Kobiela *et al.*, “Magnetic instrumentation and other applications of magnets in NOTES,” *Videosurgery and Other Miniinvasive Techniques*, vol. 7, no. 2, p. 67, 2012, doi: 10.5114/wiitm.2011.25665.
- [77] R. R. Mummadi and P. J. Pasricha, “The eagle or the snake: platforms for NOTES and radical endoscopic therapy,” *Gastrointestinal Endoscopy Clinics of North America*, vol. 18, no. 2, pp. 279–289, 2008, doi: 10.1016/j.giec.2008.01.005.
- [78] P. Swain, R. Ewers, R. Peh, and V. Sadaat, “New measurement methods and a randomized comparison of force transmission using flexible endoscopes and instruments before and after the application of Shapelock™ technology,” *Gastrointestinal Endoscopy*, vol. 61, no. 5, AB241, 2005, doi: 10.1016/S0016-5107(05)01298-8.
- [79] Roemheld Hilma Stark, *Wissenswertes über Hydraulikzylinder* (accessed: Jun. 28 2022).
- [80] D. Will and N. Gebhardt, Eds., *Hydraulik: Grundlagen, Komponenten, Systeme: 2.3.3 Luft und Wasser in der Druckflüssigkeit*. Berlin, Heidelberg: Springer Berlin Heidelberg, 2014.
- [81] N. Patel, C. Seneci, G.-Z. Yang, A. Darzi, and J. Teare, “Flexible platforms for natural orifice transluminal and endoluminal surgery,” *Endoscopy international open*, vol. 2, no. 02, E117-E123, 2014, doi: 10.1055/s-0034-1377171.
- [82] P. R. Bonenberger, *The first snap-fit handbook: Creating and managing attachments for plastics parts: 6.3 Cantilever Hook Design Rules of Thumb*: Carl Hanser Verlag GmbH Co KG, 2016.
- [83] P. Cantillon-Murphy, T. P. Cundy, N. K. Patel, G.-Z. Yang, A. Darzi, and J. P. Teare, “Magnets for therapy in the GI tract: a systematic review,” *Gastrointestinal Endoscopy*, vol. 82, no. 2, pp. 237–245, 2015, doi: 10.1016/j.gie.2014.11.007.
- [84] R. Diaz, G. Davalos, L. K. Welsh, D. Portenier, and A. D. Guerron, “Use of magnets in gastrointestinal surgery,” *Surgical endoscopy*, vol. 33, no. 6, pp. 1721–1730, 2019, doi: 10.1007/s00464-019-06718-w.
- [85] M. Albach, *Elektrotechnik: Das stationäre Magnetfeld*, 1st ed.: Pearson Deutschland GmbH, 2011.
- [86] FORMLABS, *Guide & Material Data - Using Tough 1500 Resin*. [Online]. Available: [https://support.formlabs.com/s/article/Using-Tough-1500-Resin?language=en\\_US](https://support.formlabs.com/s/article/Using-Tough-1500-Resin?language=en_US) (accessed: Jun. 28 2022).

- 
- [87] M. Keuerleber, P. Eyerer, H. Schüle, A. Radtke, O. Altmann, and W. P. Loh, “Gestalten, Fügen, Berechnungsansätze und Simulation EDV-unterstützter Konstruktionen und Auslegung von Kunststoffbauteilen,” in *Polymer Engineering*: Springer, 2008, pp. 466–544.
- [88] J. Kunz, S. Bachmann, and M. Studer, “Filmgelenke dehnungsbezogen auslegen,” *Kunststoffe*, vol. 97, no. 12, pp. 129–132, 2007.
- [89] G. Erhard, *Konstruieren mit Kunststoffen*: Hanser München, 1993.
- [90] T. B. Frick, D. D. Marucci, J. A. Cartmill, C. J. Martin, and W. R. Walsh, “Resistance forces acting on suture needles,” *Journal of biomechanics*, vol. 34, no. 10, pp. 1335–1340, 2001, doi: 10.1016/S0021-9290(01)00099-9.
- [91] K. D. Butz *et al.*, “Prestress as an optimal biomechanical parameter for needle penetration,” *Journal of biomechanics*, vol. 45, no. 7, pp. 1176–1179, 2012, doi: 10.1016/j.jbiomech.2012.01.049.
- [92] C. Heinle, *Simulationsgestützte Entwicklung von Bauteilen aus wärmeleitenden Kunststoffen*, 2012.
- [93] N. Hannoschöck, *Wärmeleitung und -transfer - Grundlagen der Wärme- und Stoffübertragung*, 2018.
- [94] S.-H. Lee, Y.-K. Park, D.-J. Lee, and K.-M. Kim, “Colonoscopy procedural skills and training for new beginners,” *World Journal of Gastroenterology: WJG*, vol. 20, no. 45, p. 16984, 2014.
- [95] Esska.de, *Technische Daten PU-Schlauch*. [Online]. Available: <https://www.esska.de/shop/Polyurethan-Schlauch-klar-Innen-%C3%98-2-bis-11-mm-Aussen-%C3%98-3-bis-16-mm-10-bis-16-bar-50-m-Preis-per-Rolle--7030KLAR1111-3340>
- [96] D. Roppenecker, “Entwicklung und Validierung eines generativ gefertigten Snake-Like Manipulators für die minimal-invasive Chirurgie,” Technische Universität München, 2017.
- [97] FORMLABS, *Rigid 4000 Resin*. [Online]. Available: <https://formlabs.com/store/materials/rigid-resin/> (accessed: Jun. 28 2022).
- [98] FORMLABS, *Form wash time settings 2021*. [Online]. Available: [https://support.formlabs.com/s/article/Form-Wash-Time-Settings?language=en\\_US](https://support.formlabs.com/s/article/Form-Wash-Time-Settings?language=en_US) (accessed: Jun. 28 2022).
- [99] FORMLABS, *Form Cure time and temperature settings 2021*. [Online]. Available: <https://s3.amazonaws.com/servicecloudassets.formlabs.com/media/Finishing/Post-Curing/115001414464-Form%20Cure%20Time%20and%20Temperature%20Settings/FormCurePost-CureSettings.pdf> (accessed: Jun. 28 2022).

- 
- [100]D. Will and N. Gebhardt, Eds., *Hydraulik: Grundlagen, Komponenten, Systeme: 3.1 Druckentstehung und -fortpflanzung*. Berlin, Heidelberg: Springer Berlin Heidelberg, 2014.
- [101]N. Suzuki, Hattori, A., Tanoue, K., Satoshi, I., Konishi, K., Tomikawa, M., Kenmotsu, H., and M. Hashizume, Eds., *Scorpion shaped endoscopic surgical robot for NOTES and SPS with augmented reality functions*: Springer, 2010.
- [102]B. S. Peters, P. R. Armijo, C. Krause, S. A. Choudhury, and D. Oleynikov, “Review of emerging surgical robotic technology,” *Surgical Endoscopy And Other Interventional Techniques*, vol. 32, no. 4, pp. 1636–1655, 2018, doi: 10.1007/s00464-018-6079-2.
- [103]J. Breuninger, R. Becker, A. Wolf, S. Rommel, and A. Verl, *Generative Fertigung mit Kunststoffen: Konzeption und Konstruktion für Selektives Lasersintern*: Springer-Verlag, 2012.
- [104]M. Mahvash and V. Hayward, “Haptic rendering of cutting: A fracture mechanics approach,” *1545-1143*, 2001.
- [105]S. P. DiMaio and S. E. Salcudean, “Simulated interactive needle insertion,” *Proceedings 10th Symposium on Haptic Interfaces for Virtual Environment and Teleoperator*, pp. 344–351, 2002, doi: 10.1109/HAPTIC.2002.998979.
- [106]T. T. Kararli, “Comparison of the gastrointestinal anatomy, physiology, and biochemistry of humans and commonly used laboratory animals,” *Biopharmaceutics & drug disposition*, vol. 16, no. 5, pp. 351–380, 1995, doi: 10.1002/bdd.2510160502.
- [107]A. Schneider and H. Feussner, *Biomedical engineering in gastrointestinal surgery: Chapter 6: Classical (Open) surger*: Academic Press, 2017.
- [108]S. Schmid-Gaiser, *Elektro-wissen: Wirkung des elektrischen Stromes auf den Menschen*. [Online]. Available: <http://elektro-wissen.de/Tipps/Wirkung-des-elektrischen-Stroms-auf-den-Menschen.php> (accessed: May 7 2021).
- [109]A. Schneider and H. Feußner, *Biomedical endingeering in gastrointestinal surgery: Chapter 9: Combined Laparocopic Endosocopic Procedures and Natural Orifice Transluminal Endoscopic Surgery (NOTES)*: Academic Press, 2017.
- [110]D. Chen, Y. Yun, and Deshpande, Ashish, D., “Experimental characterization of bowden cable friction,” *2014 IEEE international conference on robotics and automation (ICRA)*, 2014.
- [111]C. C. P. Santos, C. P. Pesce, R. Salles, Franzini, Guilherme, R., R. T. Goncalves, and R. Morini, “An experimental assessment of the hysteresis behavior of umbilical cables under cyclic traction,” 2017.